

**INTERFACIAL ELECTROCHEMISTRY OF
COLLOIDAL RUTHENIUM DIOXIDE
AND
CATALYSIS OF THE PHOTOCHEMICAL
GENERATION OF HYDROGEN FROM WATER**

ONTVANGEN

25 MEI 1977

CB-KARDEX

BIBLIOTHEEK
LANDBOUWUNIVERSITEIT
WAGENINGEN

CENTRALE LANDBOUWCATALOGUS



0000 0212 1255

40151

Promotor: dr. J. Lyklema, hoogleraar in de Fysische en Kolloïdchemie
Co-promotor: dr. H. P. van Leeuwen, universitair hoofddocent

N 08201, 1148

J. M. Kleijn

**INTERFACIAL ELECTROCHEMISTRY OF COLLOIDAL
RUTHENIUM DIOXIDE AND CATALYSIS OF THE
PHOTOCHEMICAL GENERATION OF HYDROGEN FROM WATER**

Proefschrift
ter verkrijging van de graad van
doctor in de landbouwwetenschappen,
op gezag van de rector magnificus,
dr. C. C. Oosterlee,
in het openbaar te verdedigen
op woensdag 10 juni 1987
des namiddags te vier uur in de aula
van de Landbouwuniversiteit te Wageningen



ISW 484 861

Who wills,
Can.
Who tries,
Does.
Who loves,
Lives.

Anne McCaffrey
(from "Dragonflight")

STELLINGEN

1. Kolloïdaal rutheniumdioxide is een goed alternatief voor kolloïdaal platina als katalysator van de fotochemische produktie van waterstof.

Dit proefschrift, hoofdstukken 3, 4 en 5

2. Methylviologeën is een verre van ideale elektronenmediator in fotochemische systemen voor watersplitsing.

Dit proefschrift, hoofdstuk 5

3. In "sacrificiële" modelsystemen voor fotochemische watersplitsing wordt geen water gesplitst.

4. Grensstromen voor protonreduktie vanuit gebufferde systemen worden primair bepaald door de bufferkapaciteit en niet door de pH.

Dit proefschrift, hoofdstuk 3

5. Bij de interpretatie van gegevens omtrent ionadsorptie in het grensvlak tussen een gedispergeerde katalysator en een oplossing dient men zich ervan bewust te zijn dat tijdens het katalytisch proces de potentiaal van de katalysator bepaald kan zijn door redoxkoppels.

6. De door Galizzioli et al. gevonden helling van de Tafellijn voor de waterstofvormingsreaktie aan rutheniumdioxide-filmelektroden is eerder een aanwijzing voor het optreden van het Volmer-Tafel mechanisme dan van het Volmer-Heyrovský mechanisme.

D. Galizzioli, F. Tardini en S. Trasatti, J. Appl. Electrochem. 5 (1975) 203-214

7. De door Thibault en Rinaudo gegeven analyse van hun geleidbaarheidsmetingen aan pectine-oplossingen met verschillende tegenionen is onzorgvuldig, omdat de eventuele invloed van de aard van de tegenionen op het molair geleidingsvermogen van het polyion niet is nagegaan.

J. F. Thibault en M. Rinaudo, Biopolymers 24 (1985) 2131-2143

8. Trifunac et al. leggen ten onrechte verband tussen de dielektrische verliezen in een microgolf-trilholte en de "kapaciteit" van die trilholte.

A. D. Trifunac, R. G. Lawler, D. M. Bartels en M. C. Thurnauer, Prog. Reaction Kinetics 14 (1986) 43-156
9. Neeman et al. interpreteren hun ^{13}C -NMR spektra van plantecelprotoplasten van *Nicotiana tabacum* onjuist, omdat ze geen rekening houden met de omzetting van het aangeboden substraat glucose tot fructose en sucrose.

M. Neeman, D. Aviv, H. Degani en E. Galun, Plant. Physiol. 77 (1985) 374-378
10. Bij zelfdiffusiemetingen met behulp van NMR wordt ten onrechte het relaxatiegedrag van vloeistoffen aan wanden verwaarloosd.

J. E. Tanner, J. Chem. Phys. 69 (1978) 1748-1754
G. van Woensel, proefschrift, Katholieke Universiteit Leuven (1985)
11. Het lezen van science fiction verruimt het wereldbeeld.
12. Invoering van een basisinkomen voor iedereen versterkt de bestaande man-vrouw rolpatronen.
13. Omdat er voor een volledige embryonale ontwikkeling zowel paternale als maternale chromosomen nodig zijn, is de suggestie in de feministische literatuur dat kinderen krijgen zonder tussenkomst van een man mogelijk is dankzij de moderne voortplantingstechnieken, onjuist.

J. McGrath en D. Solter, J. Embryol. Exp. Morph. 97 Suppl. (1986) 277-289
J. Zipper, Lover 87/1 (1987) 23-31

Mieke Kleijn

Interfacial electrochemistry of colloidal ruthenium dioxide and catalysis of the photochemical generation of hydrogen from water

Wageningen, 10 juni 1987

Aan mijn ouders

Aan Fred

VOORWOORD

In dit proefschrift zijn de resultaten van een vier jaar durend onderzoeksproject aan de vakgroep Fysische en Kolloïdchemie vastgelegd. Bij het onderzoek zijn vele mensen binnen en buiten de vakgroep betrokken geweest en op deze plaats zou ik hen allen hartelijk willen bedanken.

Een aantal mensen heeft een bijzondere rol vervuld bij de totstandkoming van dit werk, zoals mijn promotor Hans Lyklema. Hoewel zijn drukke werkzaamheden hem vaak elders bezig hielden, vond hij toch steeds tijd om mij met goede raad en kritische opmerkingen verder op weg te helpen.

Mijn co-promotor Herman van Leeuwen ben ik erg dankbaar voor zijn begeleiding bij de elektrode-experimenten. Verder waren de vele discussies met hem en zijn kritisch commentaar op het manuscript voor mij zeer waardevol.

Martien Cohen Stuart was aanvankelijk betrokken bij het project in verband met het idee om het rutheniumdioxide sol te stabiliseren met behulp van polymeren. Ondanks zijn vele originele suggesties bleek dit niet mogelijk en daardoor verviel helaas het plan om systematisch de invloed van polymeeradsorptie op de waterstofproductie te bestuderen.

Veel van de in dit proefschrift beschreven experimenten zijn op een nauwgezette manier uitgevoerd door Erna Rouwendal. Haar grote betrokkenheid bij het onderzoek en haar hulp bij het bedenken van experimenten waren een grote stimulans voor mij.

Eric van Bennekom heeft tijdens zijn stage bijgedragen aan dit onderzoek. Zijn resultaten zijn verwerkt in dit boekje.

Ben Spee, Willem van Maanen, Henny van Beek, Louis Verhagen en Ronald Wegh zorgden voor de "logistieke" en technische ondersteuning. Anneke Hoekstra en Gerrit Buurman hebben de vele figuren in dit boekje op een voortreffelijke manier getekend.

Tenslotte wil ik mijn vriend Fred bedanken voor zijn solidariteit en morele steun. Ook in experimenteel opzicht heeft hij bijgedragen aan dit onderzoek door mij te helpen met ESR experimenten. Het is jammer dat we, wegens het schrijven van proefschriften, geen tijd hadden om deze af te ronden.

Mieke Kleijn
voorjaar 1987

CONTENTS

1. GENERAL INTRODUCTION	
1.1 The conversion and storage of solar energy	1
1.2 Natural photosynthesis	2
1.3 The photochemical splitting of water in heterogeneous systems	4
1.4 Outline of this work	7
1.5 References	9
2. PREPARATION AND CHARACTERIZATION OF RUTHENIUM DIOXIDE SAMPLES	
2.1 Introduction	13
2.2 Materials	16
2.3 Preparation of ruthenium dioxide	16
2.3.1 Preparation	16
2.3.2 Washing procedure	17
2.4 Transmission Electron Microscopy (TEM)	17
2.5 X-ray diffraction	18
2.6 BET gas adsorption	19
2.6.1 Specific surface area	19
2.6.2 Surface porosity	20
2.7 XPS/AES surface analysis	22
2.8 Colloidal stability of RuO ₂ sols	24
2.9 Conclusions	26
2.10 Acknowledgements	26
2.11 References	26
3. DOUBLE LAYER STRUCTURE AND HYDROGEN EVOLUTION REACTION AT THE RuO ₂ /SOLUTION INTERFACE	
3.1 Introduction	29
3.2 Experimental	30
3.2.1 Materials	30
3.2.2 Potentiometric acid-base titrations	30
3.2.3 Electrophoretic mobility measurements	32
3.2.4 Preparation of RuO ₂ film electrodes	32
3.2.5 Voltammetric experiments	32
3.3 Results and discussion	34

3.3.1 The surface charge on RuO_2 in the presence of indifferent electrolyte	34
3.3.2 The surface charge and ionic composition of the double layer in the presence of specifically adsorbing ions	38
3.3.3 Adsorption of Cl^- at the point of zero charge	44
3.3.4 Hydrogen evolution at RuO_2 film electrodes	46
3.4 Conclusions	52
3.5 Acknowledgements	53
3.6 References	53
 4. ADSORPTION OF SENSITIZER, ELECTRON RELAY, AND ELECTRON DONOR AT THE RuO_2 /SOLUTION INTERFACE AND ELECTRON TRANSFER BETWEEN ELECTRON RELAY AND THE RuO_2 CATALYST SURFACE	
4.1 Introduction	57
4.2 Experimental	58
4.2.1 Materials	58
4.2.2 Adsorption experiments	59
4.2.3 Potentiometric acid-base titrations	59
4.2.4 Electrophoretic mobility measurements	60
4.2.5 Voltammetric experiments	60
4.3 Results and discussion	60
4.3.1 Adsorption of $\text{Ru}(\text{bipy})_3^{2+}$	60
4.3.2 Adsorption of EDTA	60
4.3.3 Adsorption of MV^{2+}	62
4.3.4 Electron transfer between methylviologen and RuO_2	70
4.4 Conclusions	72
4.5 Acknowledgements	72
4.6 References	73
 5. PHOTOGENERATION OF HYDROGEN IN THE $\text{Ru}(\text{bipy})_3^{2+}/\text{MV}^{2+}/\text{EDTA}/\text{colloidal RuO}_2$ SYSTEM	
5.1 Introduction	75
5.2 Experimental	77
5.2.1 Materials	77
5.2.2 Irradiation procedure	78
5.2.3 Gas analysis	79

5.2.4 Incident light intensity	79
5.2.5 Measurement of $\text{Ru}(\text{bipy})_3^{2+}$ and methylviologen concentrations	80
5.2.6 In situ measurement of $\text{MV}^{+\bullet}$ concentration	81
5.3 Results	82
5.3.1 Variation of hydrogen production with time	82
5.3.2 Formation and disappearance of $\text{MV}^{+\bullet}$ in the absence of catalyst	83
5.3.3 Influence of light intensity, $\text{Ru}(\text{bipy})_3^{2+}$, and EDTA concentration	84
5.3.4 H_2 pressure and buffer capacity	86
5.3.5 Hydrogen production as a function of RuO_2 amount and methylviologen concentration	86
5.3.6 Influence of stirring rate	89
5.3.7 Temperature dependency	91
5.3.8 Influence of the presence of stabilizing agents	92
5.4 Discussion	92
5.4.1 The induction time	92
5.4.2 Termination of the hydrogen production	93
5.4.3 Limiting factors in hydrogen generation under steady state conditions	95
5.5 Conclusions	100
5.6 Acknowledgements	101
5.7 References	102
6. A KINETIC MODEL FOR THE $\text{Ru}(\text{bipy})_3^{2+}/\text{MV}^{2+}/\text{EDTA}/\text{colloidal RuO}_2$ SYSTEM FOR PHOTOGENERATION OF HYDROGEN	
6.1 Introduction	105
6.2 The model	106
6.2.1 Flux equation for the homogeneous reactions	106
6.2.2 The rate of the excitation reaction	109
6.2.3 Flux equations for the heterogeneous reactions	110
6.2.4 Overall picture	112
6.3 Results and discussion	115
6.3.1 The rate of the unidentified side-reaction of $\text{MV}^{+\bullet}$	115
6.3.2 Effects of the model parameters ϕ_g , b , and m	116
6.3.3 Parameter ranges	118

6.3.4 Simulation of the steady state as a function of RuO ₂ amount	119
6.3.5 Steady state simulations as a function of light intensity and composition of the reaction solution	122
6.3.6 Time-evolution of the MV ⁺ concentration upon illumination	126
6.4 Conclusions	128
6.5 References	129
7. SUMMARY, CONCLUSIONS, AND PERSPECTIVES	131
SAMENVATTING	136
CURRICULUM VITAE	141

CHAPTER 1

GENERAL INTRODUCTION

1.1 THE CONVERSION AND STORAGE OF SOLAR ENERGY

The conversion of solar energy into electrical and chemical energy might be an important option to meet the world's future needs. The earth receives at its surface about 3×10^{24} J per year [1], which is roughly 10,000 times the current annual energy demand. However, the low power density of the sun's radiation ($100\text{--}300 \text{ W/m}^2$) and the necessity to convert and store the solar energy in a readily available form have always stood in the way of large-scale utilization.

The energy crisis of the seventies, which led to a substantial increase of the costs of fossil fuels, resulted in extensive programs for research and development of alternative energy sources. The possibilities to use solar energy were re-examined.

The subject of the present thesis is motivated by solar energy conversion problems and therefore, some of the current systems and methods will be briefly reviewed. For further information, we will refer to more comprehensive reviews and major papers.

Solar energy conversion systems can be roughly divided in three categories:

- Photovoltaic solar cells, which convert incident light into electricity. The devices are all-solid. The absorption of photons by a semiconducting material leads to excitation of electrons from the valence band to the conduction band; the positive hole left behind in the valence band and the electron in the conduction band are then free to move through the semiconductor and the external circuit until they recombine [2,3].
- Photochemical and photoelectrochemical systems: absorption of photons by dye molecules or semiconductors (dispersed or as electrodes) in solution, leads to useful chemical and electrochemical reactions. In this way, fuels or other (bio)chemical compounds and/or electricity can be produced [4-13].

- Thermal systems: (concentrated) sunlight generates high temperatures, which can be used for heating or to drive chemical reactions [13,14].

The development of photovoltaic solar cells has progressed so well that they are commercially available for several years already. Especially the amorphous silicon cells are well-known.

In contrast to solar heating and photovoltaic cells, research into the photochemical conversion and storage of solar energy is largely at the basic stage. Nevertheless, there is certainly potential for important advances, and the solution of some of the fundamental problems involved will have implications for a much broader range of applications than just solar energy conversion. (For example, for heterogeneous catalysis processes in general, and for the selective synthesis of fine chemicals.)

Within the area of photochemical solar energy conversion, considerable attention has been paid to the production of hydrogen and oxygen from water in heterogeneous photosystems (suspensions of catalyst particles or semiconductor powders). Harriman [10,11,15] has described the main developments in this field during the last 15 years. We will return to this subject in section 1.3.

As a fuel, hydrogen is cleaner and more efficient than fossil fuels. The necessity to store hydrogen at very low temperature or under high pressure makes its application less convenient, but alternative ways to store it are being developed (e.g. storage of hydrogen as a metal hydride [16-18]). Hydrogen is also needed in the production of ammonia, fertilizers, fats and oils, and in the refining of fossil fuels [19,20].

1.2 NATURAL PHOTOSYNTHESIS

Storing solar energy as a chemical fuel, derived from readily available compounds like water, is a well-established phenomenon and green plants, algae, and some types of bacteria have done so for about a billion of years.

In the photosynthetic process of green plants and algae, water is decomposed into oxygen and reduction equivalents, the latter being used for production of carbohydrates (e.g. glucose):



In attempts to construct solar energy devices for water-dissociation, it is useful to look towards the mechanism of photosynthesis [21-25].

Figure 1.1 shows a schematic view of the thylakoid membrane of a plant chloroplast. The reaction center proteins I and II span the membrane. Each reaction center contains an electron donor (chlorophyll a, P680 and P700; P denotes "primary electron donor") and electron acceptors (Q_1 , a plastoquinone, in photosystem II; A_1-A_2 , a complex containing chlorophyll a and a Fe-S center, in photosystem I). Light is absorbed by an antenna system of pigments, mostly chlorophylls, which transfer the excitation energy to P680 or P700, followed by a highly efficient charge separation process within the reaction centers. The latter process provides the oxidative power for the splitting of water at the donor side of the reaction center. The primary photochemical reactions within the reaction centers result in vectorial electron transfer to the electron acceptors, yielding an electrical potential across the membrane [23]. This potential is used to drive biochemical reactions. At the acceptor side of photosystem I reduction of NADP occurs. Reduced NADP is a prerequisite for the conversion of CO_2 into carbohydrates.

Not only H_2O is used as the source of electrons in natural photosynthesis; photosynthetic bacteria use more strongly reduced compounds, e.g. H_2S or succinate.

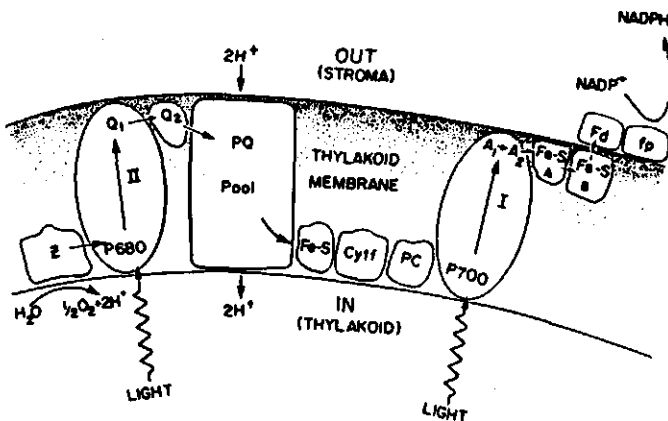


FIGURE 1.1: Schematic cross section of the thylakoid membrane showing the various components involved in electron transport from H_2O to $NADP^+$. (Taken from reference [13]).

1.3 THE PHOTOCHEMICAL SPLITTING OF WATER IN HETEROGENEOUS SYSTEMS

From the natural photosynthesis process, it becomes clear that generally the following components are necessary for the photochemical decomposition of water into oxygen and hydrogen (the latter instead of reduction equivalents in the biological system): 1) a light absorbing compound, 2) a charge-separating device acting as an electron pump, 3) two catalysts, one for oxygen production and one for hydrogen production.

Production of hydrogen from water in a photochemical system was first achieved by Shilov et al. [26] and Lehn and Sauvage [27]. Hydrogen formation occurred at the expense of some added electron donor. The work of Shilov and Lehn and Sauvage generated world-wide interest, and since then many studies of modified and improved versions of the system have been published [28-50]. The basic concept is to use a finely dispersed catalyst as the medium to couple one-electron reactions in solution with the two-electron process of hydrogen formation. The following steps lead to hydrogen evolution (figure 1.2):

- light excitation of a photosensitive compound, the **sensitizer S**
- quenching of the excited electron of S^* by an electron-transfer compound, the **electron relay R** (charge separation)
- electron transfer from R^- to H^+ via the catalyst
- formation of H_2 at the catalyst surface and subsequent desorption
- scavenging of the oxidized sensitizer S^+ by the **sacrificial electron donor D**
- irreversible decomposition of the oxidation product D^+ .

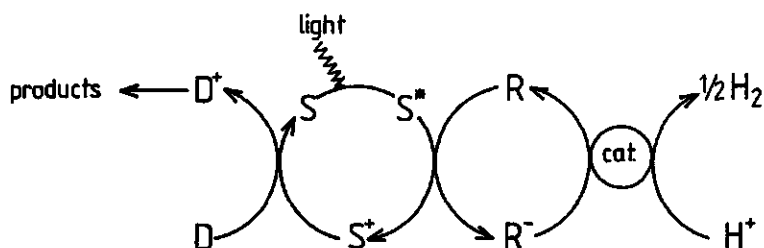


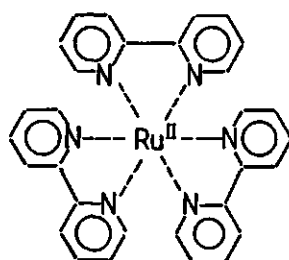
FIGURE 1.2: Scheme for sacrificial photoproduction of hydrogen.

An overview of various substances used in these so-called "sacrificial systems" as sensitizer, electron relay, electron donor, and catalyst can be found in reference [51].

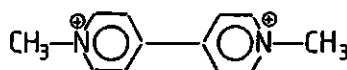
Among the possible photosensitizers, the ruthenium trisbipyridyl complex ($\text{Ru}(\text{bipy})_3^{2+}$; figure 1.3a) has aroused the most interest. This complex is very stable in aqueous solution, does not undergo ligand photodissociation, and shows a large molar absorptivity in the visible region of the solar spectrum ($\lambda_{\text{max}} \approx 452 \text{ nm}$). The life time of the excited state is relatively long ($0.6 \mu\text{s}$ [29,33]) and allows participation in redox reactions, in which it can act either as a reductor or as an oxidator (standard redox potentials: $E^0(\text{Ru}(\text{bipy})_3^{3+}/\text{Ru}(\text{bipy})_3^{2+*}) = -0.86 \text{ V/NHE}$, $E^0(\text{Ru}(\text{bipy})_3^{2+*}/\text{Ru}(\text{bipy})_3^{+}) = 0.84 \text{ V/NHE}$ [52,53]).

The most commonly used and one of the most efficient electron relays is methylviologen (MV^{2+} ; figure 1.3b), also known under the name paraquat if used as a herbicide. The ease of reduction of MV^{2+} ($E^0(\text{MV}^{2+}/\text{MV}^{+*}) = -0.45 \text{ V/NHE}$ [54]), the stability of the MV^{+*} radical, and the strong absorption of light in the visible spectrum range by MV^{+*} , make methylviologen a convenient candidate for fundamental studies.

Popular electron donors are EDTA (ethylenediaminetetraacetic acid) and TEOA (triethanolamine), which are rapidly decomposed when oxidized. In most systems for sacrificial hydrogen production, Pt is used as the catalyst.



ruthenium trisbipyridyl
(a)



methylviologen
(b)

FIGURE 1.3: The most commonly used photosensitizer (a) and electron relay (b) in systems for photogeneration of hydrogen.

In the general scheme of figure 1.2, the first steps can be replaced by direct excitation of electrons in suspended semiconductor materials [55,56]. The catalyst for hydrogen production, e.g. Pt, can be dispersed on the semiconductor surface. For excitation of electrons from the valence band into the conduction band, photons with an appropriate energy are required and only a narrow band of the solar spectrum is effective. Moreover, the radiation required is generally in the UV range (for semiconductors with a band gap of ca. 3 eV, like TiO_2 , WO_3 , and SrTiO_3), although some less photostable semiconductor materials have a small band gap and absorb visible light (e.g. CdS , $\alpha\text{-Fe}_2\text{O}_3$, and GaAs). Use of a sensitizer which injects electrons into the conduction band of the semiconductor, can enlarge the coverage of the solar spectrum [55,57]. The study of semiconductor suspensions is at the moment by far the most popular area of solar photochemistry [10,11].

For the sacrificial production of oxygen from water, also numerous photochemical systems have been proposed [58-66]. Here, the evolved gas is produced at the expense of a sacrificial electron acceptor, e.g. $\text{S}_2\text{O}_8^{2-}$ or Ce^{4+} ions.

The main limitation of sacrificial systems is, of course, the consumption of the sacrificial compounds. However, besides their scientific value, these systems might be of practical interest for the destruction of waste materials, which can function as electron donor (e.g. S^{2-} ions [67]) or as electron acceptor. In this respect, we are close to mimicking bacterial photosynthesis.

If, in the general scheme given in figure 1.2, the sacrificial electron donor D is replaced by a catalyst which can oxidize water under reduction of S^+ , then in theory one would obtain a "cyclic system" for complete water dissociation. However, in practice substantial problems are encountered: recombination of intermediate photoproducts should be prevented, the catalysts must be selective for H_2 and O_2 production, respectively, and the products must be separated.

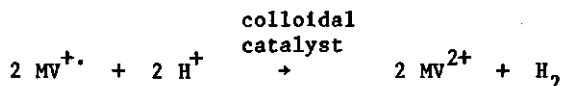
In natural photosynthesis, the abovementioned problems are bypassed through a high degree of organization and compartmentalization in protein matrices and phospho-lipid membranes [23,68]. Especially the well-defined architecture of the protein matrix, recently unraveled by Delsenhofer et al. [69], is not easily mimicked. However, the need for compartmentalization in artificial systems has been recognized for some time [68,70,71];

micelles, micro-emulsions, monolayers, bilayers, organized multilayers, polymers, vesicles, and colloidal semiconductors have been used to that end [55,57,68,72,73].

All photochemical systems developed to decompose water into H_2 , O_2 , or both still suffer from short life times and low efficiencies [10,21,74]. After the first rapid developments and optimism about their economical impact, no breakthrough has come yet to construct a practical solar energy storage device based on artificial photosynthesis, although there have been many spin-off results and fundamental advances in the basis sciences [68]. It is still a long way before the photolysis of water provides a realistic alternative energy source.

1.4 OUTLINE OF THIS WORK

With methylviologen as the electron relay, the central process in the photoproduction of hydrogen is



and any factor affecting this overall reaction is of wide interest. The objective of the present work is to gain insight into this heterogeneous process. Especially the colloid-chemical and electrochemical properties of the catalyst, the interactions between electron relay and catalyst surface, and their role in the mechanism of hydrogen formation have been the subject of our investigations.

From the various systems for sacrificial photoproduction of hydrogen, the one first described by Amouyal et al. [28] was chosen to study the abovementioned overall reaction. Besides MV^{2+} as the electron relay, this system consists of $\text{Ru}(\text{bipy})_3^{2+}$ as the sensitizer, EDTA as the electron donor, and colloidal Pt as the catalyst. This system is now well-characterized with respect to the homogeneous reactions. It is generally used as a reference for testing new sensitizers, electron relays, electron donors and catalysts [51].

A serious disadvantage of Pt and MV^{2+} containing systems is the destruction of the electron relay during the hydrogen evolution process; Pt catalyzes the irreversible hydrogenation of methylviologen [33,36,51,54]. Colloidal

ruthenium dioxide, often used to catalyze the photo-oxidation of water [58,59,61], can also be used for the water reduction reaction [32,37,41]. RuO_2 is more specific than Pt, in the sense that it does not catalyze the hydrogenation of methylviologen [37]. Therefore, RuO_2 was chosen as the "model" catalyst compound in the present study.

Colloidal RuO_2 was prepared by thermal decomposition of RuCl_3 and characterized by various techniques, with emphasis on its surface properties. The colloidal stability and the effects of stabilizing agents are briefly discussed (chapter 2).

Chapter 3 is concerned with the basic interfacial and electrochemical properties of colloidal RuO_2 . The electric double layer properties have been studied by potentiometric acid-base titrations in combination with electrophoretic mobility measurements. On this basis it will be demonstrated how quantitative data on specific adsorption can be obtained by a thermodynamic analysis of the ionic composition of the electric double layer. The specific adsorption of Cl^- on RuO_2 is taken as an example. To gain insight into the electrocatalytic properties of RuO_2 , RuO_2 film electrodes have been prepared and their basic characteristics have been studied by means of voltammetric experiments.

In chapter 4 the adsorption of the different components of the hydrogen production system at the surface of the catalyst RuO_2 is investigated. Special attention will be paid to the interaction between methylviologen and the RuO_2 surface.

Experiments concerning the complete hydrogen evolution system are described and discussed in chapter 5. The influence of the composition of the reaction mixture and other experimental conditions (e.g. light intensity and temperature) on the hydrogen production rate will be evaluated.

In chapter 6 a quantitative model for the water reduction system is presented, based on flux equations for the formation and consumption of MV^+ in the solution and at the surface of the catalyst. The model is tested by using the experimental results of chapter 5.

Finally, in chapter 7 the conclusions of this work are summarized and problems deserving further attention are indicated.

1.5 REFERENCES

1. P. Böger, *Biotechnol.*, Vortr. Hauptversamml. MNU 74th, Metzlersche Verlagsbuchhandlung, Stuttgart (1983) pp 101-108
2. S. Wagner, in "Photochemical Conversions", Symp. June 15-17, 1983, Lausanne, A. M. Braun (ed.), Press. Polytech. Romandes Lausanne (1983) pp 235-268
3. A. L. Fahrenburch, and R. H. Bube, in "Fundamentals of Solar Cells", Academic Press, New York (1983)
4. J. S. Connolly, and J. A. Turner, in "Photochemical Conversions", Symp. June 15-17, 1983, A. M. Braun (ed.), Press. Polytech. Romandes Lausanne (1983) pp 73-131
5. L. P. Bicelli, *Surf. Technol.* **20** (1983) 357-381
6. A. J. Bard, *J. Electroanal. Chem.* **168** (1984) 5-20
7. "Photochemical Conversion and Storage of Solar Energy", Part A and B, J. Rabani (ed.), Weizmann Science Press, Jerusalem (1982)
8. C. Kutal, *J. Chem. Educ.* **60** (1983) 882-887
9. K. Kalyansundaram, and M. Grätzel, *Photochem. Photobiol.* **40** (1984) 807-821
10. A. Harriman, *Photochem.* **16** (1985) 539-552
11. A. Harriman, *Photochem.* **17** (1986) 601-631
12. D. H. M. W. Thewissen, A. H. A. Tinnemans, C. W. de Kreuk, and A. Mackor, *Chem. Mag.* (1984) 472-473
13. J. R. Bolton, and M. D. Archer, in "Intersol 85", Proc. 9th Bienn. Congr. Int. Sol. Energy Soc., E. Bilgen, and K. G. T. Hollands (eds.), Pergamon, New York (1986) pp 1843-1859
14. W. Luft, *Int. J. Sol. Energy* **3** (1984) 25-40
15. A. Harriman, *J. Photochem.* **25** (1984) 33-36
16. H. Wenzl, *Metall* **34** (1980) 407-412, 647-653
17. M. S. Bawa, and R. R. Chang, *J. Sol. Energy Eng.* **107** (1985) 355-357
18. B. Luxenburger, *Brennst.-Wärme-Kraft* **37** (1985) 322-327
19. J. O'M. Bockris, B. Dandapani, D. Cocke, and J. Choroghchian, *Int. J. Hydrogen Energy* **10** (1985) 179-201
20. W. Balthasar, *Int. J. Hydrogen Energy* **9** (1984) 659-668
21. C. Laane, *PT/Procestechneik* **38** (1983) 27-32
22. G. Porter, *Proc. R. Inst. G. B.* **55** (1983) 133-147
23. P. Mathis, *Photosynth. Res.* **8** (1986) 97-111

24. O. Hirayama, K. Uya, J. Hiramatsu, H. Yamada, and K. Moriwaki, *Agric. Biol. Chem.* **50** (1986) 891-897
25. F. G. H. Van Wijk, Ph. D. Thesis, Wageningen Agricultural University (1987)
26. A. E. Shilov, B. V. Korayin, and T. S. Dzhabier, *Dokl. Akad. Nauk.* **233** (1977) 620-625
27. J. M. Lehn, and J. P. Sauvage, *Nouv. J. Chim.* **1** (1977) 449-455
28. A. Moradpour, E. Amouyal, P. Keller, and H. B. Kagan, *Nouv. J. Chim.* **2** (1978) 547-549
29. K. Kalyansundaram, J. Kiwi, and M. Grätzel, *Helv. Chim. Acta* **61** (1978) 2720-2730
30. M. W. W. Adams, K. K. Rao, and D. O. Hall, *Photobiochem. Photobiophys.* **1** (1979) 33-38
31. G. M. Brown, B. S. Brunschwig, C. Creutz, J. F. Endicott, and N. Sutin, *J. Am. Chem. Soc.* **101** (1979) 1298-1303
32. E. Amouyal, P. Keller, and A. Moradpour, *J. Chem. Soc., Chem. Commun.* (1980) 1019-1020
33. P. Keller, A. Moradpour, E. Amouyal, and H. Kagan, *Nouv. J. Chim.* **4** (1980) 377-384
34. P. A. Brugger, P. Cuendet, and M. Grätzel, *J. Am. Chem. Soc.* **103** (1981) 2923-2927
35. A. Harriman, and G. Porter, *J. Chem. Soc., Faraday Trans. 2* **77** (1981) 833-844
36. O. Johansen, A. Launikonis, J. W. Loder, A. W.-H. Mau, W. H. F. Sasse, J. D. Swift, and D. Wells, *Aust. J. Chem.* **34** (1981) 981-991
37. P. Keller, A. Moradpour, and E. Amouyal, *J. Chem. Soc., Faraday Trans. 1* **78** (1982) 3331-3340
38. H. Dürr, G. Dürr, K. Zengerle, B. Reis, and A. M. Braun, *Chimia* **37** (1983) 245-248
39. Z. C. Bi, and H. T. Tien, *Int. J. Hydrogen energy* **9** (1984) 717-722
40. K. Hashimoto, T. Kawai, and T. Sakata, *Nouv. J. Chim.* **8** (1984) 693-700
41. E. Amouyal, and P. Koffi, *J. Photochem.* **29** (1985) 227-242
42. F. Bergaya, D. Challal, J. J. Fripiat, and H. Van Damme, *Nouv. J. Chim.* **9** (1985) 721-724
43. R. C. Bhardwaj, C. M. Jadhav, and M. M. T. Khan, *Res. Ind.* **30** (1985) 6-8
44. J. L. Bourdelande, J. Camps, J. Font, P. De March, and E. Brillas, *J.*

- Photochem. **30** (1985) 437-444
45. D. N. Furlong, D. Wells, and W. H. F. Sasse, *J. Phys. Chem.* **89** (1985) 1922-1928
 46. V. E. Maier, and V. Yu. Shafirovich, *J. Chem. Soc., Chem. Commun.* (1985) 1063-1065
 47. A. W.-H. Mau, O. Johansen, and W. H. F. Sasse, *Photochem. Photobiol.* **41** (1985) 503-509
 48. I. Okura, T. Kita, S. Aono, and N. Kaji, *J. Mol. Catal.* **33** (1985) 341-343
 49. R. Simarro, S. Cervera-March, and S. Esplugas, *Int. J. Hydrogen Energy* **10** (1985) 221-226
 50. I. Okura, *Biochim.* **68** (1986) 189-199
 51. E. Amouyal, *Sci. Pap. Inst. Phys. Chem. Res.* **78** (1984) 220-231
 52. L. J. Fitzpatrick, H. A. Goodwin, A. Launikonis, A. W.-H. Mau, and W. H. F. Sasse, *Aust. J. Chem.* **36** (1983) 2169-2173
 53. V. Balzani, and F. Boletta, *Comments Inorg. Chem.* **2** (1983) 211-226
 54. A. Harriman, and G. Porter, *J. Chem. Soc., Faraday Trans. 2* **78** (1982) 1937-1943
 55. M. Grätzel, *Mod. Aspects Electrochem.* **15** (1983) 83-165
 56. M. Grätzel, *NATO Adv. Sci. Inst., Ser. C*, vol **146**, no Photoelectrochem., Photocatal., Photoreact. (1985) 217-238
 57. E. Borgarello, J. Kiwi, E. Pelizzetti, M. Visca, and M. Grätzel, *J. Am. Chem. Soc.* **103** (1981) 6324-6329
 58. J. Kiwi, and M. Grätzel, *Chimia* **33** (1979) 289-291
 59. J. M. Lehn, J. P. Sauvage, and R. Ziessel, *Nouv. J. Chim.* **4** (1980) 355-358
 60. V. Yu. Shafirovich, N. K. Khannanv, and V. V. Strelets, *Nouv. J. Chim.* **4** (1980) 81-86
 61. G. Blondeel, A. Harriman, G. Porter, D. Urwin, and J. Kiwi, *J. Phys. Chem.* **87** (1983) 2629-2636
 62. E. Borgarello, and E. Pelizzetti, *Inorg. Chim. Acta* **91** (1984) 295-300
 63. J. Desilvestro, D. Duonghong, J. M. Kleijn, and M. Grätzel, *Chimia* **39** (1985) 102-103
 64. P. A. Christensen, W. Erbs, and A. Harriman, *J. Chem. Soc., Faraday Trans. 2* **81** (1985) 575-580
 65. K. Tanaka, S. Murata, and K. Harada, *Sol. Energy* **34** (1985) 303-308
 66. R. Ramaraj, A. Kira, and M. Kaneko, *Angew. Chem.* **98** (1986) 824-825

67. D. H. M. W. Thewissen, A. H. A. Tinnemans, M. Eeuwhorst-Reinten, K. Timmer, and A. Mackor, *Nouv. J. Chim.* **7** (1983) 191-194
68. J. H. Fendler, *J. Phys. Chem.* **89** (1985) 2730-2740
69. J. Deisenhofer, O. Epp, K. Miki, R. Huber, and H. Michel, *J. Mol. Biol.* **180** (1984) 385-398
70. G. Porter, M. D. Archer, *Interdisp. Sci. Rev.* **1** (1976) 119-143
71. M. Calvin, *Acc. Chem. Res.* **11** (1978) 369-374
72. M. Kaneko, N. Takabayashi, Y. Yamanuchi, and A. Yamada, *Bull. Chem. Soc. Jpn.* **57** (1984) 156-161
73. M. Calvin, *Can. J. Chem.* **61** (1983) 873-880
74. T. W. Ebbesen, B. L. Tembe, and J. J. Kozak, *J. Phys. Chem.* **88** (1984) 683-688

PREPARATION AND CHARACTERIZATION OF RUTHENIUM DIOXIDE SAMPLES

2.1 INTRODUCTION

Ruthenium dioxide (RuO_2), an in water insoluble solid, is the most stable oxide of ruthenium and it decomposes in $\text{Ru} + \text{O}_2$ only at high temperatures (above 1000°C , [1]). It crystallizes in the rutile structure, like many other metal dioxides, e.g. TiO_2 (rutile), VO_2 , CrO_2 , IrO_2 , PtO_2 , SnO_2 and SiO_2 [2]. Its crystal structure is given in figure 2.1. Single crystals of RuO_2 have a rod-like morphology and are shiny dark blue [1].

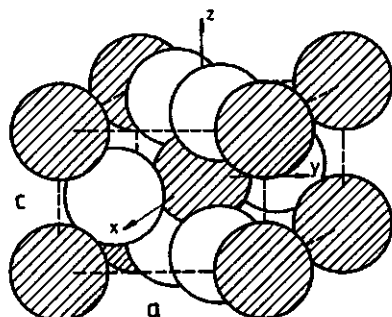


FIGURE 2.1: Unit cell of ruthenium dioxide (two elemental formulas RuO_2). From ref. [2].

● ruthenium atoms; ○ oxygen atoms.

The rutile-type crystal has a tetragonal symmetry; the metal atoms are positioned in the corners and the centre of the unit cell. Each metal atom is surrounded by six O atoms. Lattice constants at room temperature: $a = 0.449 \text{ nm}$, $c = 0.311 \text{ nm}$ [1-4].

Among the oxides of transition metals, RuO_2 , together with a few other oxides (e.g. IrO_2 , TlO), holds a particular position, because it exhibits a metallic conductivity [1,2,5]. An overview of some of its physical and chemical properties is given in table 2.1.

TABLE 2.1: Physical and chemical properties of RuO₂.

property		references
mol. weight	133.07 g/mole	[6]
specific density	6.97 g/cm ³	[6]
crystalline form	rutile-type, tetragonal, d. blue	[1,2,4,6]
coord. number of Ru	6	
lattice constants	a = 0.4491 nm, b = 0.3650 nm, c = 0.3106 nm	
electron configuration	Ru(4d ⁴)	[2]
solubility	insoluble in hot and cold water, acid; soluble in fused alkali	[6]
electr. conductivity	metallic	[1,2,5]
single crystals	2-3 × 10 ⁴ Ω ⁻¹ cm ⁻¹ (comp. Cu: 5.9 × 10 ⁵ Ω ⁻¹ cm ⁻¹ Ru: 1.4 × 10 ⁵ Ω ⁻¹ cm ⁻¹)	[1,2]
pressed powders	10 ⁻⁵ Ω ⁻¹ cm ⁻¹	[1]
films on electrodes	10 ² -10 ⁴ Ω ⁻¹ cm ⁻¹	[2,7]
enthalpy of formation	-ΔH ⁰ = 298-307 kJ/mole	[1,2]
decomposition reaction	RuO ₂ ⇌ Ru + O ₂ (eq. pO ₂ is 1 atm at 1580 °C)	[1]

RuO₂ is of considerable interest for the electrochemical industry as a corrosion resistant material for anodic evolution of chlorine and oxygen, due to its low overpotential for both processes [8]. Since the early seventies, the carbon electrodes traditionally used in chlorine industry are increasingly replaced by titanium anodes coated with RuO₂ + TiO₂ mixed oxide layers [9]. Nowadays 80 % of the world chlorine production is based on these new electrode materials [10]. Several comprehensive review articles concerning electrocatalytic and structural properties of RuO₂ based electrodes have been published [2,8,11].

RuO₂ also finds a wide applicability as a chemically stable material for making resistors and interconnections in integrated circuits [12,13].

Renewed interest in RuO₂ has been stimulated by studies of water decomposition processes to store solar energy (see chapter 1). Colloidal RuO₂, often dispersed on the surface of n-type semiconductor particles, is now generally used for catalytic oxygen generation from water in sacrifi-

cial or cyclic model systems [14-16]. Amouyal et al. [17,18] were the first to report that colloidal RuO_2 is also an effective redox catalyst for the photogeneration of hydrogen from water. The reductive catalytic properties of RuO_2 have also been recognized elsewhere in electrochemistry [19].

There are several procedures to prepare the compound which is usually referred to as ruthenium dioxide [2,20]. It can be prepared as large single crystals, as a powder, or as a layer on a support. Single crystals can be obtained by chemical vapor transport [1]. In this procedure, RuO_2 is transported in the vapor phase by oxygen at high temperature and deposited at lower temperature. This is the only known method to give the pure stoichiometric compound.

The RuO_2 to be used in this work as a catalyst for photo-induced hydrogen production, had to meet the following criteria: a large specific surface area (colloidal size particles) and a well-defined solid phase and surface. One of the methods to obtain colloidal RuO_2 is chemical precipitation from solution [21]. However, the resulting material is an hydrous oxide with large deviations from stoichiometry. The method of preparation chosen here is the thermal decomposition route as described by Ardizzone et al. [22]. RuCl_3 is decomposed at elevated temperatures under oxygen, giving an oxide powder with an overall composition of $\text{RuO}_x\text{Cl}_y\text{H}_z$ [7,23]. As the temperature of preparation is raised, the oxide particles grow better, a fact which manifests itself in a decrease in specific surface area and an increase in stoichiometry and crystallinity [2,7,22]. Therefore, by varying the temperature of preparation, a compromise can be found with respect to a large catalytic active surface area on the one hand, and a sufficient degree of crystallinity and surface cleanliness on the other.

The procedure of preparation and specific thermal treatment also affect the surface properties and catalytic properties. For example, the point of zero charge of colloidal RuO_2 depends significantly on the preparation temperature [20,22,24]. The catalytic activities of RuO_2 powders for O_2 evolution and their corrosion stabilities improve if they are heated at moderate temperatures (ca. 150 °C); the catalytic activities decline if higher temperatures are applied [25,26]. The effects of preparation procedure and thermal treatment on the reductive catalytic properties of RuO_2 are not clear.

2.2 MATERIALS

All chemicals used were analytical reagent grade. Solutions were prepared with water that was purified by reverse osmosis and subsequently passed through a millipore Super-Q system (conductivity $< 0.8 \mu\text{S/cm}$).

Oxygen gas used in the preparation of RuO_2 was of technical quality ($> 99.5 \text{ vol\% O}_2$, $< 0.35 \text{ vol\% Ar}$, $< 0.15 \text{ vol\% H}_2\text{O}$) and used without further purification.

2.3 PREPARATION OF RUTHENIUM DIOXIDE

2.3.1 Preparation

RuO_2 was prepared in small batches, from 1-5 g RuCl_3 as the starting material. RuCl_3 , a brown, strongly hygroscopic powder, was dried in an oven at $90\text{--}100^\circ\text{C}$ for 1-2 hours, and subsequently crushed and milled in an agate mortar. Oxidation (upon thermal decomposition) to RuO_2 was carried out during 6 hours in a quartz crucible in a small furnace, at the selected temperature and under an oxygen stream of ca. 20 l/hr. Temperatures applied are 700°C (the actual temperature in the furnace varied during preparation from 700 to 715°C), 600°C ($600\text{--}615^\circ\text{C}$), 300°C ($307\text{--}314^\circ\text{C}$), and 400°C ($405\text{--}420^\circ\text{C}$), respectively. After cooling down, the material was crushed and milled again, and the oxidation treatment was repeated for another 6 hours at the same temperature. This procedure was followed because the material tends to form small aggregates, in the interior of which some undecomposed RuCl_3 might be present [22].

The total weight of the samples was measured before and after the heat treatments. During the first treatment 0.64-0.67 g of material was formed from 1 g of RuCl_3 ($M_{\text{RuO}_2}/M_{\text{RuCl}_3} = 0.642$). The total loss of weight during the second treatment was always less than 1 %. The RuO_2 powder formed has a blue color, which is darker as the applied decomposition temperature is lower.

For simplicity, the RuO_2 samples will henceforth be designated as $\text{RuO}_2(700)$, $\text{RuO}_2(600)$ etc., where the number in brackets denotes the preparation temperature.

2.3.2 Washing procedure

Freshly prepared RuO_2 powder was dispersed in water by ultrasonic vibration. After settling of the RuO_2 particles, the supernatant was removed and examined with respect to pH, conductivity, and Cl^- content. The presence of Cl^- was detected potentiometrically using an Ag/AgCl electrode. This first portion of supernatant generally had a low pH value (2-3). Clean water was added to the RuO_2 powder, and it was dispersed again ultrasonically.

The washing procedure was repeated at high, low, and neutral pH values (KOH and HNO_3 were used to adjust the pH, and in some cases KNO_3 was added to promote the settling of the particles) until no Cl^- could be detected anymore and the conductivity of the supernatant was less than $2 \mu\text{S}/\text{cm}$. The RuO_2 was dried at 80°C and stored in an exsiccator.

2.4 TRANSMISSION ELECTRON MICROSCOPY (TEM)

Electron microscopy analysis was carried out using formvar-coated 200 MESH copper grids, covered with evaporated carbon to avoid charging and to stabilize the membrane. Droplets of freshly prepared RuO_2 suspensions, adjusted to pH 3 and ultrasonically vibrated to promote dispersion, were brought onto the grids and the particles were allowed to settle for some minutes. The excess solution was soaked off and the grids were dried at room temperature before being examined in a Philips T400 electron microscope.

In all samples examined a considerable degree of aggregation was observed, despite the sonification. Samples of $\text{RuO}_2(700)$ and $\text{RuO}_2(600)$ show angular particles of irregular shape (figure 2.2a). The sizes of the particles range from 0.1 to $10 \mu\text{m}$. The particles of $\text{RuO}_2(300)$ are much smaller; the sizes of most of them range from several nm to tens of nm. Their shapes are not well-defined. Larger particles appeared to be lumps of small particles. Samples of $\text{RuO}_2(400)$ show particles of a more or less rectangular shape (figure 2.2b), with sides commonly between 5 and 50 nm (average size $25 \times 15 \text{ nm}$, calculated from 30 well distinguishable particles). The crystallinity of individual particles was investigated by electron microdiffraction. These particles appeared to be monocrystalline.

Neither addition of polymers (PMA , PVA , dextran; see table 2.2) to

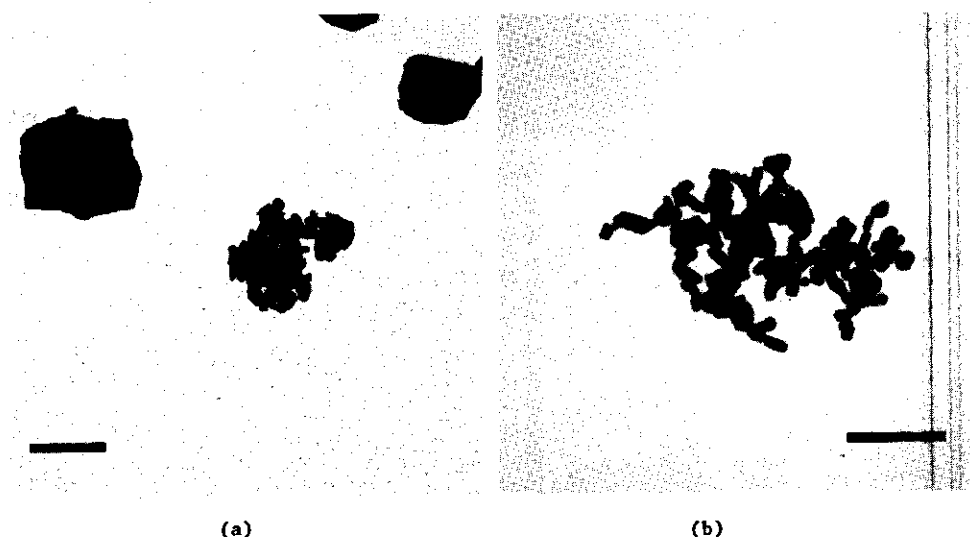


FIGURE 2.2: TEM micrographs of RuO_2 particles. a) preparation temperature ca. 700 °C, the bar refers to 2 μm ; b) preparation temperature ca. 400 °C, the bar refers to 100 nm.

$\text{RuO}_2(400)$ dispersions, nor covering the grids with polymers (gelatine, poly-L-lysine) prior to deposition of the dispersions, nor varying the pH of the dispersions, did affect the general picture of aggregation.

In order to find out if the size of the RuO_2 particles changes when kept in solution, TEM micrographs were made of $\text{RuO}_2(400)$ dispersions, after storage times of several days up to several weeks at different pH values. No changes in size or morphology were observed at low or neutral pH, but at pH values higher than 8, the boundaries of the particles become more vague and edges are rounded.

2.5 X-RAY DIFFRACTION

X-ray diffraction diagrams were obtained with a Guinier camera (Enraf Nonius FR 552) using cobalt $K_{\alpha 1}$ radiation ($\lambda = 0.178890$ nm).

RuO_2 samples prepared at 700 and 600 °C give sharp diffraction lines, exactly positioned at the literature lattice spacing values of RuO_2 [27]. In the diagrams of $\text{RuO}_2(300)$ and $\text{RuO}_2(400)$ samples, some line broadening is

observed, but the positions of the lines are not changed. This line broadening can be due to the small size of the crystallites [28], and may, to some extent, also be attributed to local disorder.

Pizzini et al. [7] have reported X-ray diffraction results on thick, polycrystalline RuO_2 films, obtained by thermal decomposition of RuCl_3 on metallic and oxidic substrates. A shift of the diffraction lines with respect to those for pure RuO_2 was found, which increased as the preparation temperature was lowered. This observation was attributed to incorporation of Cl in the crystal lattice, changing the dimensions of the unit cell. Chemical analysis revealed a Cl content of 4.77 and 3.85 wt% for layers obtained at 300 and 400 °C, respectively. Since in the present study no shift in the X-ray line positions could be observed, it is concluded that our RuO_2 samples are more stoichiometric than the RuO_2 films of reference [7].

2.6 BET GAS ADSORPTION

The specific surface area and surface porosity of $\text{RuO}_2(400)$ samples were investigated by BET (Brunauer-Emmet-Teller) N_2 adsorption and desorption in a Carlo Erba Sorptomatic 1800 apparatus. Before outgassing at 100 °C, the samples were dried at 80-100 °C.

2.6.1 Specific surface area

The BET surface areas (S_{BET}) of $\text{RuO}_2(400)$ samples vary from batch to batch, probably because it is not possible to create exactly identical preparation conditions with respect to temperature and oxygen stream. The values found for S_{BET} range from 21.5 to 28.3 m^2/g . Within each batch the reproducibility of the adsorption isotherms and S_{BET} was satisfactory: the values of S_{BET} from duplicate measurements differ 1-2 m^2/g . No ageing phenomena have been observed for dry nor wet stored samples.

From the BET surface area an equivalent radius for spherical particles can be calculated. Using $S_{\text{BET}} = 3/\rho r$, where r is the particle radius and ρ the specific density of the solid, the equivalent particle radius obtained varies from 15 to 20 nm for the different batches.

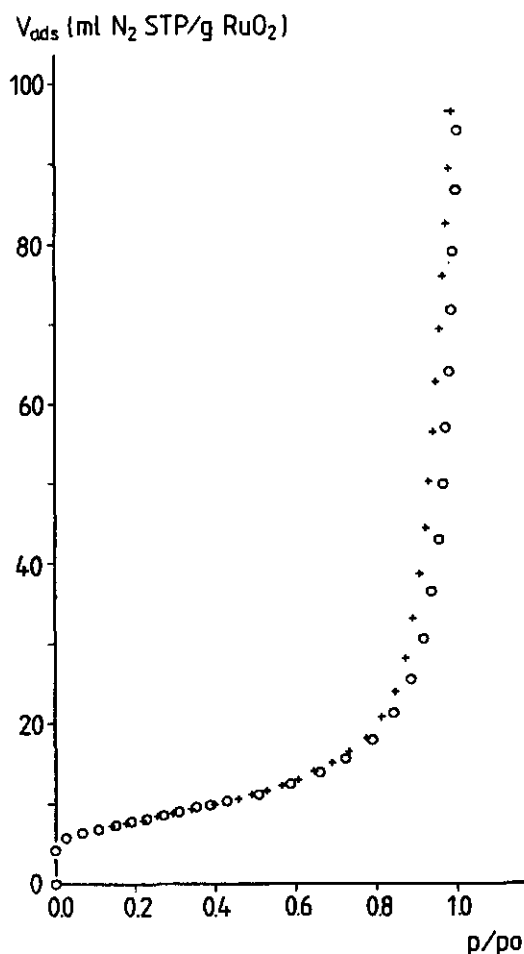


FIGURE 2.3: N_2 adsorption (O) and desorption (+) isotherms for $RuO_2(400)$.

2.6.2 Surface porosity

The N_2 adsorption isotherm (figure 2.3) may be characterized as a type II isotherm in the BDDT (Brunauer-Demming-Demming-Teller) classification [29]. This type of isotherm is generally found for non-porous solids. The adsorption and desorption isotherms exhibit a slight degree of hysteresis in the range $p/p_0 > 0.7$ (p/p_0 is the relative vapor pressure of the adsorbate), which indicates capillary condensation in mesopores (width 2-50 nm, [29]). The BET constant c , which is related to the difference in

heats of adsorption in the first and subsequent adsorption layers, has a rather high value ($100 < c < 300$). In figure 2.3, this can be inferred from the sharp knee in the isotherms in the low pressure range.

The extent of microporosity can be assessed by comparing the adsorption data with those for a non-porous reference solid. An elegant way to perform this comparison is by construction of a so-called t -plot [30]. In such a plot the volume of gas adsorbed at a given relative pressure is plotted against the average thickness t of the adsorbed layer on the non-porous reference at the same relative pressure. (A monolayer of adsorbed N_2 has a thickness of 0.354 nm.) When the sample under study is non-porous and the surface has the same chemical nature as the reference solid, a straight line through the origin is obtained. Microporosity results in a downward deviation of the t -plot, whereas capillary condensation leads to an upward deviation [29]. Here, a standard isotherm is chosen on the basis of the BET constant c , as recommended by Lecloux and Pirard [31]. This isotherm resembles the N_2 adsorption isotherm of non-porous silica.

In figure 2.4 the resulting t -plot is shown. For low values of t , a

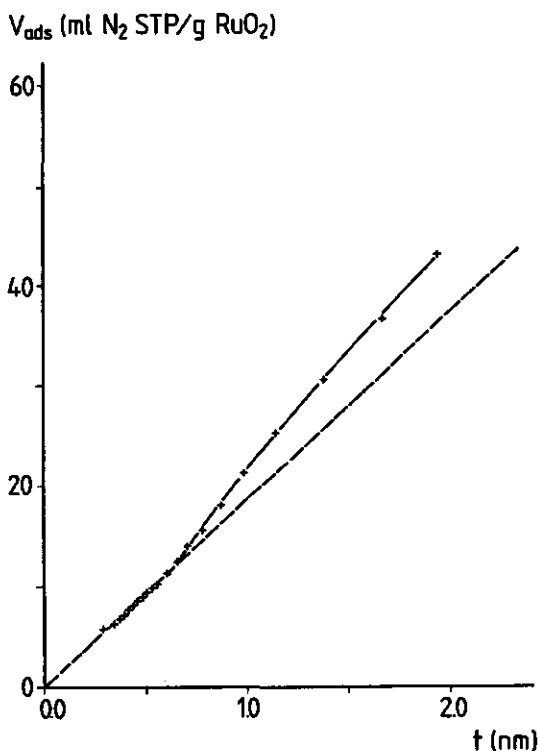


FIGURE 2.4: t -plot for $RuO_2(400)$.

straight line through the origin is obtained, which implies that the appropriate standard is used. The surface area, S_t , calculated from this part of the plot is $29.9 \text{ m}^2/\text{g}$ ($S_{\text{BET}} = 28.3 \text{ m}^2/\text{g}$ for this particular RuO_2 sample). No indication for microporosity is found. Above $t \approx 0.6 \text{ nm}$ ($p/p_0 \approx 0.5$) a gradual upward deviation from the standard is observed, which indicates the presence of pores with radii exceeding 2 nm [29]. The t -plot does not become linear again below $t \approx 1.3 \text{ nm}$, corresponding to high values of p/p_0 (> 0.9). Apparently, there is no upper limit to the pore sizes. Probably, we are dealing with pores in aggregates and compacts of RuO_2 particles.

2.7 XPS/AES SURFACE ANALYSIS

A comprehensive evaluation of the XPS (X-ray Photoelectron Spectroscopy)/AES (Auger Electron Spectroscopy) technique can be found, for example, in references [32,33]. Suffice it to say that under soft X-ray irradiation in ultra high vacuum photoelectrons are ejected from the solid, having a kinetic energy, E_k , related to their binding energy, E_b , in the solid. The XPS spectrum is obtained by scanning E_k of all ejected electrons. Peaks are observed at discrete values of E_k , corresponding to particular values of E_b . From these peaks the origin of the electrons can be characterized, and information is obtained concerning the species being ionized.

XPS/AES is a surface specific technique, since only electrons from the outer 2-15 atom layers gain enough kinetic energy to escape from the solid. So-called Auger electrons have a relatively low kinetic energy and therefore are more surface specific than the photoelectrons.

Surface analysis of RuO_2 was carried out in a Leybold-Heraeus type LHS-10 XPS/AES apparatus, provided with a Hewlett-Packard dedicated computer. A $\text{Mg K}\alpha$ excitation source was applied (energy 1253.6 eV) at the operating conditions of 13 kV and 20 mA . Spectral lines were identified by comparing them with standard values [34].

Two samples were analyzed: a freshly prepared (not washed) sample of $\text{RuO}_2(400)$ (sample A) and a washed sample of the same material (sample B). In figure 2.5 the corresponding XPS/AES spectra are shown. In sample A the presence of Cl was clearly detectable; other impurities could not be detected. The overall composition of the surface, calculated from the integrated intensities of the spectral lines, is 62 at% O, 34 at% Ru and 5 at% Cl (\pm

10 % rel.). If there were a homogeneous distribution of Cl throughout the sample, the ratio of the integrated intensities of the Cl-Auger peak and the Cl-2p peak, $I(\text{Cl-Auger})/I(\text{Cl-2p})$, would be 0.12 under the applied conditions. However, the experimental $I(\text{Cl-Auger})/I(\text{Cl-2p})$ was found to be 0.6, which points to the Cl in the sample being mainly present at the surface. This is confirmed by an XPS/AES spectrum obtained after Ar^+ ion bombardment of the surface. Consequently, the Cl coverage of the very surface layer must be greater than 5 at%. Model calculations according to Gallon [35,36] and Kuyers [37], assuming a monolayer coverage, indicate that 30 at% of the surface is covered by Cl atoms.

The overall composition of the surface of sample B (washed) is 65 at% O, 34 at% Ru and 1 at% Cl. The ratio $I(\text{Cl-Auger})/I(\text{Cl-2p})$ is ca. 0.4, indicating that also in this sample there is some Cl surface enrichment.

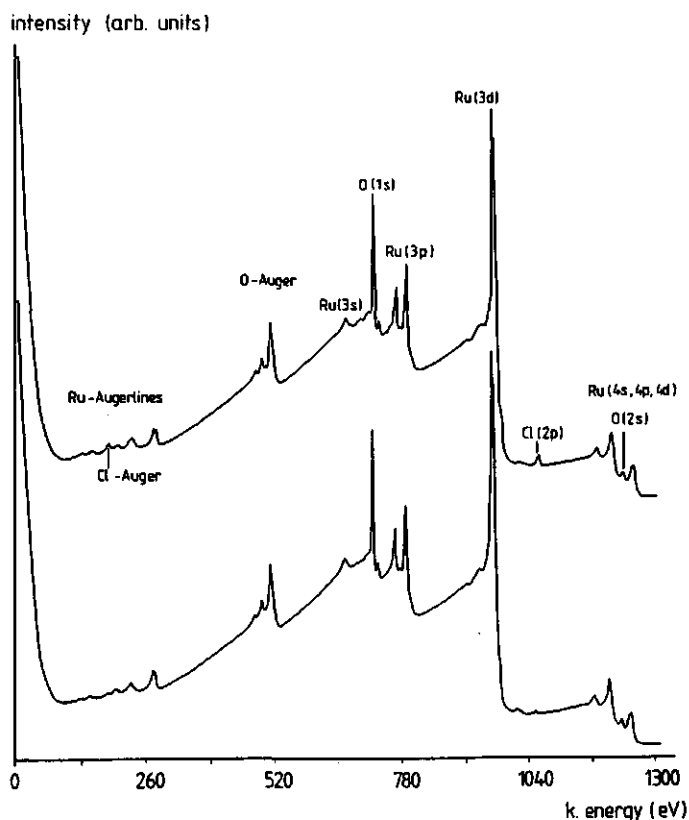


FIGURE 2.5: XPS/AES spectra for a freshly prepared (upper line) and a washed (lower line) $\text{RuO}_2(400)$ sample.

2.8 COLLOIDAL STABILITY OF RuO₂ SOLS

In an aqueous system for photogeneration of hydrogen, the degree of dispersion of the colloidal catalyst is of course of importance. Coagulation of catalyst particles might have a negative influence on the photolysis efficiency by the loss of accessibility of catalytic surface area.

Dispersions of RuO₂(400) appeared to be colloid-chemically very unstable. Without added electrolyte, the RuO₂ particles settle within a few hours after being dispersed by ultrasonic vibration in the pH range 4-6. (The point of zero charge of RuO₂(400) is ca. pH 5.7; see chapter 3.) In the presence of 0.1 M KNO₃, a clear supernatant is obtained within a few minutes over the whole pH range. This ionic strength is comparable to that of the reaction solution for photoproduction of hydrogen (see chapter 5).

The strong tendency of RuO₂ particles to aggregate could be due to a large Hamaker constant, caused by the metallic conductivity and the high specific density of the solid.

A variety of polymers and surfactants (table 2.2) was examined with respect to their ability to stabilize RuO₂(400) sols. The degree of stabi-

TABEL 2.2: Polymers and surfactants used to stabilize RuO₂ sols.

polymer/surfactant	mol. weight (g/mole)	nature
polyvinyl alcohol (PVA) /Konam	183,000	non-ionic, 88% -OH groups, 12 % -COOH groups
polyvinyl pyrrolidone (PVP) /BASF	933,000	non-ionic, cyclic amide groups
polymethacrylic acid (PMA) /BDH	26,000	anionic, at low pH uncharged, -COOH groups
polyethylene oxide (PEO) /Hoechst	35,000	non-ionic, polyether
Polybrene /Aldrich	?	cationic, quaternary N ⁺
Synperonic NPE 1800 /ICI *)	2,180	non-ionic surfactant
dextran T70 /Pharmacia	64,400	non-ionic, polysaccharide
gelatine /Merck	67,000	protein, at low pH pos. charged (i.e.p. at pH 6)

*) See reference [38]

lization was measured qualitatively in coagulation tubes. Generally, a concentrated solution of the polymer in question was mixed with a RuO_2 dispersion at pH 3.5 (no electrolyte present). Immediately before and after mixing, the RuO_2 dispersion was ultrasonically vibrated for 5-10 minutes. The ratio polymer/ RuO_2 varied from 1 to 10 mg polymer per m^2 RuO_2 surface area.

No difference in stability could be observed between RuO_2 dispersions with and without polymer. On addition of KNO_3 (final concentration 0.01-0.1 M), none of the polymers used could prevent settling of most of the RuO_2 within a few hours, although in some cases (PVA, PVP, PMA, dextran) the supernatant remained slightly turbid for longer periods. Changing of the mixture procedure, pH, or sol concentration did not improve these results.

In order to find out whether or not adsorption takes place, the amount of PMA adsorbed on $\text{RuO}_2(400)$ was determined by depletion measurements. In two 35 ml PMA solutions (initial concentration 450 mg/l; pH 3.85 and 0.01 M KNO_3) 25 resp. 9 mg RuO_2 was dispersed. After equilibration overnight, during which the tubes containing the dispersions were rotated end-over-end, the dispersions were centrifuged. The equilibrium concentration PMA in the supernatants was measured by potentiometric titration with 0.1 N KOH under N_2 atmosphere. Adsorbed amounts of 0.78 and 1.3 mg PMA/ m^2 RuO_2 were found at equilibrium concentrations of 59 and 65 mg/l respectively. These values are in general agreement with experimental data concerning polymer adsorption on solid colloidal particles [39].

In conclusion, attempts to stabilize RuO_2 sols with polymers were unsuccessful, although -at least in the case of PMA- adsorption at the RuO_2 surface does take place. It is not clear why the particles are not sterically stabilized to an appreciable extent. Maybe the sonification process does not break down the aggregates into primary particles due to strong Vanderwaals forces, or the aggregation process is so fast that conglomerates of particles are trapped within one polymer network. Perhaps preparation of RuO_2 by chemical precipitation in solution [21] in the presence of stabilizing agents would result in a stable sol with separate primary particles, but this preparation route was not tested (see section 2.1).

2.9 CONCLUSIONS

On the basis of the TEM and X-ray diffraction results, it was decided to use RuO_2 prepared at ca. 400 °C as the catalyst for the sacrificial photoproduction of hydrogen from water. Although the thermal decomposition of RuCl_3 resulted in crystalline RuO_2 at all preparation temperatures applied, the particles of the RuO_2 samples obtained at 700 and 600 °C are barely of colloidal size (0.1-10 μm), whereas the shape of the 300 °C particles is rather undefined. The RuO_2 prepared at 400 °C consists of small (5-50 nm), rectangular particles, the morphology resembling that of unit crystals grown by chemical vapor transport [1].

The BET surface area of $\text{RuO}_2(400)$ varies roughly from 20 to 30 m^2/g . The particles are not microporous; pores with radii larger than 2 nm are probably interstitial holes in conglomerates of particles. Cl impurities are mainly present at the surface of the particles and the larger part can be removed by a simple washing procedure.

The colloidal stability of $\text{RuO}_2(400)$ dispersions is low and can hardly be improved by adding polymers.

2.10 ACKNOWLEDGEMENTS

The following people are gratefully acknowledged: mr. H. Elerie and mrs. E. Bouw (TFDL, Wageningen) for their kind assistance with the electron microscope, dr. J. van Doesburg and prof. dr. L. van der Plas (Department of Soil Science, Agricultural University) for carrying out the X-ray diffraction and interpretation of the results, Anton Korteweg and Marcel Paalman for the BET measurements, dr. A. Pijpers (DSM Central Laboratories, Geleen) for the XPS/AES analyses, and Erna Rouwendal for the investigations with respect to the colloidal stability of RuO_2 .

2.11 REFERENCES

1. H. Schäfer, G. Schneidereit, and W. Gerhardt, Z. Anorg. Allgem. Chem. **319** (1963) 327-336
2. S. Trasatti, and G. Lodi, in "Electrodes of Conductive Metallic Oxides", Part A, S. Trasatti (ed.), Elsevier, Amsterdam (1980) pp 301-358
3. C.-E. Boman, Acta Chem. Scand. **24** (1970) 116-122

4. W. E. O'Grady, Lj. Atanasoska, F. H. Pollak, and H. L. Park, J. Electroanal. Chem. **178** (1984) 61-68
5. J. M. Honig, in "Electrodes of Conductive Metallic Oxides", Part A, S. Trasatti (ed.), Elsevier, Amsterdam (1980) pp 1-98
6. "Handbook of Chemistry and Physics", 58th ed., The Chem. Rubber Publ. Co., Cleveland (1977)
7. S. Pizzini, G. Buzzanca, C. Mari, L. Rossi, and S. Torchio, Mater. Res. Bull. **7** (1972) 449-462
8. S. Trasatti, and W. E. O'Grady, in "Advances in Electrochemistry and Electrochemical Engineering", H. Gerischer, and C. W. Tobias (eds.), John Wiley, New York (1981) pp 177-261
9. O. DeNora, Chem.-Ing.-Tech. **42** (1970) 222-230
10. H. Bartelt, Wiss. Z. Humboldt-Univ. Berlin, Math.-Naturwiss. Reihe **34** (1985) 50-55
11. D. M. Novak, B. V. Tilak, and B. E. Conway, Mod. Aspects Electrochem. **14** (1982) 195-318
12. D. J. Peddler, Electrocomp. Sci. Tech. **2** (1976) 259-265
13. M. W. Schafer, and J. Armstrong, IBM Tech. Disc. Bull. **20** (1978) 4633-4640
14. K. Kalyansundaram, and M. Grätzel, Helv. Chim. Acta **62** (1979) 2432-2441
15. E. Borgarello, J. Kiwi, E. Pelizzetti, M. Visca, and M. Grätzel, J. Am. Chem. Soc. **103** (1981) 6324-6329
16. G. Blondeel, A. Harriman, G. Porter, D. Urwin, and J. Kiwi, J. Phys. Chem. **87** (1983) 2629-2636
17. E. Amouyal, P. Keller, and A. Moradpour, J. Chem. Soc., Chem. Commun. (1980) 1019-1020
18. P. Keller, A. Moradpour, and E. Amouyal, J. Chem. Soc., Faraday Trans. **1** **78** (1982) 3331-3340
19. W. Gissler, and A. J. McEvoy, Sol. Energy Mater. **10** (1984) 309-316
20. A. Daghetti, G. Lodi, and S. Trasatti, Mater. Chem. Phys. **8** (1983) 1-90
21. C. Iwakura, K. Irao, and H. Tamura, Electrochim. Acta **22** (1977) 335-338
22. S. Ardizzone, P. Siviglia, and S. Trasatti, J. Electroanal. Chem. **122** (1981) 395-401
23. G. Lodi, G. Zucchini, A. De Battisti, E. Sivieri, and S. Trasatti, Mater. Chem. **3** (1978) 179-188
24. P. Siviglia, A. Daghetti, and S. Trasatti, Colloids Surfaces **7** (1983) 15-27

25. A. Mills, C. Lawrence, and R. Enos, J. Chem. Soc., Chem. Commun. (1984) 1436-1438
26. A. Mills, and S. Giddings, in "Sixth International Conference on Photochemical Conversion and Storage of Solar Energy", Paris, July 21-25, 1986, Book of Abstracts, p C67
27. "Joint Committee on Powder Diffraction Standards" (1971)
28. H. P. Klug, and L. E. Alexander, in "X-ray Diffraction Procedures", John Wiley & Sons, New York (1962) pp 491-538
29. S. J. Gregg, and K. S. W. Sing, in "Adsorption, Surface Area and Porosity", 2nd ed., Academic Press, London (1982)
30. B. C. Lippens, and J. H. De Boer, J. Catal. 4 (1965) 319-330
31. A. Lecloux, and J. P. Pirard, J. Colloid Interface Sci. 70 (1979) 265-281
32. G. Ertl, and J. Klüppers, in "Low Energy Electrons and Surface Chemistry", Verlag Chemie, Weinheim (1974) pp 17-51, 67-84
33. M. W. Roberts, Adv. Catal. 29 (1980) 55-95
34. "Handbook of X-ray Photoelectron Spectroscopy", Perkin-Elmer, Eden Prairies, Minn. (1979)
35. T. E. Gallon, Surf. Sci. 17 (1969) 486-489
36. D. C. Jackson, T. E. Gallon, and A. Chambers, Surf. Sci. 36 (1973) 381-394
37. F. J. Kuyers, Ph. D. Thesis, State University Leiden, The Netherlands (1978)
38. A. Van den Boomgaard, Ph. D. Thesis, Wageningen Agricultural University, The Netherlands (1985)
39. M. A. Cohen Stuart, T. Cosgrove, and B. Vincent, Adv. Colloid Interface Sci. 24 (1986) 143-239

DOUBLE LAYER STRUCTURE AND HYDROGEN EVOLUTION REACTION AT THE
RuO₂/SOLUTION INTERFACE

3.1 INTRODUCTION

Measurement of the surface charge (σ_0) on colloidal particles at various electrolyte concentrations by means of potentiometric titration with potential-determining ions, provides useful information on the basic double layer properties. For example, one can determine the pristine point of zero charge (p.p.z.c.), a notion of Bowden et al. [1,2] and reintroduced by Lyklema [3]. For oxides it is defined as the pH where the surface charge is zero in the absence of specific adsorption, and it reflects the intrinsic protolytic nature of the interface. It is also possible to study specific adsorption of certain ions at the oxide/solution interface, because their presence has a drastic effect on the σ_0 -pH curves.

In this chapter the double layer properties of colloidal RuO₂ in indifferent electrolyte (KNO₃) and the adsorption of Cl⁻ were studied, using the potentiometric titration technique in combination with electrophoretic mobility measurements. It is demonstrated how quantitative data on specific adsorption can be obtained from σ_0 and ζ -potential measurements without introducing an inner layer model, like the ones based on surface complexation or site binding. The analysis is based on purely thermodynamic arguments combined with diffuse double layer theory, and therefore has a general validity. Double layer properties of colloidal RuO₂ have been studied before only by Siviglia et al. [4,5]. These authors have investigated the dependence of the p.p.z.c. on the procedure used in preparing this oxide. Siviglia et al. have also reported the specific adsorption of Cl⁻ ions on RuO₂. Overviews on the basic properties of the oxide/electrolyte interface in general are given in references [6,7].

In addition, the hydrogen evolution reaction (HER) at the surface of RuO₂ film electrodes was investigated, because of the basic role of RuO₂ in the photolysis of water. The material used in preparing the films was -as

much as possible- identical to the colloidal RuO_2 used in the water photo-reduction experiments (chapter 5).

Over the past century, the HER at Pt and other electrodes has been extensively studied and the discussion about the possible mechanisms of the reaction is still going on (see for example references [9-12]). It goes beyond the limits of this work to try to unravel the reaction path of hydrogen evolution at RuO_2 in detail. Attention is rather focussed on relationships between the rate of H_2 formation, the overpotential of the RuO_2 film electrode, and the proton availability in solution, parameters that can be exploited in modelling the hydrogen photoproduction system (chapter 6). The electrochemical investigations comprised the measurement of current versus potential characteristics.

A number of studies concerning the behavior of certain types of RuO_2 films on metal supports have been conducted before by Trasatti and coworkers [13-21] and the (photo)electrochemical behavior of semiconductors coated with RuO_2 has been studied by McEvoy and Gissler [22,23].

3.2 EXPERIMENTAL

3.2.1 Materials

All chemicals used were reagent grade. Water was purified by reverse osmosis and subsequently passed through a Millipore Super-Q system (conductivity $< 0.8 \mu\text{S}/\text{cm}$).

Colloidal RuO_2 was prepared by thermal decomposition of RuCl_3 under an oxygen stream at 405-420 °C. After preparation it was washed thoroughly at high and low pH to remove residual Cl. Details on the preparation and characterization of colloidal RuO_2 are described in chapter 2. The BET specific surface area of the RuO_2 batch used here is $21.5 \text{ m}^2/\text{g}$.

3.2.2 Potentiometric acid-base titrations

Potentiometric acid-base titrations of aqueous dispersions of RuO_2 were carried out at 20 °C in an air-tight titration vessel. Details of the cell and procedure have been described previously [24,25]. Each experiment consisted of a series of titrations on the same RuO_2 sample in at least three different electrolyte concentrations, in order to determine the rel-

ative position of the σ_0 -pH curves.

The volume of the solutions was about 50 ml, containing 1-2 gram of RuO_2 . At these low concentrations of solid, the suspension effect is negligible [24]. The solutions were stirred magneticcally, except just before and during pH measurements. Nitrogen was continuously flushed through the system to purge the solutions from CO_2 . Before entering the system, the N_2 was purified and moistened by passing over a soda-lime column and repeated bubbling through pure water.

An HP (Hewlett-Packard) 3497A Data Acquisition Unit and an HP 85 microcomputer were used to control and monitor the experiments. Starting at low pH, aliquots of 0.1 N KOH were added stepwise by a Metrohm Multi-Dosimat 655 automatic buret. For each point of the titration, a period of at least 25 minutes was given for equilibration and after this time a pH drift of less than 0.005 pH unit per 5 minutes was used as the criterion for equilibrium. Back-titration to low pH was done in one or two steps with 0.1 N acid (HNO_3 or HCl , equilibration overnight).

For pH measurements, a glass-electrode (Schott N1180) and an $\text{Ag}/\text{AgCl}/3.5 \text{ M KCl}$ reference electrode (Schott B2920) were used. In the case of titration in the presence of KNO_3 , the reference electrode was connected to the cell through a salt-bridge, containing the same electrolyte solution as the cell, to prevent leakage of KCl into the cell. For the titrations in the presence of KCl , no salt bridge was used, but a reference electrode with a very low KCl leak was selected. In none of these cases stirring had a significant effect on the EMF of the cell. Before and after every experiment, the electrodes were calibrated using two fresh buffers (pH 4.00 and 7.00, Titrisol, Merck).

Blank titrations were carried out in the same way as dispersion titrations and the experimental curves for all electrolyte solutions were found to agree within 0.03 pH unit with curves calculated using tabulated activity coefficients [26]. The blank curves were reproducible within 0.01 pH unit. In KNO_3 the surface charge is defined as $\sigma_0 = F(\Gamma_{\text{HNO}_3} - \Gamma_{\text{KOH}})$, where Γ stands for the surface concentration of the substance named, in other electrolytes the corresponding equation is used. The experimental blanks are used to correct for the changes in H^+ and OH^- amounts in the solution.

After each experiment, the oxide sample was repeatedly washed at high and low pH, to completely remove the electrolyte. In this way a RuO_2 sample could be used several times. It was found that during the first experiment

on a RuO_2 sample, equilibrium is sometimes achieved only after a long time, and the σ_0 -pH curves then obtained are not reproducible. However, the results of second and later experiments are reproducible within $0.2 \mu\text{C}/\text{cm}^2$. Only those results will be reported. During the course of many titrations, the BET surface area of the RuO_2 particles did not change.

3.2.3 Electrophoretic mobility measurements

The electrophoretic mobility of RuO_2 particles as a function of pH was measured at 20°C in a Mk II Zeta Sizer microelectrophoresis apparatus of Malvern Instruments Ltd.

3.2.4 Preparation of RuO_2 film electrodes

RuO_2 film electrodes were prepared by depositing a layer of colloidal RuO_2 particles on 0.1 mm thick Pt plates of 0.5 cm^2 total surface area. The plates were connected to a glass tube with a thin Pt wire.

Prior to deposition the Pt support was etched in hot 20 % HCl and rinsed with millipore water, to obtain a clean surface and a good adhesion. RuO_2 particles were dispersed in 2-propanol and the Pt plate was repeatedly dipped in this dispersion, the solvent being evaporated in a hot air stream, until the surface of the plate was totally covered with RuO_2 . To prevent the RuO_2 from being washed off during experiments, the film was sintered in a furnace at 700°C for about 4 hours.

Electron micrographs of the obtained surface are shown in figure 3.1. The thickness of the RuO_2 films is approximately $6 \mu\text{m}$, obtained by weighing the material deposited on the supports (ca. 2 mg) and using the specific density of crystalline RuO_2 ($6.97 \text{ g}/\text{cm}^3$).

3.2.5. Voltammetric experiments

Experiments were carried out at room temperature in a three-electrode cell with a Pt plate (ca. 3 cm^2 surface area) as counter electrode and an $\text{Ag}/\text{AgCl}/3.5 \text{ M KCl}$ reference electrode (Schott B2920).

Single sweep and cyclic voltammetric curves were measured at various scan rates, in $0.025 \text{ M KNO}_3/\text{HNO}_3$ solutions of different pH values and in a 0.05 M acetate buffer solution of pH 4.6. Before each experiment, the solu-

tion was flushed for at least 30 minutes with nitrogen gas, which had been passed through a BTS catalyst column to remove residual oxygen. During the measurements N_2 was passed over the solution.

Potentials were applied from a Princeton Applied Research Polarographic Analyzer model 174A and i-E curves were recorded on an HP 7040A X-Y plotter.

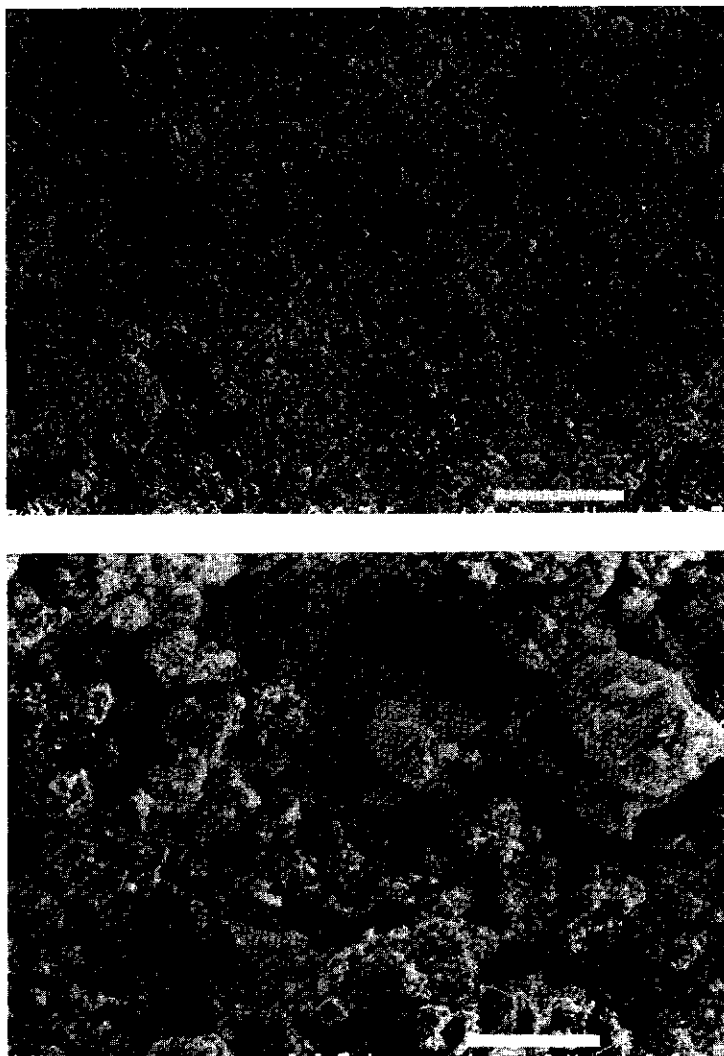


FIGURE 3.1: Electron micrographs of a RuO_2 film on a Pt substrate (Jeol JSM 35C scanning electron microscope). The bars refer to 100 μm (upper picture) and 10 μm (lower picture).

3.3 RESULTS AND DISCUSSION

3.3.1 The surface charge on RuO_2 in the presence of indifferent electrolyte

In figure 3.2 σ_0 -pH curves for RuO_2 at three different KNO_3 concentrations are given. A sharp common intersection point (c.i.p.) is found at pH 5.75 ± 0.05 . Electrophoretic mobility measurements show that the iso-electric point (i.e.p.) is situated at pH 5.8, independent of KNO_3 concentration (figure 3.3). Therefore, the c.i.p. is identified as the pristine point of zero charge (p.p.z.c.) and it is concluded that there is no specific adsorption of K^+ or NO_3^- ions.

Siviglia et al. [5] have measured a p.p.z.c. of 5.1 for RuO_2 prepared at 400 °C. They found that the p.p.z.c. shifts to higher pH values with

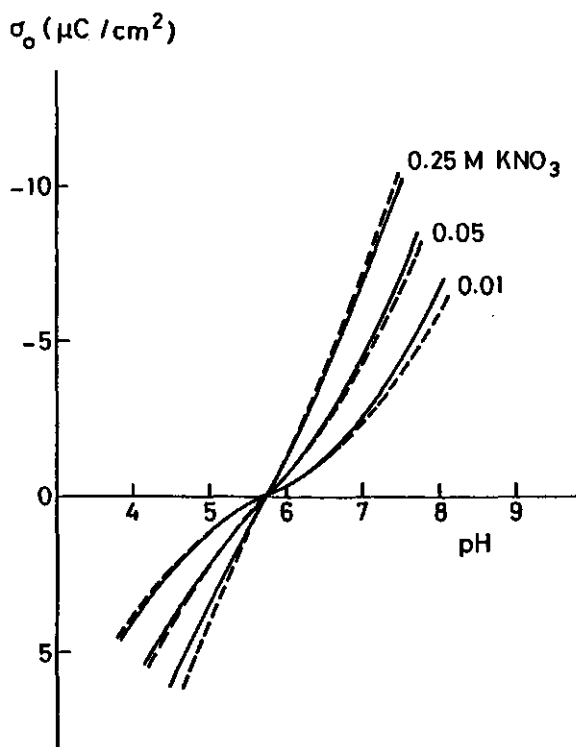


FIGURE 3.2: Surface charge on RuO_2 in the presence of KNO_3 .

— experimental curves, ---- calculated curves (for details see the text).

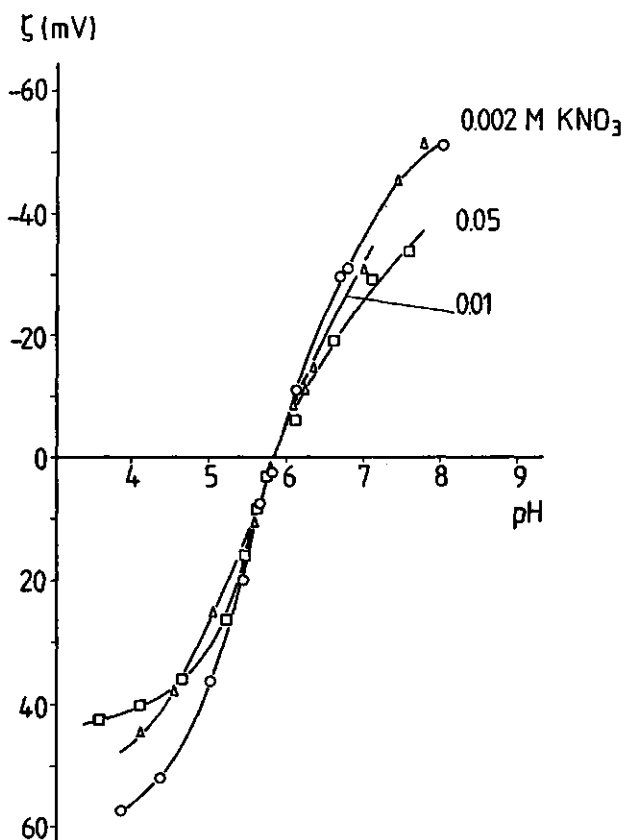


FIGURE 3.3: ζ -potentials of RuO_2 in various KNO_3 solutions.

increasing preparation temperature of the oxide, with an upper limit of pH 7.3 for pure RuO_2 (obtained by chemical vapor transport). This variation in the p.p.z.c. has been interpreted in terms of changes in the RuO_2 lattice dimensions, due to variation in the residual chlorine content, which decreases with increasing preparation temperature. Therefore, the position of the p.p.z.c. seems to be a measure of the stoichiometry of (the surface region of) the oxide. (See also chapter 2.)

For RuO_2 film electrodes Nernst behavior has been reported [5,18,19]. This means that the potential difference between bulk oxide and bulk solution obeys Nernst's law, and because RuO_2 is a metallic conductor (no space charge distribution in the solid phase), this indicates also Nernst behavior of the surface potential.

Capacitance-pH curves can be obtained by differentiation of the curves in figure 3.2, using the Nernst equation. From the minima in these capacitance curves, located at the point of zero charge, it is possible to determine an "electrochemical" surface area and the capacitance of the inner part of the double layer. The procedure has been suggested by Parsons and Zobel [27] and formerly used for the RuO_2 /solution interface by Siviglia et al. [5]. In this method the total capacitance of the double layer C (experimentally found as a capacitance per gram of substance) is divided into an inner layer capacitance C_i (independent of electrolyte concentration, per m^2) and a capacitance of the diffuse double layer C_d (per m^2) in series. Assuming that for the electrolyte concentrations applied, these two components of C refer to the same microscopic surface area S (m^2/g), then:

$$\frac{1}{C} = \frac{1}{S} \left(\frac{1}{C_i} + \frac{1}{C_d} \right) \quad (3.1)$$

The capacitance of the diffuse double layer at the p.z.c. was calculated numerically, using the Gouy-Chapman theory and assuming spherical geometry (which is, in view of the small size of the particles, more appropriate than using flat geometry as has been done in reference [5]). From a plot of $1/C$ versus $1/C_d$ (figure 3.4) an inner layer capacitance of about $300 \mu\text{F}/\text{cm}^2$ and an electrochemical surface area S_{EC} of $21.5 \text{ m}^2/\text{g}$ are found. S_{EC} is identical to the surface area obtained from BET measurements, in contrast to the findings for AgI colloids, for which S_{EC} is much higher than S_{BET} [28].

In comparison with AgI and Hg [28,29], the inner layer capacitance found for RuO_2 is fairly high. This seems to be a common characteristic of many oxide/electrolyte interfaces. The σ_0 -pH curves for TiO_2 (rutile) and $\alpha\text{-Fe}_2\text{O}_3$ (hematite) have essentially the same shape as those for RuO_2 [30]. In this respect SiO_2 (silica) and Al_2O_3 exhibit a different behavior [31,32]. Their surface charge densities and differential capacitances are lower than for AgI and Hg near their p.z.c.'s, but they are much higher far from the p.z.c. Only on SiO_2 and Al_2O_3 extremely high surface charges are found, up to $100 \mu\text{C}/\text{cm}^2$ and more.

A high inner layer capacitance in the classical Gouy-Chapman-Stern-Grahame model would mean a rather thin Stern layer and/or a high relative dielectric constant in the Stern layer, ϵ_s . Based on the experimental data on AgI, for which C_i is about $30 \mu\text{F}/\text{cm}^2$, it is commonly accepted that ϵ_s has a low value (< 20), but this is not necessarily true for oxides. The

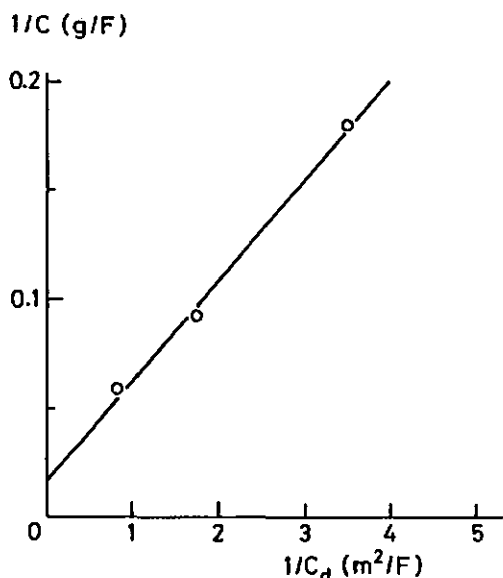


FIGURE 3.4: Reciprocal capacitance plot for determining the specific surface area and the inner layer capacitance of RuO_2 in the presence of KNO_3 .

"water-like" nature of the oxide interface can result in more orientational freedom for the water molecules than at the hydrophobic AgI -interface, and therefore ϵ_s can be higher. However, even if for ϵ_s the bulk value of 80 is taken, the Stern layer thickness would be only about 0.25 nm, the size of one water molecule. Therefore, one could assume that the concept of a charge-free Stern layer is not adequate for oxides. The surface of the oxide is covered with OH-groups, which are in close contact with surrounding water molecules. The surface charge (a shortage or excess of protons in the interface) could perhaps be spread over the surface OH-groups and the first water layer(s). In this way the counter ions can closely approach the surface charge and screen it efficiently. In such a picture of the inner layer, the notions "surface charge" and "Stern layer" lose their physical meaning.

Nevertheless, large part of $\sigma_0(\text{pH})$ can already be accounted for in terms of a very simple double layer model, i.e. a diffuse layer and a charge free inner layer with a high and constant capacitance. This is illustrated in figure 3.2 for RuO_2 in KNO_3 ($C_1 = 300 \mu\text{F}/\text{cm}^2$). The experimental curves are slightly asymmetrical, showing a somewhat higher capacitance at the negatively charged oxide surface.

3.3.2 The surface charge and ionic composition of the double layer in the presence of specifically adsorbing ions

Figure 3.5 shows σ_0 -pH curves for RuO_2 at various KCl concentrations. The origin of the charge axis was determined by first titrating without added electrolyte. There is no c.i.p. and the p.z.c. moves to higher pH values with increasing KCl concentration. This indicates specific adsorption of Cl^- ions.

A possible explanation for the affinity of Cl^- ions for the RuO_2 surface can be found in the preparation procedure, which involves RuCl_3 as the

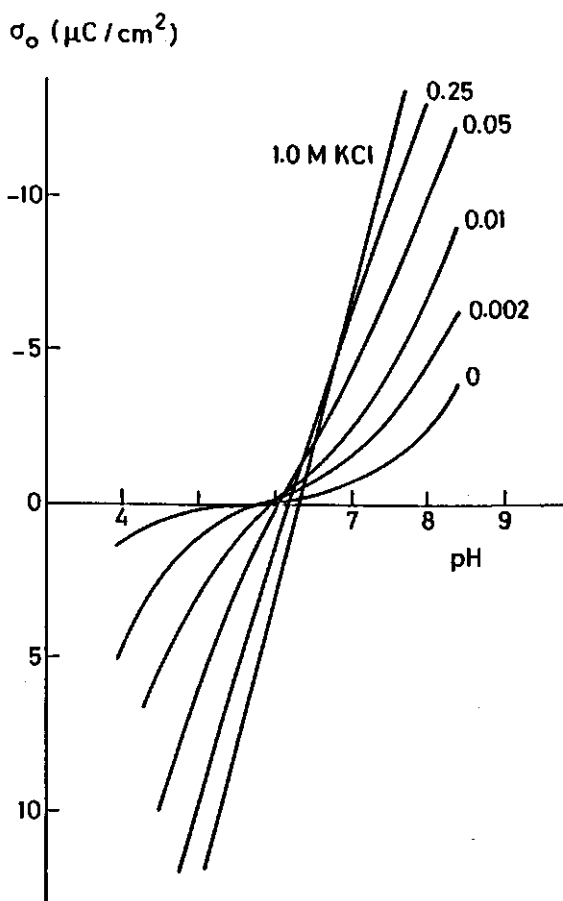


FIGURE 3.5: Surface charge on RuO_2 in various KCl solutions.

starting material. As outlined in chapter 2, the surface of the freshly prepared oxide is contaminated with Cl, of which the greater part can be removed by washing at low and high pH. It can be imagined that Cl^- ions fit well into any remaining binding sites. Siviglia et al. [5] have also found specific adsorption of Cl^- and from their σ_0 -pH curves it is obvious that the affinity of Cl^- for the RuO_2 surface decreases with increasing preparation temperature and consequently with decreasing residual Cl content.

From a set of σ_0 -pH curves at different electrolyte concentrations, it is possible to determine the ionic composition of the electric double layer [3,33-36]. Thermodynamic analysis of the adsorption of the various species at the oxide/electrolyte interface gives, in the case of a 1:1 electrolyte [3,35]:

$$\left(\frac{\partial \sigma_+}{\partial \sigma_0}\right)_{c_s} = \frac{1}{2} \left(\frac{\partial \text{pH}}{\partial \log f_{\pm} c_s}\right)_{\sigma_0} - \frac{1}{2} \quad (3.2a)$$

$$\left(\frac{\partial \sigma_-}{\partial \sigma_0}\right)_{c_s} = -\frac{1}{2} \left(\frac{\partial \text{pH}}{\partial \log f_{\pm} c_s}\right)_{\sigma_0} - \frac{1}{2} \quad (3.2b)$$

In these expressions σ_+ and σ_- are the contributions to the counter charge of cations and anions, respectively, c_s is the electrolyte concentration, and f_{\pm} is the mean activity coefficient. The term $(\partial \text{pH} / \partial \log f_{\pm} c_s)_{\sigma_0}$ is the Esin-Markov coefficient β and it is a function of c_s and σ_0 (or pH). β can be obtained from the experimental σ_0 -pH curves by determining the tangents of plots of the pH as a function of $\log f_{\pm} c_s$ at constant σ_0 values.

Integration gives σ_+ and σ_- :

$$\sigma_+(c_s, \sigma_0) = \frac{1}{2} \int_0^{\sigma_0} \beta(c_s, \sigma_0) d\sigma_0 - \frac{1}{2} \sigma_0 + K(c_s) \quad (3.3a)$$

$$\sigma_-(c_s, \sigma_0) = -\frac{1}{2} \int_0^{\sigma_0} \beta(c_s, \sigma_0) d\sigma_0 - \frac{1}{2} \sigma_0 - K(c_s) \quad (3.3b)$$

$K(c_s)$ is identical to $\sigma_+(\sigma_0=0)$; because of electroneutrality, $\sigma_+(\sigma_0=0) = -\sigma_-(\sigma_0=0)$. If there is no specific adsorption, $\sigma_+ = \sigma_- = 0$ at the p.z.c., which is in that case identical to the p.p.z.c. Then, $K(c_s) = 0$ for all c_s .

The problem is to determine $K(c_g)$ in the presence of specifically adsorbing ions. Levine [36] has proposed several procedures to estimate this integration constant, but for our purposes and experimental results none of these methods has practical meaning. Fortunately, the combination of potentiometric titrations with electrokinetic studies can solve the problem. At the i.e.p. the diffuse part of the counter charge is zero. The specifically adsorbed charge is then, except for the sign, equal to the surface charge and with this knowledge the integration constants can be calculated.

As an example the experimental results on RuO_2 in the presence of KCl have been analyzed, using equations (3.2) and (3.3). For the mean activity coefficient tabulated values were used [26]. In figure 3.6 the Esin-Markov coefficients as a function of σ_0 are given for the different KCl concentrations.

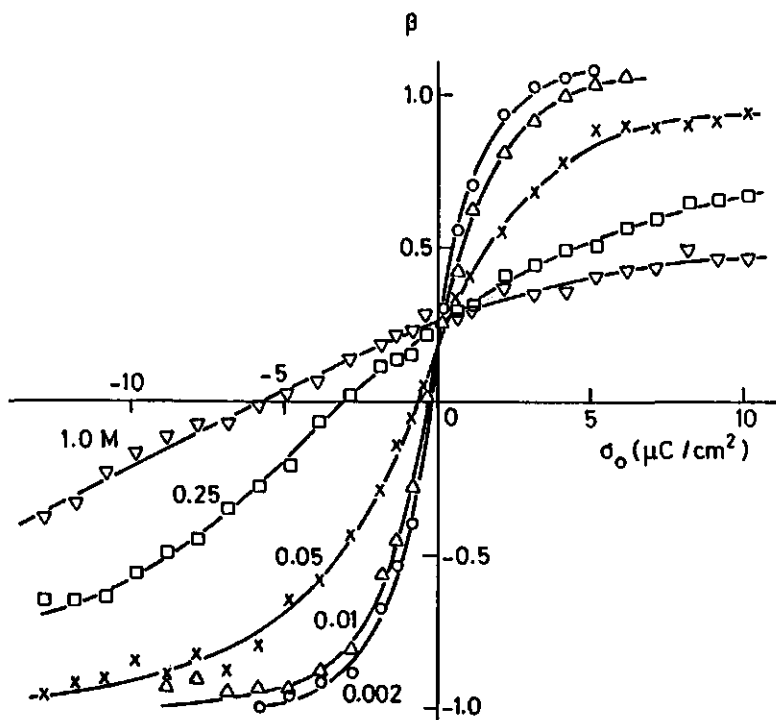


FIGURE 3.6: Esin-Markov coefficients as a function of surface charge for RuO_2 in various KCl solutions.

For the lowest KCl concentrations (0.002, 0.01 and 0.05 M), the ζ -potentials of RuO_2 are given in figure 3.7. It is for practical reasons not possible to measure electrophoretic mobilities at higher electrolyte concentrations. It may be noted that the ζ -pH curves have a c.i.p. at or near the p.p.z.c. As expected, the i.e.p. shifts to lower pH values with increasing KCl concentration.

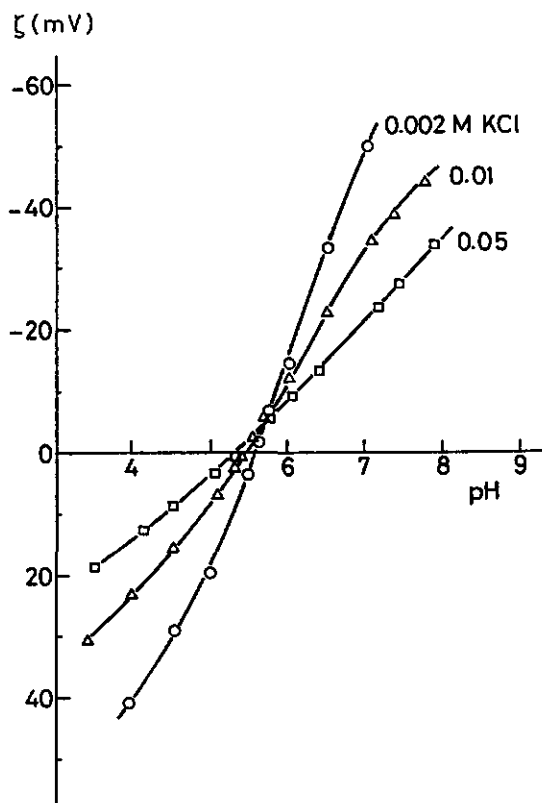


FIGURE 3.7: ζ -potentials of RuO_2 in the presence of KCl.

Using the values found for the i.e.p.'s, the integration constants $K(c_{\text{KCl}})$ were determined and they are listed in table 3.1. For 0.25 M KCl, K could be estimated by extrapolating the β - σ_0 curve in figure 3.6 to $\beta = -1$ and carrying out the integration. At high negative surface charge there is no specific adsorption of Cl^- any more and the contribution of Cl^- ions to

TABLE 3.1 Some characteristics of the electric double layer on RuO_2 in KCl solutions and the specific adsorption of Cl^- at the p.z.c.

c_{KCl} (M)	i.e.p.	σ_0 (i.e.p.) ($\mu\text{C}/\text{cm}^2$)	K ($\mu\text{C}/\text{cm}^2$)	$\sigma_{-,1}(\sigma_0=0)$ ($\mu\text{C}/\text{cm}^2$)	$\psi_d(\sigma_0=0)^a)$ (mV)
0.002	5.60	0.20	0.08	-0.13	-12
0.01	5.45	1.33	0.37	-0.60	-25
0.05	5.35	3.78	0.94	-1.51	-29
0.25 $b)$	5.1	8.7	2.3	-3.6	-31

^{a)} ψ_d is calculated from σ_d , using Gouy-Chapman theory.

^{b)} $\sigma_{-,1}$, σ_0 (i.e.p.) and the i.e.p. are based on the estimated value of K.

the counter charge becomes constant ($\partial\sigma_-/\partial\sigma_0 = 0$). The level of the maximum negative adsorption of Cl^- is given by the Gouy-Chapman theory of the diffuse double layer [33]. For 1:1 electrolytes:

$$\sigma_- = A (1 - e^{-F\psi_d/2RT}) \quad (3.4)$$

with $A = \sqrt{2RT\epsilon c_g}$; ϵ is the dielectric constant and ψ_d the potential of the diffuse double layer. F , R and T have their usual meanings. From equation (3.4) it follows that the theoretical limiting value of σ_- at high negative ψ_d is equal to A ($= 5.88 \sqrt{c_g} \mu\text{C}/\text{cm}^2$ with c_g in mol/l).

In figure 3.8 the calculated ionic composition of the double layer on RuO_2 as a function of σ_0 is given. The limiting values for σ_- at negative surface charge are indicated. For 0.01 and 0.05 M KCl, σ_- approaches this limit very well within the range of σ_0 values attainable by our technique.

The surface charge for which $\beta = 0$ is different for each KCl concentration, corresponding with the fact there is no c.i.p. in the σ_0 -pH curves. For $\beta = 0$, $(\partial\sigma_+/\partial\sigma_0) = (\partial\sigma_-/\partial\sigma_0) = -\frac{1}{2}$. Under these conditions, cation and anion adsorption are equally sensitive to changes in the surface charge. Obviously, at this point the affinity of Cl^- ions to the interface due to specific adsorption together with electrostatic repulsion is equal to the affinity of K^+ ions due to electrostatic attraction only. The point where $\beta = 0$ can therefore be called an "equal affinity point" rather than an "equal compensation point" [3]. In figure 3.8 these points are indicated with arrows.

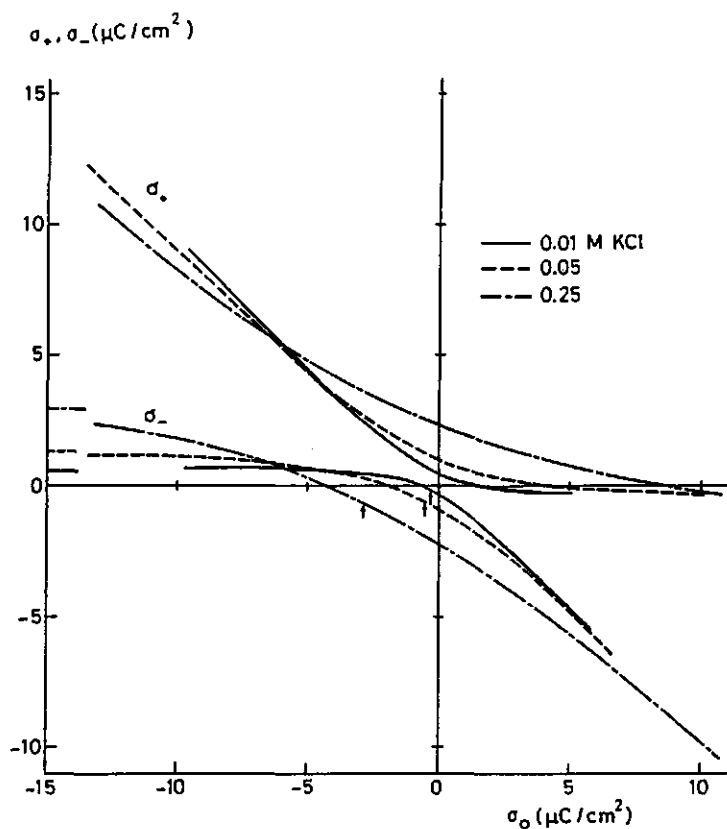


FIGURE 3.8: Ionic components of charge of the double layer on RuO_2 at various concentrations of KCl. The arrows indicate the surface charge where $\beta = 0$. The theoretical limiting values of σ_- at high negative surface charge are indicated.

If there is no specific adsorption of K^+ , the intersection points of the σ_+ curves with the σ_0 -axis are the i.e.p.'s. From the shapes of these curves it is clear that $\sigma_0(\text{i.e.p.})$ is rather sensitive to specific adsorption. At the intersection points of the σ_- curves with the σ_0 -axis, the specifically adsorbed amount of Cl^- is equal to the negative adsorption of Cl^- in the diffuse double layer.

3.3.3 Adsorption of Cl^- at the point of zero charge

From equation (3.3b) it follows that at the p.z.c. the total adsorption of Cl^- is equal to $-K$ ($\mu\text{C}/\text{cm}^2$) or K/F ($\mu\text{mol}/\text{cm}^2$). Part of this adsorbed amount is situated in the diffuse double layer:

$$\sigma_- = -K = \sigma_{-,i} + \sigma_{-,d} \quad (3.5)$$

in which $\sigma_{-,i}$ is the specifically adsorbed charge and $\sigma_{-,d}$ the contribution of Cl^- to the diffuse counter charge. The latter contribution is positive, because it is due to a deficit of Cl^- ions (negative adsorption). For 1:1 electrolytes the Gouy-Chapman theory of the diffuse double layer gives [33]:

$$\sigma_{-,d} = \frac{\sigma_d}{2} + A - \sqrt{\left(\frac{\sigma_d}{2}\right)^2 + A^2} \quad (3.6)$$

where σ_d is the total diffuse charge, which, at the p.z.c., is equal to $-\sigma_{-,i}$. Therefore, at $\sigma_0 = 0$:

$$\sigma_d = -\sigma_{-,i} = K + \sigma_{-,d} \quad (3.7)$$

From equations (3.6) and (3.7) $\sigma_{-,d}$ and $\sigma_{-,i}$ at $\sigma_0 = 0$ can be found:

$$\sigma_{-,d} = \frac{K A}{K + A} \quad (3.8a)$$

$$\sigma_{-,i} = -\frac{K (K + 2A)}{K + A} \quad (3.8b)$$

In table 3.1 an overview is given and in figure 3.9 the specific adsorption of Cl^- ions on RuO_2 at the p.z.c. is given as a function of c_{KCl} . The adsorption of Cl^- is much lower than that reported for $\text{TiO}_2/\text{RuO}_2$ electrodes [37,38]. It would have been impossible to detect it by direct analytical measurements. The limited number of data only allows an analysis in terms of a Langmuir isotherm equation, revealing a saturation coverage of $4.4 \times 10^{-11} \text{ mol}/\text{cm}^2$ and a standard molar Gibbs energy of adsorption $\Delta_{\text{ads}}G^\circ$

of about -6.6 RT. However, the shape of the adsorption isotherm in figure 3.9 indicates a strong repulsive interaction between the adsorbed ions, making this analysis tentative. Attempts to fit the data with a Frumkin-Fowler-Guggenheim isotherm equation [39,40] showed that $\Delta_{\text{ads}}G^\circ$ lies between -5 and -6.5 RT, and that the saturation coverage is higher than found with Langmuir. Since at the p.z.c. the specifically adsorbed ions have no coulombic interaction with the oxide surface, $\Delta_{\text{ads}}G^\circ$ does not contain an electrical contribution and is a pure "specific" adsorption energy.

It is also possible to calculate $\sigma_{-,1}$ for $\sigma_0 \neq 0$, by computing the value of σ_d from σ_+ , again assuming σ_+ to be totally diffuse. The advantages of these experimental methods and calculations over direct analytical measurements are the greater sensitivity for specific adsorption and the fact that information on the surface charge is obtained simultaneously. The adsorption of species at constant surface charge or at constant pH can be determined and discrimination between specific and "diffuse" adsorption is possible. However, it must be realized that in the calculations of σ_+ and σ_- using equations (3.3) accumulation of experimental errors takes place, which limits the accuracy of this analysis.

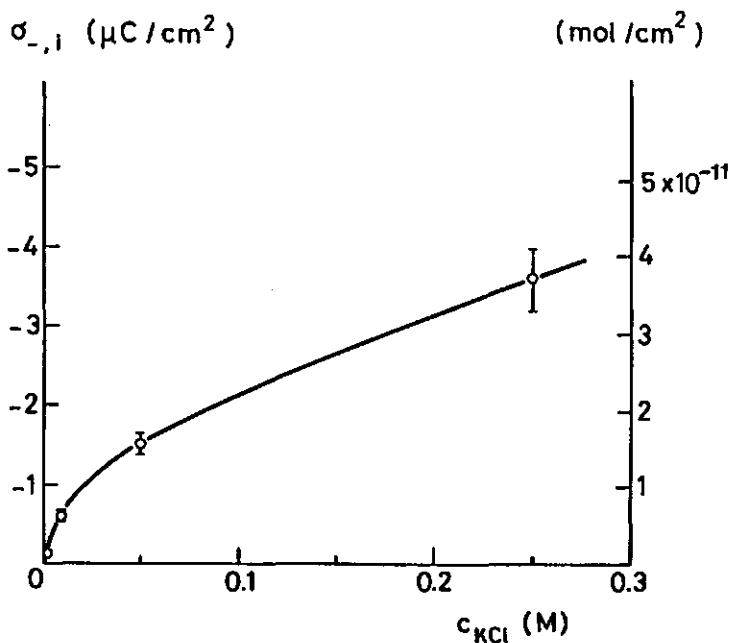


FIGURE 3.9: Specific adsorption of Cl^- on RuO_2 at $\sigma_0 = 0$.

3.3.4 Hydrogen evolution at RuO_2 film electrodes

The metallic behavior of RuO_2 gives an opportunity to study electron transfer reactions at the surface of RuO_2 film electrodes [13-17]. However, the RuO_2 films appeared to be not resistant to prolonged H_2 evolution at high overpotentials. Mechanical destruction due to gas evolution in pores leads to collapse of the film with the deposition of RuO_2 powder at the bottom of the cell. Hydrogen evolution during short periods at moderate overpotentials (0 to -150 mV) does not permanently modify the electrodes.

Figure 3.10 shows current density-potential (i - E) curves for a RuO_2 film electrode in an unbuffered 0.025 M KNO_3 solution of pH 4.6 at different scan rates. The film shows a capacitive behavior, exhibiting a charging process on the forward scan and a corresponding discharging process on the reverse scan. In region I, up to about -0.35 V, no electron transfer reactions take place at the electrode surface. The magnitude of the current is approximately linear with the scan rate, as can be expected for a pure charging current. From the current densities and scan rates the double

current density

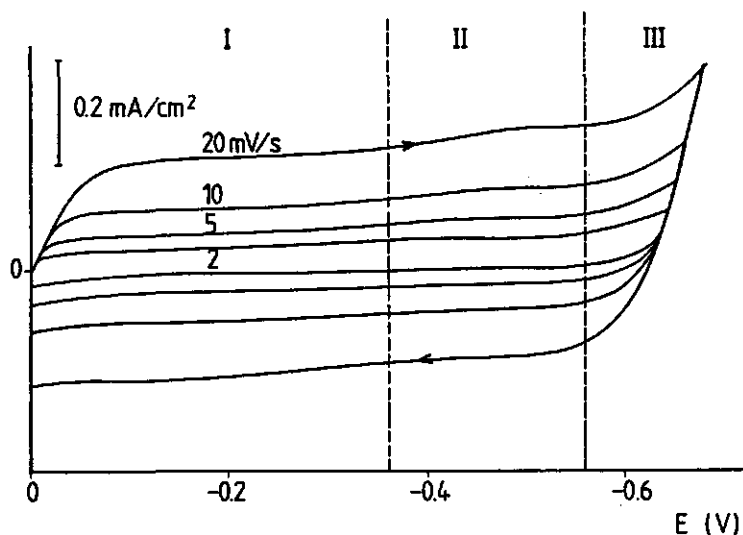


FIGURE 3.10: i - E curves for a RuO_2 film electrode in 0.025 M KNO_3 of pH 4.6. In region I no electron transfer reactions take place, in region II H^+ is reduced, and in region III reduction of H_2O occurs.

layer capacitance C of the film can be calculated. For different RuO_2 film electrodes C was found to vary from 12 to 28 mF per cm^2 of geometrical surface area. The total double layer capacitance of colloidal RuO_2 at this KNO_3 concentration and pH value is ca. 70 μF per cm^2 microscopic area (from potentiometric acid-base titrations). From these values, a ratio between the effective surface area and the geometrical surface area of the RuO_2 film electrodes in the order of a few hundreds is obtained. Considering the nature of the surface (figure 3.1) and roughness factors found for platinumized Pt electrodes [41,42], this is a reasonable result. Because the thickness of the double layer in 0.025 M KNO_3 is only about 2 nm, the effective area of the RuO_2 electrode will be approximately identical to the real microscopic area.

At low scan rates (< 0.5 mV/s), the charging current is relatively small and this fact facilitates investigation of the hydrogen evolution reaction (HER). By way of comparison the HER on smooth Pt electrodes (0.5 cm^2) was also studied. Cyclic voltammetric experiments in the potential range of H^+ reduction were performed in 0.025 M $\text{KNO}_3/\text{HNO}_3$ solutions of various pH values (pH 1.6, 2.6, 3.6, and 4.6) and in a 0.05 M acetate buffer solution of pH 4.6. Gas evolution proceeded in an undisturbed manner (no stirring). After one complete voltammetric cycle, remaining gas bubbles were removed mechanically from the electrode. In figure 3.11 some of the voltammograms obtained for RuO_2 film electrodes and smooth Pt electrodes are displayed. During a cathodic sweep H^+ reduction occurs and H_2 evolution can be observed. On the anodic scan the remaining hydrogen is re-oxidized and gives rise to an "anodic dissolution" current, the magnitude of which depends on the duration and rate of the preceding H^+ reduction. This phenomenon is already known for Pt [43] and is here also observed for the RuO_2 film electrodes, pointing to chemical reversibility of the H^+ reduction. This finding is different from the results of Galizzioli et al. [16], who concluded that the oxide is not able to dissociate molecular hydrogen. However, after being subjected to hydrogen evolution at moderate overpotentials, the RuO_2 film electrode loses the potential of the hydrogen couple faster than Pt. In this respect our results run parallel with those of Galizzioli et al. [16].

Current density-potential plots for the HER can be analyzed in terms of the cathodic Tafel equation [44], which applies in the region where re-oxidation of H_2 is negligible and mass transfer of protons to the surface

current density (mA/cm²)

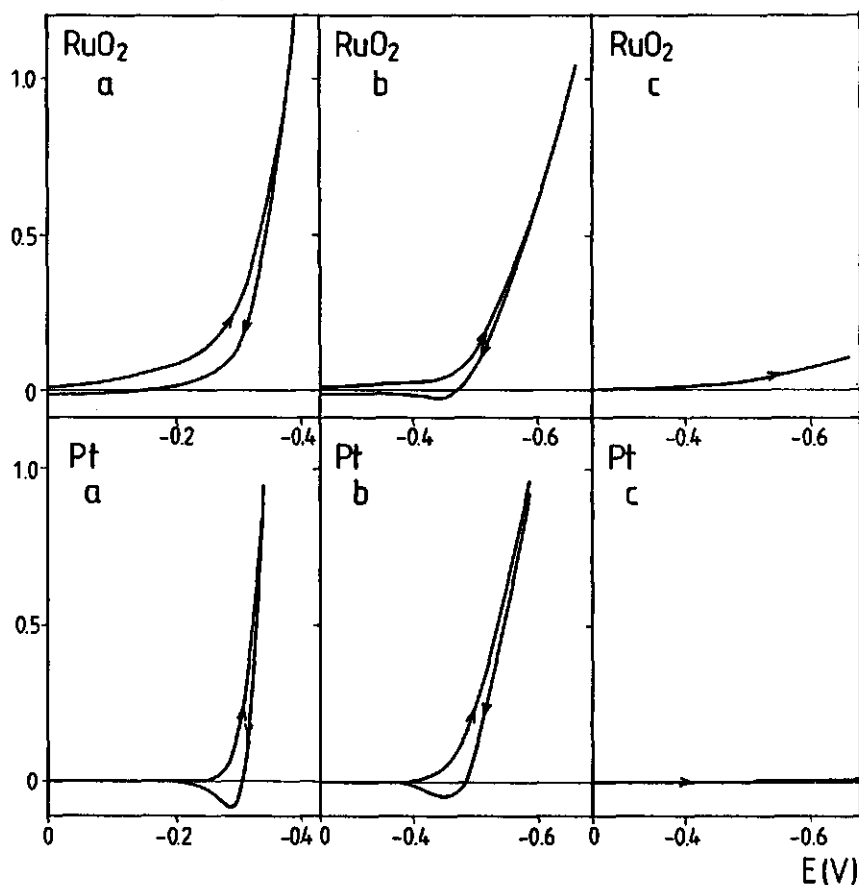


FIGURE 3.11: i - E curves for the HER on a RuO_2 film electrode and a smooth Pt electrode. Scan rate 0.5 mV/s, no stirring. a) 0.025 M HNO_3 , pH 1.6; b) 0.05 M acetate buffer, pH 4.6; c) 0.025 M KNO_3 , pH 4.6.

is not rate-limiting:

$$\eta = \frac{RT}{\alpha nF} (\ln i_0 - \ln i) \quad (3.9)$$

where η denotes the overpotential ($E - E_{\text{eq}}$, with E_{eq} the equilibrium potential for the H^+/H_2 couple), α the transfer coefficient, n the number of electrons involved in the rate determining step and i_0 the exchange current

density. Current densities i and i_0 are referred to the macroscopic surface area; for the RuO_2 film electrodes their real values will be lower by a factor of a few hundreds, depending on the surface roughness.

For unbuffered 0.025 M KNO_3 solutions of $\text{pH} > 2.6$, the low H^+ concentrations resulted in low mass transport limited current densities (i_L) and analysis in terms of the Tafel equation was not very well possible. Under conditions of non-stirring, the values for i_L for RuO_2 film electrodes and Pt electrodes were approximately the same and linear with H^+ concentration. This confirms that the surface irregularities on the RuO_2 electrode surface (order 10^{-7} – 10^{-5} m) are relatively small with respect to the thickness of the diffusion layers (order 10^{-4} m for the scan rate used). Stirring caused an increase of i_L , which was slightly larger for the RuO_2 film electrodes, in accordance with an increase in the effective electrochemical surface area with decreasing diffusion layer thickness.

Figure 3.12 gives representative "Tafel plots" (η as a function of $\log i$) for RuO_2 and Pt in 0.025 M HNO_3 ($\text{pH} 1.6$) and 0.05 M acetate buffer

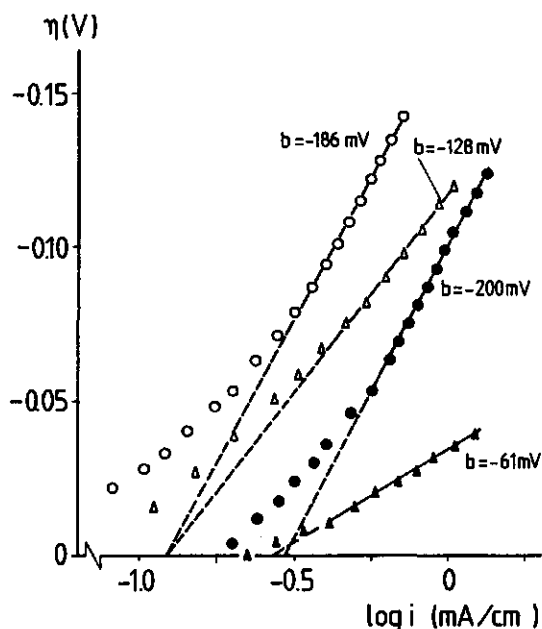


FIGURE 3.12: Tafel plots for the HER on a RuO_2 film electrode and a smooth Pt electrode. Open symbols: RuO_2 ; closed symbols: Pt. O, ●: 0.05 M acetate buffer, pH 4.6; Δ, ▲: 0.025 M HNO_3 , pH 1.6.

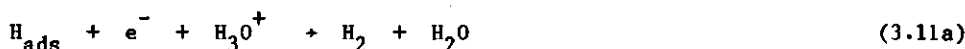
of pH 4.6. The slopes b of the linear part of the Tafel plots are indicated. Extrapolation of the Tafel lines to $\eta = 0$ yields the exchange current density i_0 . Values found for b and i_0 vary somewhat between different RuO₂ film electrodes (four electrodes were investigated with respect to the HER). Average values are listed in table 3.2. The large differences between b for RuO₂ and for Pt at pH 1.6 indicate that there is little or no influence of the platinum substrate on the behavior of the RuO₂ films. Considering the surface roughness of the RuO₂ films, i_0 per cm² real surface area is by some orders of magnitude smaller than for Pt.

Galizzoli et al. [16] have reported a Tafel slope of -60 mV for the HER on Ta-supported RuO₂ films in 1 M HClO₄ solutions; i_0 values found by these authors vary from 0.023 to 0.037 mA/cm². The HER on Pt is usually studied in 1 M solutions of strong acids. Reported values for b range from -30 to -120 mV and for i_0 from 0.25 to 2.5 mA/cm² [8-11,16]. The electrocatalytic properties of Pt for the HER depend strongly on the "activity" or "cleanliness" of the electrode and hence on the electrochemical pretreatment [9].

For the hydrogen evolution reaction, two reaction paths are generally accepted [9,10]. Both paths start with a primary discharge step (the Volmer reaction), which involves the formation of adsorbed H



but there are two options for the second step: an electrochemical desorption step (the Heyrovský reaction)



or a surface recombination step (the Tafel reaction)



Criteria for the determination of the reaction mechanism include the Tafel slope b . For example, a slope of ca. -120 mV can indicate either reaction path. A low value for b points to the Volmer-Tafel mechanism, with the Tafel reaction as rate determining step [9]. However, a conclusive decision about the mechanism cannot be made only on the basis of b values. A conclu-

sion that can be reached here is that, for both Pt and RuO₂, the mechanism for hydrogen evolution changes on going from a solution of strong acid (pH 1.6) to an acetate buffer solution (pH 4.6).

For the HER on Pt a parallel pathway has been proposed [9], i.e. the discharge step can be followed by both the electrochemical desorption step and the recombination step. The relative contributions of the different steps to the overall reaction rate can change with overpotential and pH. In alkaline solutions b is more negative and i_0 is smaller than in acid solutions. Galizzioli et al. [16] proposed (on the basis of the value of the Tafel slope of -60 mV and other -rather unclear- arguments) the Volmer-Heyrovský path for the HER on RuO₂ in 1 M HClO₄. The Heyrovský reaction was considered to be the rate determining step.

TABLE 3.2: Average electrode kinetic parameters for the HER on RuO₂ and Pt.

solution	electrode	b *) (mV)	i_0 *) (mA/cm ² geom. area)	approximate value of α
0.025 M HNO ₃ (pH 1.6)	RuO ₂	-127 (-121/-133)	0.12 (0.104/0.123)	0.5
	Pt	-56 (-51/-61)	0.28 (0.283/0.283)	1.0
0.05 M acetate (pH 4.6)	RuO ₂	-174 (-163/-186)	0.091 (0.071/0.123)	0.33
	Pt	-200	0.30	0.29

*) Numbers in brackets denote the range in which values for b and i_0 were found.

For modelling the hydrogen photoproduction system (chapter 6) the most important results reported here are those on RuO₂ in 0.05 M acetate buffer solution of pH 4.6, since this is the medium generally used in such systems (see chapter 5 and references therein). The complete Tafel plot (figure 3.12) is very well described by the Butler-Volmer equation [44]:

$$i = i_0 \left(e^{-\alpha n f \eta} - e^{(1-\alpha) n f \eta} \right) \quad (3.12)$$

using $n = 1$ and the obtained values for the Tafel slope and i_0 ; $f = F/RT$. This establishment again points to the chemical reversibility of the HER on RuO₂.

From figure 3.11 it can be concluded that for H⁺ reduction from a buffer

solution, the rate of the reaction is not determined by the concentration of free H^+ (compare the i - E plots for the buffered and unbuffered solutions of pH 4.6). A solution of 0.05 M acetate buffer of pH 4.6 has the same total concentration of H^+ as a 0.025 M HNO_3 solution. A remarkable finding is therefore that, for RuO_2 as well as for Pt, the i_0 values obtained in these two solutions are approximately the same. Acetic acid appears to be a labile proton donor, so that the protons associated with the buffer are also available for the HER in the considered potential range. This fact has been frequently overlooked in literature [45-47].

3.4 CONCLUSIONS

The pristine point of zero charge of the colloidal RuO_2 used throughout this work is positioned at $pH\ 5.75 \pm 0.05$. The surface charge-pH curves show similar characteristics as found for other oxides, the most striking feature being the high capacitance of the inner part of the double layer. The surface charge as a function of pH can be fitted satisfactorily with a simple double layer model.

From the analysis of the ionic composition of the double layer in the presence of Cl^- , which adsorbs specifically at the RuO_2 /solution interface, it is concluded that interfacial electrochemical studies of oxides, together with a thermodynamic analysis, can reveal specific adsorption at low levels, even below analytical detectability.

Evolution of hydrogen at moderate overpotentials does not modify the electrochemical behavior of RuO_2 film electrodes. This process appears to be chemically reversible. The mechanism in 0.05 M acetate buffer (pH 4.6) differs from that in 0.025 M HNO_3 (pH 1.6). In the buffer, the rate of hydrogen evolution is determined by the concentration of potentially available protons, i.e. by $[H^+] + [HAc]$. For this medium, which is used in the hydrogen photoproduction system, the slope of the Tafel line is ca. -174 mV ($\alpha = 0.33$) and the exchange current density is ca. 0.09 mA per cm^2 geometrical surface area of the electrodes. The true exchange current density is smaller by a factor depending on the roughness of the electrodes.

3.5 ACKNOWLEDGEMENTS

Thanks are due to Erna Rouwendal and Eric Van Bennekom for conducting electrophoretic mobility measurements. The RuO₂ film electrodes have been prepared by Erna Rouwendal, who also assisted in performing the voltammetric experiments. Mrs. A. Clerkx (TFDL, Wageningen) is kindly acknowledged for taking SEM micrographs of RuO₂ films.

3.6 REFERENCES

1. J. W. Bowden, A. M. Posner, and J. P. Quirk, *Aust. J. Soil Res.* **15** (1977) 121-136
2. M. A. F. Pyman, J. W. Bowden, and A. M. Posner, *Aust. J. Soil Res.* **17** (1979) 191-195
3. J. Lyklema, *J. Colloid Interface Sci.* **99** (1984) 109-117
4. S. Ardizzzone, P. Siviglia, and S. Trasatti, *J. Electroanal. Chem.* **122** (1981) 395-401
5. P. Siviglia, A. Daghetti, and S. Trasatti, *Colloids Surfaces* **7** (1983) 15-27
6. D. N. Furlong, D. E. Yates, and T. W. Healy, in "Electrodes of Conductive Metallic Oxides", Part B, S. Trasatti (ed.), Elsevier, Amsterdam (1981) pp 367-432
7. A. Daghetti, G. Lodi, and S. Trasatti, *Mater. Chem. Phys.* **8** (1983) 1-90
8. J. O'M. Bockris, *Mod. Aspects Electrochem.* **1** (1954) 180-276
9. B. E. Conway, and L. Bai, *J. Electroanal. Chem.* **198** (1986) 149-175
10. A. Saraby-Reintjes, *Electrochim. Acta* **31** (1986) 251-254
11. K. Machida, and M. Enyo, *Bull. Chem. Soc. Jpn.* **59** (1986) 725-731
12. A. K. Vijh, and A. Bélanger, *Int. J. Hydrogen Energy* **11** (1986) 147-151
13. S. Trasatti, and G. Buzzanca, *J. Electroanal. Chem.* **29** (1971) App.1-App.5
14. S. Pizzini, G. Buzzanca, C. Mari, L. Rossi, and S. Torchio, *Mater. Res. Bull.* **7** (1972) 449-462
15. D. Galizzioli, F. Tardini, and S. Trasatti, *J. Appl. Electrochem.* **4** (1974) 57-67
16. D. Galizzioli, F. Tardini, and S. Trasatti, *J. Appl. Electrochem.* **5** (1975) 203-214
17. G. Lodi, E. Sivieri, A. De Battisti, and S. Trasatti, *J. Appl. Electro-*

- chem. 8 (1978) 135-143
18. G. Lodi, G. Zucchini, A. De Battisti, E. Sivieri, and S. Trasatti, *Mater. Chem.* 3 (1978) 179-188
 19. S. Trasatti, and G. Lodi, in "Electrodes of Conductive Metallic Oxides", Part A, S. Trasatti (ed.), Elsevier, Amsterdam (1980) pp 301-358
 20. S. Trasatti, and W. E. O'Grady, in "Advances in Electrochemistry and Electrochemical Engineering", H. Gerisher and C.W. Tobias (eds.), John Wiley, New York (1981) pp 177-261
 21. S. Trasatti, *Electrochim. Acta* 29 (1984) 1503-1512
 22. A. J. McEvoy, and W. Gissler, Rep. Comm. Eur. Communities, Eur. no. Eur. 9315 (1984) 59 pp.
 23. W. Gissler, and A. J. McEvoy, *Solar Energy Mater.* 10 (1984) 309-316
 24. A. Breeuwsma, Ph. D. Thesis, Wageningen Agricultural University (1973)
 25. A. Breeuwsma, and J. Lyklema, *Discuss. Faraday Soc.* 52 (1971) 324-333
 26. R. Parsons, in "Handbook of Electrochemical Constants", Butterworths, London (1959)
 27. R. Parsons, and F. G. R. Zobel, *J. Electroanal. Chem.* 9 (1965) 333-348
 28. H. J. Van den Hul, and J. Lyklema, *J. Am. Chem. Soc.* 90 (1968) 3010-3015
 29. D. C. Grahame, *Chem. Rev.* 41 (1947) 441-448
 30. L. G. J. Fokkink, A. de Keizer, J. M. Kleijn, and J. Lyklema, *J. Electroanal. Chem.* 208 (1986) 401-403
 31. Th. F. Tadros, and J. Lyklema, *J. Electroanal. Chem.* 22 (1969) 1-8
 32. C. P. Huang, and W. Stumm, *J. Colloid Interface Sci.* 43 (1973) 409-420
 33. D. C. Grahame, *J. Phys. Chem.* 21 (1953) 1054-1060
 34. D. C. Grahame, and B. A. Soderberg, *J. Phys. Chem.* 22 (1954) 449-460
 35. J. Lyklema, *J. Electroanal. Chem.* 37 (1972) 53-60
 36. S. Levine, *J. Electroanal. Chem.* 20 (1969) 403-409
 37. V. E. Kazarinov, and V. N. Andreev, *Elektrokhimiya* 13 (1977) 685-690
 38. V. E. Kazarinov, and V. N. Andreev, *Elektrokhimiya* 14 (1978) 577-582
 39. A. N. Frumkin, *Z. Phys. Chem.* 116 (1925) 466
 40. R. H. Fowler, and E. A. Guggenheim, in "Statistical Thermodynamics", Cambridge University Press, London (1965) p 558
 41. H. P. Schwan, *Biophysik* 3 (1966) 181-201
 42. E. Lamy-Pitaru, L. Benchiraf, and J. Barbier, *Appl. Catal.* 18 (1985) 117-131
 43. R. N. Adams, in "Electrochemistry at Solid Electrodes", Marcel Dekker

Inc., New York (1969) p 23

44. A. J. Bard, and L. R. Faulkner, in "Electrochemical Methods, Fundamentals and Applications", John Wiley and Sons, New York (1980)
45. D. S. Miller, A. J. Bard, G. McLendon, and J. Ferguson, J. Am. Chem. Soc. **103** (1981) 5336-5341
46. D. S. Miller, and G. McLendon, J. Am. Chem. Soc. **103** (1981) 6791-6796
47. W. J. Albery, and A. J. McMahon, J. Electroanal. Chem. **182** (1985) 1-6

CHAPTER 4

ADSORPTION OF SENSITIZER, ELECTRON RELAY, AND ELECTRON DONOR AT THE RuO₂/SOLUTION INTERFACE AND ELECTRON TRANSFER BETWEEN ELECTRON RELAY AND THE RuO₂ CATALYST SURFACE

4.1 INTRODUCTION

The methylviologen cation MV^{2+} is the most frequently used electron relay in water photolysis systems [1]. A common scheme for its operation is the generation of the radical $MV^{\cdot+}$ after electron transfer from the excited state of a photosensitizer, e.g. ruthenium trisbipyridyl $Ru(bipy)_3^{2+}$ used in the present study. The reduced form $MV^{\cdot+}$ transfers the electron to the surface of a solid catalyst (usually colloidal particles), where subsequent reduction of water takes place. (See also figure 1.1.) The interaction of methylviologen with the catalyst surface is therefore of great importance in the performance of hydrogen production systems.

Strong ("preferential") adsorption of methylviologen at the catalyst/solution interface has been described in literature for catalyst compounds like Pt and Au [2-5]. The role of methylviologen in artificial photosynthetic devices has been evaluated on this basis. On the one hand it is argued [3] that strong adsorption of methylviologen makes it easier to transfer electrons from $MV^{\cdot+}$ to the catalyst. On the other hand adsorbed methylviologen could inhibit H₂ evolution by blocking active surface sites [3,5]. To add a third consideration, electron transfer from the sensitizer in the bulk solution to the surface of the catalyst via methylviologen is certainly inhibited if the available MV^{2+} ions are strongly bound in the catalyst/solution interface, without having a certain degree of mobility.

It is likely that also adsorption of the other constituents of the sacrificial water reduction system, i.e. the sensitizer and the electron donor, influence the catalytic hydrogen evolution. Furlong and coworkers [6-8] reported on the adsorption and desorption of sensitizers and relay compounds at oxide/electrolyte interfaces, including the RuO₂/electrolyte interface. It was found that adsorption of $Ru(bipy)_3^{2+}$ and MV^{2+} occurred in

response to attractive coulombic interactions with the negatively charged oxide surface, i.e. at pH values above the iso-electric point (i.e.p.). Apart from some data on the electrophoretic mobility of hematite particles in the presence of EDTA [9], there are -to our knowledge- no reported data on the adsorption behavior of this electron donor at oxide/solution interfaces.

This chapter deals with the adsorption of $\text{Ru}(\text{bipy})_3^{2+}$, EDTA, and MV^{2+} on the colloidal catalyst RuO_2 . Special attention will be paid to adsorption under experimental conditions comparable to those generally applied in the hydrogen evolution system, as described in chapter 5. In addition, the (specific) adsorption of MV^{2+} at the RuO_2 /solution interface in the presence and absence of indifferent electrolyte is evaluated. The electron transfer between methylviologen and RuO_2 is studied by means of voltammetric experiments with RuO_2 film electrodes.

4.2 EXPERIMENTAL

4.2.1 Materials

All chemicals used were reagent grade. Ruthenium tris(2,2'-bipyridyl) dichloride hexahydrate ($\text{Ru}(\text{bipy})_3^{2+}$) was obtained from Aldrich, N,N'-dimethyl-4,4'-bipyridinium dichloride trihydrate (methylviologen, MV^{2+}) from Fluka, and disodium ethylenediamine-N,N,N',N'-tetraacetate dihydrate (EDTA) from Merck.

Water was purified by reverse osmosis and subsequently passed through a Millipore Super-Q system (conductivity $< 0.8 \mu\text{S}/\text{cm}$). Concentrated stock solutions of $\text{MV}(\text{NO}_3)_2$ were obtained by potentiometric titration of MVCl_2 solutions with AgNO_3 . The AgCl formed was removed by centrifugation.

Two batches of colloidal RuO_2 , prepared at 405-420 °C and with BET specific surface areas of 21.5 and 26.3 m^2/g , respectively, were used in the experiments. Details on the preparation and characterization are described in chapter 2.

4.2.2 Adsorption experiments

The adsorption of $\text{Ru}(\text{bipy})_3^{2+}$, MV^{2+} , and EDTA on colloidal RuO_2 was determined by batchwise depletion measurements. 40-50 mg RuO_2 was weighed out into 10 ml polycarbonate centrifuge tubes. Solutions of the adsorbate and the other electrolytes at the selected initial pH were added in appropriate aliquots. The volumes were made up to 8 ml with water of the same pH and the RuO_2 was dispersed by ultrasonic vibration. After equilibration overnight (15-20 hours), during which the tubes were rotated end-over-end, the oxide was separated by centrifugation (25 minutes, 20,000 rpm). Subsequently, the equilibrium pH and adsorbate concentrations were determined.

Measurements of pH were carried out with a combined glass-Ag/AgCl electrode (Schott N59GN), calibrated with two buffers (pH 4.00 and 7.00, Titrisol, Merck).

$\text{Ru}(\text{bipy})_3^{2+}$ concentrations were determined from absorbance measurements at 452 nm, using an Hitachi 150-20 Spectrophotometer.

For determination of methylviologen concentrations, MV^{2+} was completely reduced to MV^{+} , and detected spectrophotometrically at 396 nm wavelength. Reduction was carried out by adding 1 ml of freshly prepared sodium dithionite reagent (50 mg $\text{Na}_2\text{S}_2\text{O}_4$ /25 ml 1 M KOH) to 5 ml solution [10].

EDTA concentrations were measured by potentiometric titrations with 0.01 M $\text{Cu}(\text{NO}_3)_2$ [11,12] using a Cu^{2+} ion-selective electrode (Orion, cat. no. 942900) and a saturated calomel reference electrode (Schott B2810). To obtain 100 % Cu^{2+} -EDTA complexation during titration, the solutions (5 ml) were brought to pH 10 by adding 3 ml buffer (pH 10.00, Titrisol, Merck).

Adsorptions were calculated from the differences between initial and final adsorbate concentrations. All adsorbed amounts have been corrected for adsorption on the polycarbonate tubes by running blank experiments. In the case of spectrophotometric measurements, blank experiments were also performed to correct for light absorbance by any residual RuO_2 .

4.2.3 Potentiometric acid-base titrations

Surface charge-pH curves were obtained for RuO_2 in the presence of $\text{MV}(\text{NO}_3)_2$ with and without supporting electrolyte (KNO_3). The apparatus and procedure adopted for potentiometric acid-base titrations have been de-

scribed already in chapter 3 (section 3.2.2). Here, the Ag/AgCl reference electrode (Schott B2920) used in the titration experiments was modified in that the KCl concentration was lowered from 3.5 to 0.5 M. This was done to minimize leakage of Cl^- , which adsorbs specifically on RuO_2 (section 3.3.2), into the titration cell. Stirring had no significant effect on the EMF of the cell.

4.2.4 Electrophoretic mobility measurements

The electrophoretic mobility of RuO_2 particles as a function of pH was measured at 20 °C in a MK II Zeta Sizer microelectrophoresis apparatus of Malvern Instruments Ltd.

4.2.5 Voltammetric experiments

Preparation of the RuO_2 film electrodes as well as the equipment and procedure applied in the voltammetric experiments have been described in sections 3.2.4 and 3.2.5, respectively. Cyclic voltammetric curves were measured at various scan rates in 5×10^{-3} M MV/0.025 M KNO_3 solutions of pH 6, in the absence and in the presence of EDTA (2×10^{-3} M).

4.3 RESULTS AND DISCUSSION

4.3.1 Adsorption of $\text{Ru}(\text{bipy})_3^{2+}$

The adsorption of $\text{Ru}(\text{bipy})_3^{2+}$ at the RuO_2 surface was investigated in the presence of 0.05 M acetate buffer (pH 4.6) and 0.02 M EDTA, which are conditions generally applied in the hydrogen photoproduction system (see chapter 5). It was found that under these circumstances no measurable adsorption of the sensitizer at the catalyst/solution interface takes place.

4.3.2 Adsorption of EDTA

In figure 4.1 adsorption isotherms for EDTA on RuO_2 at pH 4.1 and pH 5.4 are shown. At both pH values, adsorption increases with equilibrium concentration until a plateau is attained. Plateau values of ca. 1.0 and 1.2 $\mu\text{mol}/\text{m}^2$, respectively, are found. From these values an area occupied

per adsorbed species of $1.4\text{--}1.7\text{ nm}^2$ is calculated, which indicates a rather close packing of EDTA ions at the surface.

In the presence of indifferent electrolyte, the surface charge of RuO_2 in the pH range 4.1–5.4 is relatively low, i.e. between 0 and $-2\text{ }\mu\text{C}/\text{cm}^2$ (see figure 3.2). In this pH range, EDTA is mainly present in the form $\text{H}_2\text{EDTA}^{2-}$ ($\text{p}K_2 \approx 6.2$, $\text{p}K_3 \approx 2.7$ [13]), which means that the plateau adsorptions represent charges of about $-9\text{ }\mu\text{C}/\text{cm}^2$. This observation clearly points to specific adsorption, which is confirmed by electrophoretic mobility measurements (figure 4.2). The i.e.p. of RuO_2 particles in $5 \times 10^{-3}\text{ M}$ EDTA is found near pH 3, ca. 1.8 pH unit lower than the pristine point of zero charge (p.p.z.c.) of RuO_2 (section 3.3.1). Similar results have been reported for the metallic oxide hematite [9].

In the hydrogen photoproduction system (pH 4.6), the EDTA concentration is generally higher than $5 \times 10^{-3}\text{ M}$, which would imply that the RuO_2 catalyst surface is covered with EDTA to an appreciable extent. Due to the high ratio EDTA/catalyst area in this system (in most cases ca. $4\text{ mmol}/\text{m}^2$), most of the EDTA is still present in the bulk solution, where it can reduce the oxidized sensitizer.

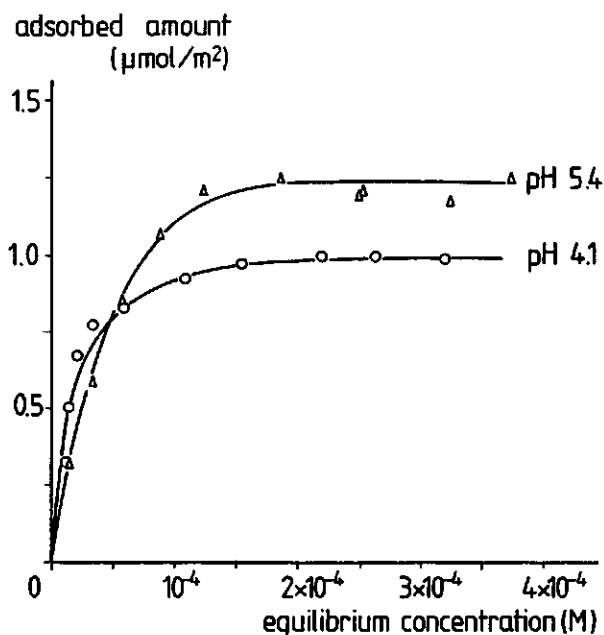


FIGURE 4.1: Adsorption isotherms of EDTA on RuO_2 . Background electrolyte $5 \times 10^{-3}\text{ M}$ KNO_3 .

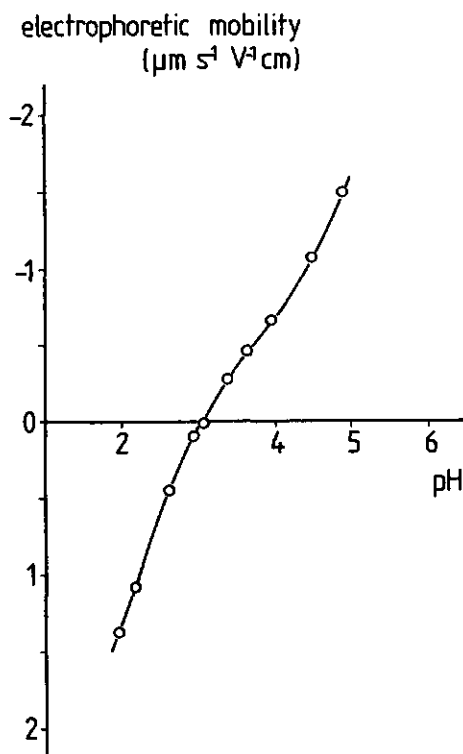


FIGURE 4.2: Electrophoretic mobility of RuO_2 particles in $5 \times 10^{-3} \text{ M EDTA}$.

4.3.3 Adsorption of MV^{2+}

The adsorption of MV^{2+} on RuO_2 in the presence of indifferent electrolyte (KNO_3) was investigated at pH values below and above the p.p.z.c. of RuO_2 . Below the p.p.z.c., no adsorption could be detected by means of depletion measurements. Adsorption isotherms at pH 7 are given in figure 4.3. In the absence of KNO_3 , the adsorption isotherm resembles that for the case where $5 \times 10^{-3} \text{ M KNO}_3$ is present, up to an equilibrium concentration of ca. $4 \times 10^{-4} \text{ M MV}^{2+}$. Above this concentration, the adsorption still increases and at $10^{-3} \text{ M MV}^{2+}$ the adsorbed amount is already ca. $1.4 \mu\text{mol/m}^2$. If methylviologen adsorbs in a flat orientation with both quaternary nitrogens adjacent to the oxide surface, the area occupied per adsorbed species would be approximately 0.9 nm^2 [6]. A close packing at the surface would then be reached when the adsorption level is about $1.8 \mu\text{mol/m}^2$.

The level of adsorption decreases with increasing ionic strength of the solution. The adsorption of MV^{2+} was also measured in the presence of phosphate buffer (pH 7), and an increase in adsorption was found with increasing buffer concentration. This is in contradiction with the observations of Furlong et al. [6], who reported that acetate and phosphate buffers produced the same effects as simple electrolytes like KNO_3 . Probably, specific adsorption of phosphate anions at the RuO_2 /solution interface induces extra adsorption of the methylviologen cation in the double layer of the oxide particles. Specific adsorption of phosphate on hematite particles is a well-known phenomenon [14].

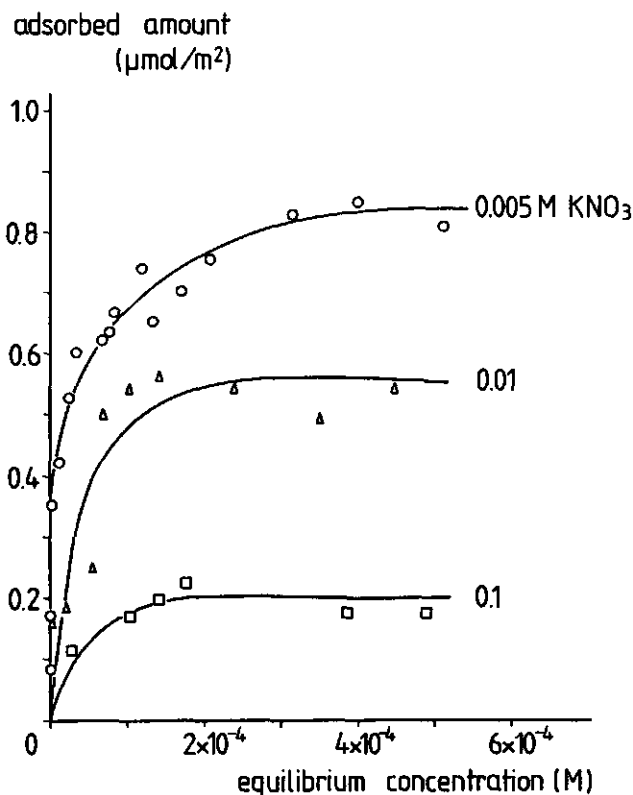


FIGURE 4.3: Adsorption isotherms of MV^{2+} on RuO_2 at various concentrations indifferent electrolyte, pH 7.

To clarify the adsorption behavior of MV^{2+} in more detail, the double layer properties of the RuO_2 /electrolyte interface in the presence of MV^{2+} were studied by means of potentiometric acid-base titrations and electrophoretic mobility measurements. Because Cl^- adsorbs specifically on RuO_2 as demonstrated in section 3.3.2, experiments were carried out using $MV(NO_3)_2$ instead of $MVCl_2$.

Surface charge-pH curves for RuO_2 in the presence of $MV(NO_3)_2$ are given in figure 4.4. The p.z.c. shifts to lower pH values with increasing $MV(NO_3)_2$ concentration and a (not entirely sharp) common intersection point is found at pH 5.3, which is lower than the p.p.z.c. Both facts indicate specific adsorption of MV^{2+} . This is confirmed by electrokinetic mobility measurements, demonstrating a shift of the i.e.p. in opposite direction (figure 4.5).

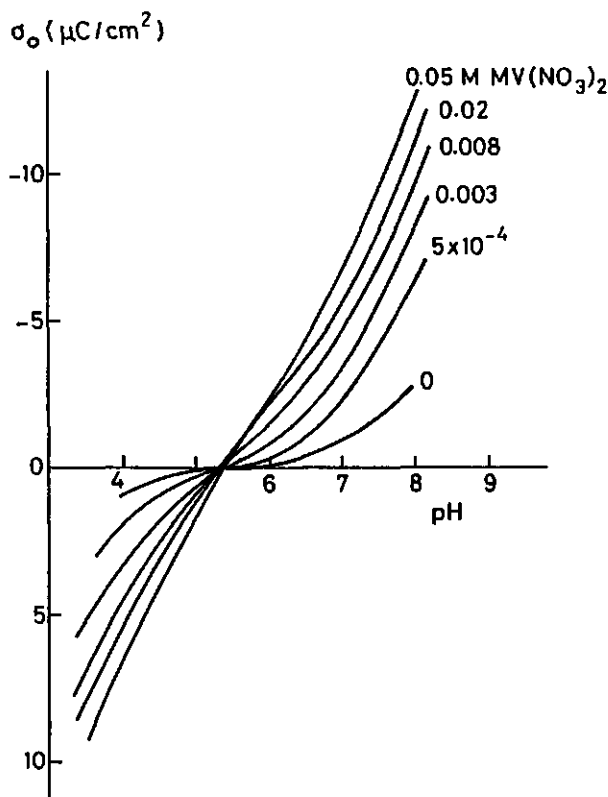


FIGURE 4.4: The surface charge of RuO_2 in the presence of methylviologen.

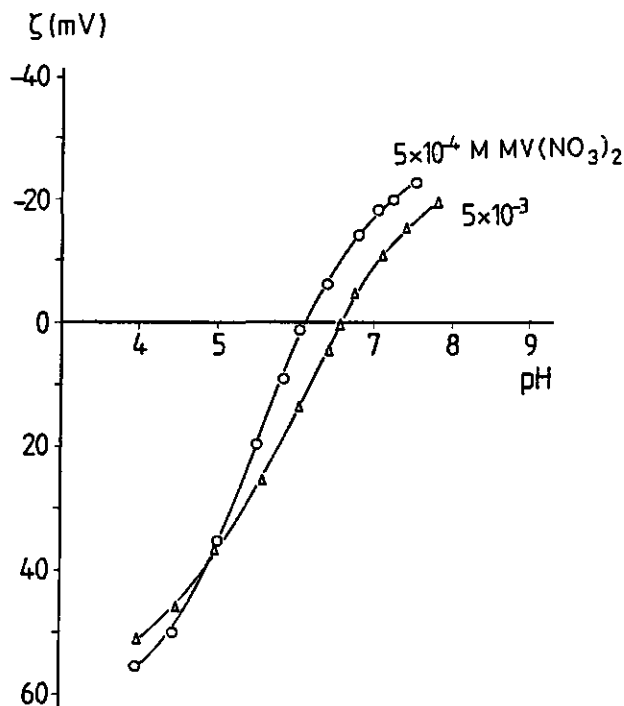


FIGURE 4.5: The ζ -potential of RuO_2 particles for two MV^{2+} concentrations.

In principle, it is possible to calculate the ionic composition of the double layer following the procedure described in section 3.3.2. Thermodynamic analysis of the adsorption of the various ionic species at the oxide/electrolyte interface gives, in the case of a 2:1 electrolyte [15,16]:

$$\left(\frac{\partial \sigma_+}{\partial \sigma_0}\right)_{c_s} = \frac{2}{3} \left(\frac{\partial \text{pH}}{\partial \log f_{\pm} c_s}\right)_{\sigma_0} - \frac{2}{3} \quad (4.1)$$

where σ_+ is the contribution to the countercharge of the bivalent cations, c_s the electrolyte concentration, and f_{\pm} the mean activity coefficient. The term $(\partial \text{pH} / \partial \log f_{\pm} c_s)_{\sigma_0}$, i.e. the Esin-Markov coefficient β , can be derived from the changes in the σ_0 -pH curves with $\text{MV}(\text{NO}_3)_2$ concentration.

Unfortunately, equation (4.1) cannot be applied unambiguously to the

experimental data displayed in figure 4.4. The main reason is that, in order to be in the range of relevance for water photoreduction, the MV^{2+} concentrations have been chosen so low that the contribution of KNO_3 , present due to titration with KOH and HNO_3 , cannot be neglected. For the lower $MV(NO_3)_2$ concentrations part of the experimentally determinable Esin-Markov coefficients is a result of the gradually increasing concentration of KNO_3 . (During the measurement of each titration curve, the KNO_3 concentration increases with ca. 10^{-3} M.) Therefore, only an analysis of the situation at the higher $MV(NO_3)_2$ concentrations will be presented here.

In figure 4.6 the Esin-Markov coefficient β is given as a function of σ_0 for 0.02 and 0.05 M $MV(NO_3)_2$. In the absence of specific adsorption, β ought to approach +1 for positive values of σ_0 and $-\frac{1}{2}$ for negative values of σ_0 [15]. For $MV(NO_3)_2$ this coefficient becomes lower than $-\frac{1}{2}$ and hence $(\partial\sigma_+/ \partial\sigma_0)$ becomes lower than -1. This means that as the surface becomes

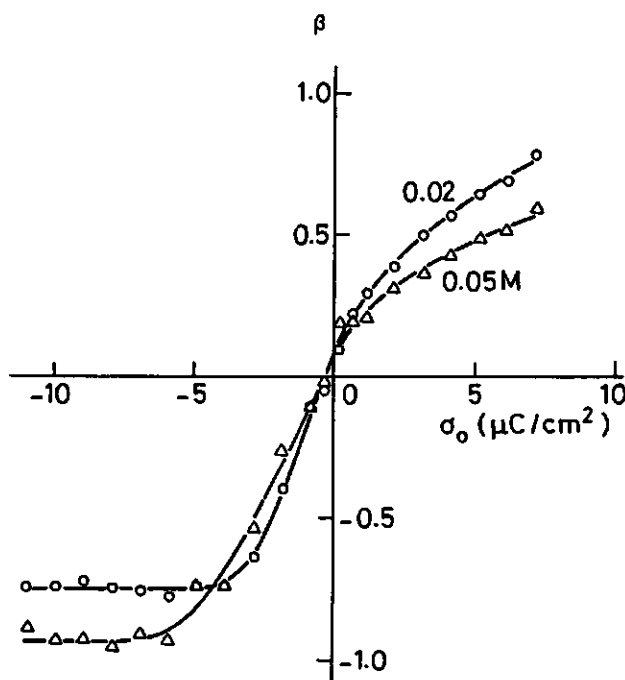


FIGURE 4.6: Esin-Markov coefficients as a function of surface charge for RuO_2 at two $MV(NO_3)_2$ concentrations.

more negative, the extra surface charge is overcompensated by extra adsorption of MV^{2+} . This superequivalent adsorption should lead to a reversal of sign of the ζ -potential. However, for these $MV(NO_3)_2$ concentrations electrokinetic data could not be obtained.

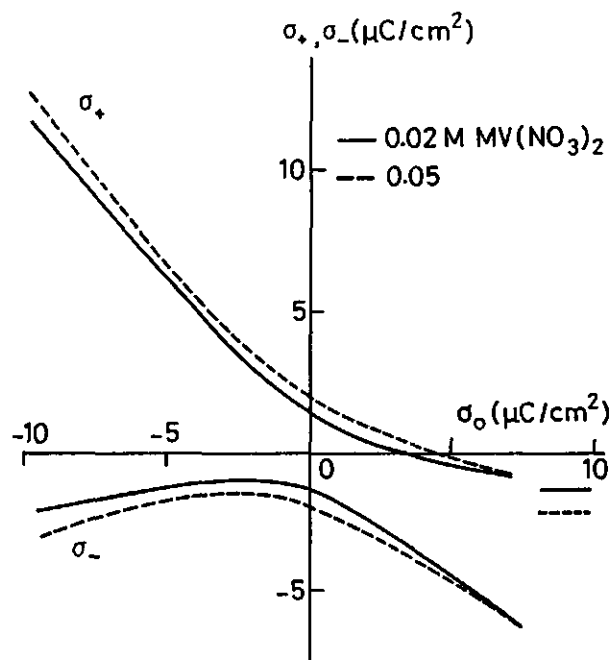


FIGURE 4.7: Ionic composition of the double layer on RuO_2 in $MV(NO_3)_2$ solutions. The theoretical limiting values of σ_+ at high positive surface charge are indicated.

Integration of equation (4.1) yields σ_+ as a function of σ_0 , apart from the integration constant $K(c_g)$. Values for $K(c_g)$ were estimated from the limiting values of σ_+ in the region of high positive surface charge [17], where specific adsorption of MV^{2+} becomes negligible. Values obtained are 1.4 ± 0.1 and $2.2 \pm 0.3 \mu C/cm^2$ for 0.02 and 0.05 M $MV(NO_3)_2$, respectively. In figure 4.7 the calculated ionic composition of the double layer is shown. The electrokinetic charge (surface charge plus specifically adsorbed charge) is positive over the entire σ_0 interval, so there is no i.e.p. any more. The amount of adsorbed MV^{2+} increases more than linearly when σ_0 becomes more negative.

The occurrence of superequivalent adsorption of MV^{2+} above the p.z.c. can also be inferred from the above described adsorption (depletion) measurements, although there is no complete quantitative agreement between the adsorption data and the results of the double layer analysis. For pH 7 and a MV^{2+} concentration of 5×10^{-4} M, an adsorption of $0.9 \mu\text{mol}/\text{m}^2$ has been found (figure 4.3), which represents a charge of $17 \mu\text{C}/\text{cm}^2$. According to the data of figure 4.4, the surface charge is only about $-2 \mu\text{C}/\text{cm}^2$. For 10^{-3} M MV^{2+} at the same pH the adsorption found was as high as $1.4 \mu\text{mol}/\text{m}^2$, i.e. $27 \mu\text{C}/\text{cm}^2$.

Figure 4.8 shows σ_0 -pH curves for RuO_2 in the presence of a constant concentration of 0.05 M KNO_3 and various $\text{MV}(\text{NO}_3)_2$ concentrations. The total ionic strength is comparable to that of the hydrogen production system. Only for 0.05 M $\text{MV}(\text{NO}_3)_2$ the p.z.c. is shifted to a significantly lower pH

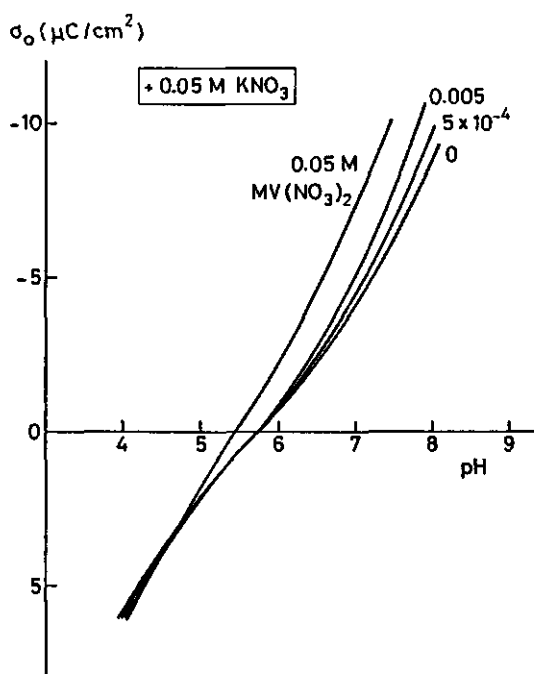


FIGURE 4.8: Surface charge of RuO_2 in various $\text{MV}(\text{NO}_3)_2$ solutions in the presence of indifferent electrolyte.

value. For the case of a mixed electrolyte (KNO_3 and $\text{MV}(\text{NO}_3)_2$), the following expression was derived:

$$\left(\frac{\partial \sigma_{\text{MV}}}{\partial \sigma_0}\right)_{c_1, c_2} = \frac{2(c_1 + c_2)}{c_1 + 3c_2} \left(\frac{\partial \text{pH}}{\partial \log f_{\pm c_2}}\right)_{\mu_{\text{KNO}_3}, \sigma_0} - \frac{2c_2}{c_1 + 3c_2} \quad (4.2)$$

in which c_1 and c_2 are the concentrations of KNO_3 and $\text{MV}(\text{NO}_3)_2$, respectively. For the curves of figure 4.8 obtained at the lower MV^{2+} concentrations, the condition of constant μ_{KNO_3} in equation (4.2) is met. Electrophoretic measurements revealed that for these methylviologen concentrations and an excess of KNO_3 , the i.e.p. is identical to that in the absence of MV^{2+} , which implies that the integration constants for calculating σ_{MV} from equation (4.2) are zero. Furthermore, in the pH region from 4.6 to 6, the differential quotient $(\partial \text{pH} / \partial \log f_{\pm c_2})_{\mu_{\text{KNO}_3}, \sigma_0}$ is approximately zero. Therefore, in this pH interval:

$$\sigma_{\text{MV}} \approx - \frac{2c_2}{c_1 + 3c_2} \sigma_0 \quad (4.3)$$

implying that for the lower $\text{MV}(\text{NO}_3)_2$ concentrations the contribution to the countercharge and the specific adsorption of MV^{2+} is negligible. It is therefore concluded that specific adsorption of MV^{2+} on RuO_2 does occur, but it is not particularly strong. The methylviologen cation is readily displaced from the double layer by an excess of K^+ , indicating that electrostatic interactions play a major role in its adsorbance. The suppression of methylviologen adsorption by indifferent electrolyte is also demonstrated by the adsorption isotherms displayed in figure 4.3.

These results indicate that in the hydrogen production system direct adsorption of MV^{2+} on the catalyst surface is not very important. However, in that system EDTA is one of the dominant electrolytes and adsorbs specifically at the catalyst surface, as shown above. It is imaginable that MV^{2+} is indirectly, via EDTA, adsorbed at the oxide/solution interface, although in solution complexation of $\text{H}_2\text{EDTA}^{2-}$ and MV^{2+} is negligible [18]. For this reason, the adsorption of MV^{2+} in the pH range 4.1-5.4 was also investigated in the presence of EDTA by means of depletion measurements. The EDTA

concentration was chosen high enough to obtain complete coverage of the RuO_2 surface with EDTA ions. No adsorption of MV^{2+} could be detected.

For the sake of completeness, adsorption of MV^{2+} was also determined under the conditions applied in the hydrogen production system, i.e. 0.05 M acetate buffer of pH 4.6 and 0.02 M EDTA. Again, no adsorption was found. A remaining uncertainty is connected with the actual potential of the RuO_2 particles during hydrogen evolution. According to the results of Siviglia et al. [19], the open-circuit potential of RuO_2 in indifferent electrolyte solutions at pH 4.6 is about +0.6 V/NHE. Under the conditions of hydrogen production, the potential of the particles is determined by the redox couples $\text{MV}^{2+}/\text{MV}^{+}$ and H^+/H_2 and is in the range between -0.45 and -0.27 V/NHE (see chapter 6). However, we do not expect too much influence from this change in potential on the adsorption of MV^{2+} (and $\text{Ru}(\text{bipy})_3^{2+}$), since the ionic strength of the reaction solution is high. This is confirmed by experiments with RuO_2 film electrodes, showing that MV^{2+} adsorption from 5×10^{-3} M methylviologen solutions containing an excess of KNO_3 is still not very important at potentials of about -0.45 V/NHE (next section).

4.3.4 Electron transfer between methylviologen and RuO_2

Cyclic voltammograms of methylviologen at a RuO_2 film electrode are shown in figure 4.9. A well-defined faradaic response is observed, centered around -625 mV versus $\text{Ag}/\text{AgCl}/3.5 \text{ M KCl}$, in agreement with the reported E^0 value for the $\text{MV}^{2+}/\text{MV}^{+}$ couple (-0.45 V/NHE [20]). Under identical conditions, in the absence of methylviologen, voltammograms of RuO_2 film electrodes only display a charging current in the potential range studied, except near -860 mV, where a considerable cathodic current is observed, due to water reduction.

The magnitudes of the cathodic peaks are in satisfactory agreement with the Randles-Ševčík equation [21] for a diffusion-controlled peak current. This indicates that adsorption of MV^{2+} at the RuO_2 /solution interface is not very important.

For a fully reversible one-electron transfer process a separation between cathodic and anodic peak of 57 mV at 20° C is predicted [21]. The increase in peak separation with increasing scan rate points to quasi-reversible behavior, i.e. the overall rate of the electrode reaction is determined by both electron transfer kinetics and mass transfer of methyl-

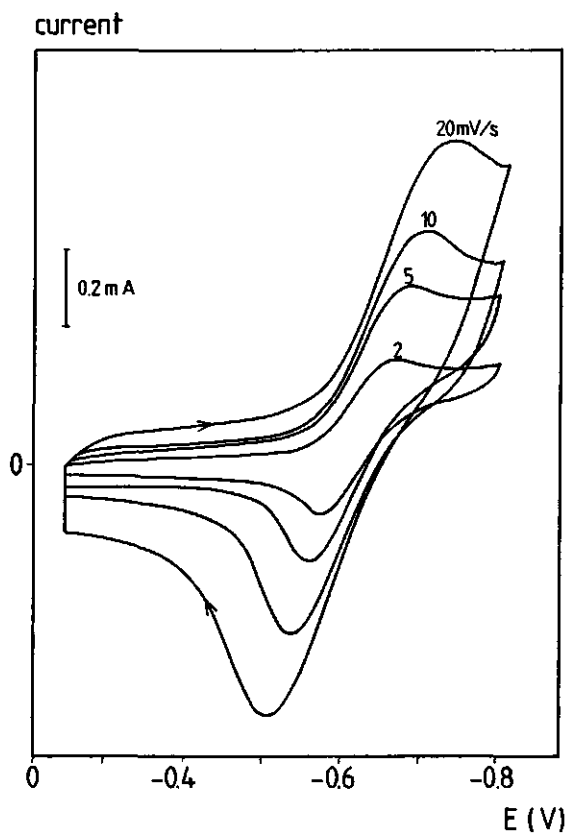


FIGURE 4.9: Cyclic voltammograms of a RuO_2 film electrode in an unstirred 5×10^{-3} M methylviologen solution of pH 6 (supporting electrolyte 0.025 M KNO_3).

viologen to the electrode. Following the method outlined by Matsuda and Ayabe [22], and using a diffusion coefficient of $8 \times 10^{-10} \text{ m}^2/\text{s}$ for both MV^{2+} and MV^{+} [5], the standard heterogeneous electron transfer rate constant k^0 was evaluated to be about $1.4 \times 10^{-5} \text{ m/s}$, with a transfer coefficient α between 0.3 and 0.4. For a smooth Pt electrode also quasi-reversible behavior with respect to the reduction and oxidation of methylviologen was found, the heterogeneous rate constant being in the order of $2 \times 10^{-5} \text{ m/s}$.

The standard heterogeneous rate constant found for the RuO_2 film electrode refers to its macroscopic area, since the surface irregularities are small compared to the thickness of the diffusion layer around the electrode

(order 10^{-4} m for the scan rates used). Taking into account the roughness of the electrode (see section 3.3.4), the true value of k^0 is considerably smaller.

The experiments were repeated in the presence of EDTA (2×10^{-3} M), yielding identical results. It is therefore concluded that the presence of EDTA does not significantly influence the electron transfer between methylviologen and RuO_2 .

4.4 CONCLUSIONS

Methylviologen exhibits specific adsorption behavior with respect to the RuO_2 surface, and at negative surface charges superequivalent adsorption can take place. However, the specific adsorption behavior is weak and no longer noticeable in the presence of an excess of indifferent electrolyte.

Under the conditions applied in the hydrogen production system (chapter 5), adsorption of the sensitizer $\text{Ru}(\text{bipy})_3^{2+}$ and the electron relay MV^{2+} at the catalyst/solution interface is not important, while there is appreciable adsorption of the electron donor EDTA. However, most of the electron donor is still present in the bulk solution, where it can reduce the oxidized sensitizer. The electron transfer from sensitizer to catalyst surface is probably favoured by the mobility of the electron relay ("hit & run" mechanism), although mass transfer of this compound is a potential rate determining step in the hydrogen production system. The electron transfer rate between methylviologen and the catalyst, as measured at RuO_2 film electrodes, takes place with a standard heterogeneous rate constant of ca. 1.4×10^{-5} m/s, and a transfer coefficient α between 0.3 and 0.4. The true heterogeneous rate constant is smaller by a factor depending on the roughness of the electrodes. In applying the results for the kinetic parameters to the hydrogen production system (chapter 6), this point will be taken into account.

4.5 ACKNOWLEDGEMENTS

Erna Rouwendal and Eric van Bennekom are gratefully acknowledged for carrying out adsorption and electrophoretic mobility measurements. RuO_2 film electrodes have been prepared by Erna Rouwendal, who also performed

the voltammetric experiments.

4.6 REFERENCES

1. E. Amouyal, *Sci. Pap. Inst. Phys. Chem. Res.* **78** (1984) 220-231
2. B. Beden, O. Enea, F. Hahn, and C. Lamy, *J. Electroanal. Chem.* **170** (1984) 357-361
3. O. Enea, *Electrochim. Acta* **30** (1985) 13-16
4. P. Crouigneau, O. Enea, and B. Beden, *J. Electroanal. Chem.* **218** (1987) 307-317
5. W. J. Albery, P. N. Bartlett, and A. J. McMahon, in "Photogeneration of Hydrogen", A. Harriman, and M. A. West (eds.), Academic Press, London (1982) pp 85-103
6. D. N. Furlong, and W. H. F. Sasse, *Colloids Surfaces* **7** (1983) 29-52
7. D. N. Furlong, and W. H. F. Sasse, *Colloids Surfaces* **7** (1983) 115-119
8. D. N. Furlong, Y.-M. Tricot, J. D. Swift, and W. H. F. Sasse, *Aust. J. Chem.* **37** (1984) 703-711
9. C.-C. Lo, E. Matijević, and N. Kallay, *J. Phys. Chem.* **88** (1984) 420-424
10. A. Calderbank, and S. H. Yuen, *Analyst* **90** (1965) 99
11. H. A. Flaschka, in "EDTA Titrations, an Introduction of Theory and Practice", 2nd ed., Pergamon Press, Oxford (1964) pp 116-117
12. T. S. West, in "Complexometry with EDTA and Related Reagents", 3rd ed., BDH Chemicals Ltd., Poole (1969) pp 181-183
13. L. G. Sillén, and A. E. Martell, in "Stability Constants of Metal-Ion Complexes", Chem. Soc. Spec. Publ. **17**, Metcalfe and Cooper Ltd., London (1964)
14. A. Breeuwsma, and J. Lyklema, *J. Colloid Interface Sci.* **43** (1973) 437-448
15. J. Lyklema, *J. Electroanal. Chem.* **37** (1972) 53-60
16. J. Lyklema, *J. Colloid Interface Sci.* **99** (1984) 109-117
17. D. C. Grahame, *J. Phys. Chem.* **21** (1953) 1054-1060
18. J. Kuczynski, and J. K. Thomas, *Langmuir* **1** (1985) 158-161
19. P. Siviiglia, A. Daggetti, and S. Trasatti, *Colloids Surfaces* **7** (1983) 15-27
20. A. Harriman, and G. Porter, *J. Chem. Soc., Faraday Trans. 2* **78** (1982) 1937-1943
21. A. J. Bard, and L. R. Faulkner, in "Electrochemical Methods, Fundamen-

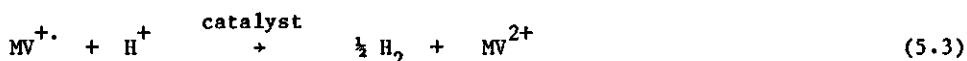
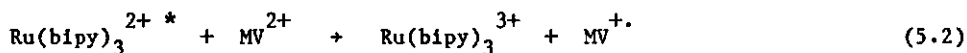
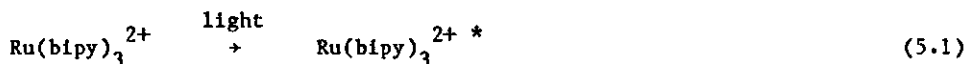
- tals and Applications", John Wiley and Sons, New York (1980)
22. H. Matsuda, and Y. Ayabe, Z. Electrochem. **59** (1955) 494-500

CHAPTER 5

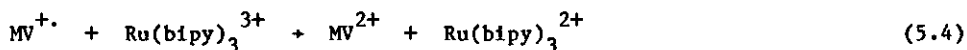
PHOTOGENERATION OF HYDROGEN IN THE Ru(bipy)₃²⁺/MV²⁺/EDTA/colloidal RuO₂ SYSTEM

5.1 INTRODUCTION

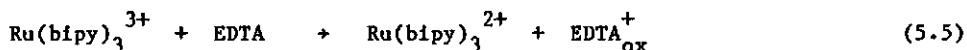
In a sacrificial system for photoproduction of hydrogen, containing ruthenium trisbipyridyl (Ru(bipy)₃²⁺) as the sensitizer and methylviologen (MV²⁺) as the electron relay, the following reactions lead to formation of hydrogen [1]:



The presence of (an excess) of an electron donor, like EDTA, prevents the undesired back-reaction



by reduction the oxidized sensitizer to the original substrate:



The oxidation product of EDTA decomposes irreversibly, hence the term "sacrificial".

It is generally accepted that reaction (5.3) does not take place in the bulk solution (see reference [2] and references therein). The reaction must take place at the surface of a catalyst and involves several steps, i.e. mass transfer of MV⁺ and H⁺ to the surface, electron transfer from MV⁺ to the catalyst, proton discharge and subsequent formation of H₂ at

the surface, and finally desorption of H_2 . Formation of hydrogen is thermodynamically feasible if

$$\log \frac{[MV^{+}]}{[MV^{2+}]} > \frac{F}{2.303 RT} E^{\circ} + pH + \frac{1}{2} \log p_{H_2} \quad (5.6)$$

where E° is the standard redox potential of the MV^{2+}/MV^{+} couple (-0.45 V/NHE [3]) and p_{H_2} denotes the partial H_2 gas pressure.

With colloidal Pt as the catalytic compound, generally stabilized by polymers or deposited on inorganic substrates, this system has been the subject of many studies [1-13]. In attempts to optimize its efficiency, the hydrogen production has been investigated as a function of the concentrations of sensitizer, electron relay, and electron donor, the pH, the amount of Pt, and the type of stabilizing agents.

Ruthenium dioxide, which is commonly used to catalyze the photo-oxidation of water, is also a suitable catalyst for water reduction [7,14,15]. It has been shown in sections 3.3.4 and 4.3.4 of this work, that the rates of hydrogen evolution and electron transfer from MV^{+} on RuO_2 film electrodes are, per microscopic surface area, much lower than on smooth Pt electrodes. This implies that more surface area of RuO_2 than of Pt is needed to obtain the same hydrogen production rate. However, in contrast to Pt, RuO_2 does not catalyze the irreversible hydrogenation of the relay methylviologen [15] and therefore appears to be a good alternative. It has also been suggested [15] that the efficiency of RuO_2 is related to its inability to dissociate H_2 , which would result in chemical irreversibility of the hydrogen evolution reaction. However, experiments with RuO_2 film electrodes conducted in our laboratory do not confirm this idea (see section 3.3.4).

Keller et al. [14,15] investigated the dependence of the hydrogen formation rate and total hydrogen yield on the pH of the reaction solution and on the amount of RuO_2 present in the system. Characterization of the RuO_2 used (commercially available, obtained from Alfa Ventron) is lacking, but it is presumably composed of small particles with a rather undefined stoichiometry (according to reference [16], the RuO_2 powder in question has a BET surface area of $67 \text{ m}^2/\text{g}$ and an i.e.p. at pH 3.3). In the range between 30 and 120 $\mu\text{mol RuO}_2$ per 30 ml solution, no effect of the catalyst

amount was observed. With respect to the pH, an optimum in hydrogen production was found around pH 5. The existence of this optimum is due to two opposite effects. A decrease in pH favours the formation of hydrogen, both from a thermodynamic and a kinetic point of view, but is also attended with loss of efficiency of the electron donor EDTA [1]. To our knowledge, no other systematic studies on the performance of the $\text{Ru}(\text{bipy})_3^{2+}/\text{MV}^{2+}/\text{EDTA}/\text{RuO}_2$ system have been reported.

In this chapter experiments are described and discussed in which the light-induced formation of hydrogen takes place at the surface of well-defined colloidal RuO_2 . On the basis of the results of Keller et al., the standard value of the pH of the reaction solution has been chosen at 4.6. The influence of the light intensity, the concentration of the various compounds in solution (including the buffer concentration), the amount of catalyst, the temperature, the stirring rate, the presence of several polymers intended to stabilize the catalyst, and the presence of H_2 in the gas phase is investigated. Besides the hydrogen formation rate and yield, the MV^{+} concentration during hydrogen evolution is also monitored. As can be deduced from equation (5.6), the concentration MV^{+} is an important parameter in the performance of the system. The experimental results obtained will be used in the next chapter to analyze the rate-limiting steps in the hydrogen production system on the basis of a kinetic model.

5.2 EXPERIMENTAL

5.2.1 Materials

All chemicals used were reagent grade. Ruthenium tris(2,2'-bipyridyl) dichloride hexahydrate was obtained from Aldrich, $\text{N,N}'$ -dimethyl-4,4'-bipyridinium dichloride trihydrate (methylviologen) from Fluka, and disodium ethylenediamine- $\text{N,N,N}',\text{N}'$ -tetraacetate dihydrate (EDTA) from Merck.

Water was purified by reverse osmosis and subsequently passed through a millipore Super-Q system (conductivity $< 0.8 \mu\text{S}/\text{cm}$).

Colloidal RuO_2 was prepared by thermal decomposition of RuCl_3 at 405-420 °C. Details on the preparation and characterization are given in chapter 2. Different batches of RuO_2 show a slight variation in BET surface area, but no significant variation in catalytic behavior with respect to hydrogen evolution was observed. In the experiments described here, a batch

with BET surface area of $21.5 \text{ m}^2/\text{g}$ was used.

Polymers and surfactant used as stabilizing agents for the RuO_2 particles are polyvinyl alcohol (PVA), polyvinyl pyrrolidone (PVP), dextran, and Synperonic NPE 1800 (see table 2.2, chapter 2).

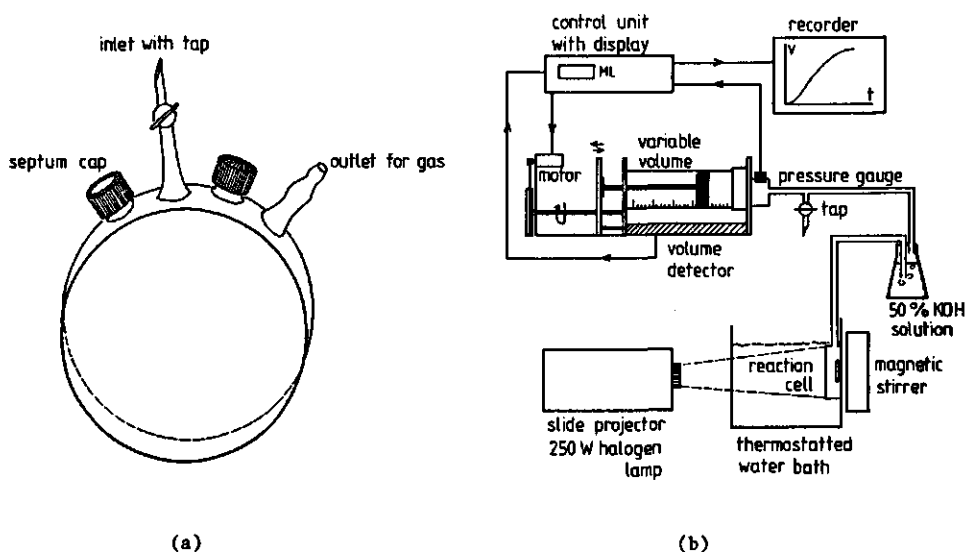


FIGURE 5.1: Schematics of experimental equipment. (a) Reaction cell, (b) experimental set-up.

5.2.2 Irradiation procedure

Steady state irradiations were carried out using a Perkeo AFS Professional slide projector (Zeiss Ikon) with a 250 W halogen lamp. Figure 5.1a shows the glass reaction cell used in the experiments. It has flat windows and is provided with an outlet for gas, an inlet with tap for gas flushing, a septum cap for taking gas samples and an extra opening for pH or temperature measurements. The reaction vessel is placed in a thermostatted water bath. The water bath has also a function as IR filter (ca. 12 cm water

between vessel and light source).

A schematic diagram of the experimental set-up is given in figure 5.1b. The reaction cell is filled with reaction solution (58 ml) and a given amount of RuO_2 , dispersed by ultrasonic vibration. Before each experiment, the system is generally deaerated for 30 minutes by nitrogen flushing. The reaction mixture is continuously stirred. The gas produced during the experiments is bubbled through a concentrated KOH solution (50 %) and collected at room temperature in a home-built volumeter, in which the total pressure is kept at 1 atmosphere (within 1 mbar). The produced volume of gas is automatically recorded as a function of irradiation time. The hydrogen production rates and total hydrogen production are determined from the slopes and plateau values of the resulting plots. Variations in the temperature of the laboratory cause variations in the total volume of the gas phase of 1 ml at the most. Leakage of gas out of the system was always less than 0.1 ml/hr.

For measurements of the temperature in the reaction cell, an electrical resistor with negative temperature coefficient (NTC) was used. The pH in the cell was measured with a small combined pH electrode (Schott).

Unless otherwise stated, the composition of the reaction solution is: 2×10^{-4} M $\text{Ru}(\text{bipy})_3^{2+}$, 5×10^{-4} M MV^{2+} , 0.02 M EDTA, and 0.05 M acetate buffer (pH 4.6). The temperature in the reaction cell is 20-21 °C.

5.2.3 Gas analysis

The collected gas was identified by gas liquid chromatography (GLC), using a Pye Unicam GCD apparatus with conductivity detector, molecular sieve column 80-100 MESH, and argon as the carrier gas. In this way H_2 and N_2 can be detected, O_2 , if present, will form a shoulder on the N_2 peak.

5.2.4 Incident light intensity

The light intensity as a function of wavelength was measured using a Photodyne Optical Power Meter model 66XLA and various interference filters (half maximum bandwidth 10-20 nm). The power meter and an interference filter were placed in a black tube at some distance behind the reaction cell, which contained clean water. Only light which passed the cell (and the water bath) in a straight line could reach the meter via the filter.

The intensity of the light falling on the reaction cell was calculated from the measured intensity, taking into account the interference filter characteristics, the divergency of the light beam and the extra glass/air transition (no correction is needed for extra glass/water transitions). The incident light intensity I_0 as a function of wavelength is given in figure 5.2. The light intensity varied somewhat in time and for different halogen lamps (generally less than 10 %).

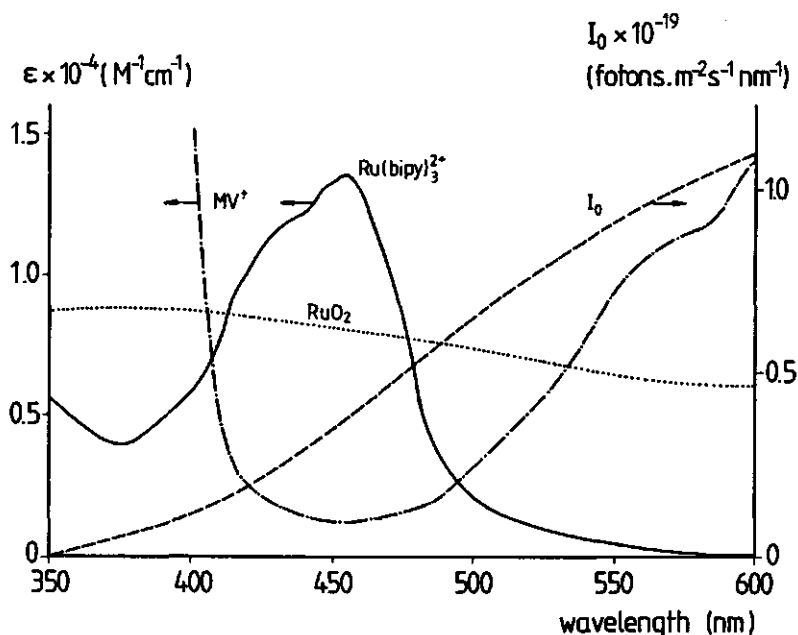


FIGURE 5.2: The incident light intensity I_0 and the absorption spectra of $\text{Ru}(\text{bipy})_3^{2+}$, MV^{+} , and RuO_2 in the wavelength interval relevant for excitation of the sensitizer. The left ordinate indicates the extinction coefficients of $\text{Ru}(\text{bipy})_3^{2+}$ and MV^{+} , the right one the light intensity. The optical density of RuO_2 at 600 nm is $1.62 \text{ g}^{-1} \text{ l cm}^{-1}$.

5.2.5 Measurement of $\text{Ru}(\text{bipy})_3^{2+}$ and methylviologen concentrations

The total methylviologen and $\text{Ru}(\text{bipy})_3^{2+}$ concentrations in the reaction mixture after illumination were determined spectrophotometrically, using an Hitachi 150-20 Spectrophotometer. First the colloidal RuO_2 (if

present) was removed by centrifugation (25 minutes, 20,000 rpm). $\text{Ru}(\text{bipy})_3^{2+}$ was detected at 452 nm wavelength, where no light is absorbed by MV^{2+} or the other components of the reaction solution. (MV^{+} , which absorbs light in the visible spectrum, is not stable in the presence of oxygen and is converted into MV^{2+} when the solution is exposed to air.) The extinction coefficient $\epsilon(452)$ of $\text{Ru}(\text{bipy})_3^{2+}$ was obtained from a standard series.

For determination of the methylviologen concentration, MV^{2+} was completely reduced to MV^{+} by adding 1 ml of freshly prepared sodium dithionite reagent (50 mg $\text{Na}_2\text{S}_2\text{O}_4$ /25 ml 1 M KOH) to 5 ml solution [17]. The radical MV^{+} exhibits a broad absorption peak around 603 nm wavelength, at which the other components of the reaction solution do not absorb light. The extinction coefficient of MV^{+} at 603 nm was found to be $1.40 \times 10^4 \text{ M}^{-1}\text{cm}^{-1}$, which is in fair agreement with values reported in literature, also for electrochemically and photochemically generated methylviologen radicals [18-20].

5.2.6 In situ measurement of MV^{+} concentration

During hydrogen production the concentration of methylviologen radicals was determined at regular time intervals by absorbance measurements at 600 nm wavelength. The light intensity transmitted through the reaction cell was measured using the optical power meter and an interference filter of 600 nm in the same way as described in section 5.2.4. (To this end the magnetic stirrer had to be removed temporarily; the measurement was done within 15 seconds.) To obtain the transmission (absorbance) of the reaction solution, the cell was lifted out of the water bath, making it possible to measure the incident light intensity I_0 too.

The concentration of MV^{+} was calculated using $l = 1.5 \text{ cm}$ (length of the light path), $\epsilon(600 \text{ nm}) = 1.4 \times 10^4 \text{ M}^{-1}\text{cm}^{-1}$, and taking into account the optical density of the RuO_2 particles. The latter value was obtained by measurements at $t = 0$ when no MV^{+} is yet present.

From experiments with different amounts of RuO_2 it was found that the optical density of the (flocculated) catalyst particles varies linearly with their concentration and the extinction coefficient at 600 nm amounts to $1.62 \text{ g}^{-1} \text{ l cm}^{-1}$.

5.3 RESULTS

5.3.1 Variation of hydrogen production with time

Under illumination of the standard reaction solution containing colloidal RuO_2 , the formation of gas bubbles is rapidly noticeable. In figure 5.3 typical V-t plots are given. After an induction time of about 20-25 minutes, the rate of gas production becomes constant. The slope of the plot at this stage is called the (steady state) rate of hydrogen production, r_{H_2} . After several hours the production rate decreases to zero.

No hydrogen evolution was observed in the absence of either MV^{2+} , $\text{Ru}(\text{bipy})_3^{2+}$, or EDTA.

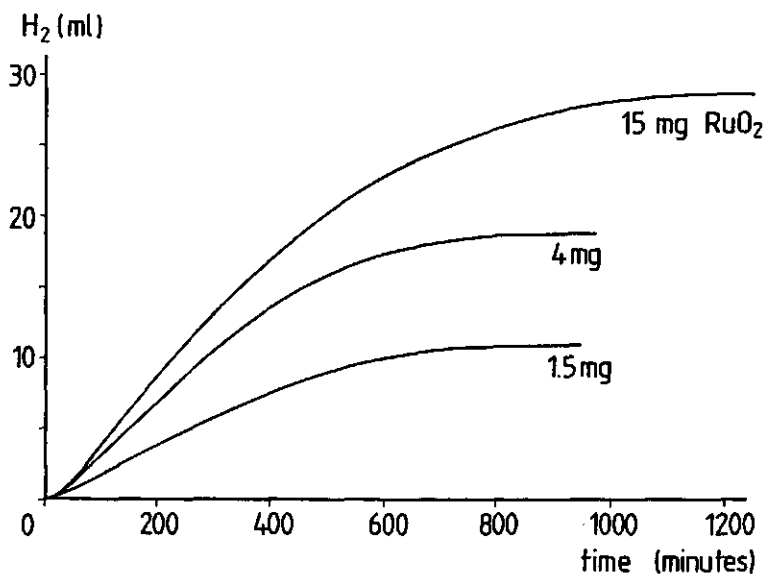


FIGURE 5.3: Hydrogen production as a function of time. Steady state rates of production are 1.3, 2.3, and 3.0 ml/hr for increasing amounts of RuO_2 .

5.3.2 Formation and disappearance of $MV^{\cdot+}$ in the absence of catalyst

In the absence of RuO_2 catalyst, the color of the reaction solution changed under illumination within a few minutes from orange (the color of $Ru(bipy)_3^{2+}$) to green, indicating accumulation of $MV^{\cdot+}$ radicals. The presence of these radicals has been confirmed by an EPR (Electron Paramagnetic Resonance) experiment and by spectrophotometrical measurements. Both the EPR and the absorption spectrum of $MV^{\cdot+}$ are easily recognized [18,21]. The rate of gas production was not significant and only a small amount of hydrogen (at the threshold of detection) could be found in the gas phase.

The light-induced formation of $MV^{\cdot+}$ in the absence of catalyst was monitored for different methylviologen concentrations (figure 5.4). After

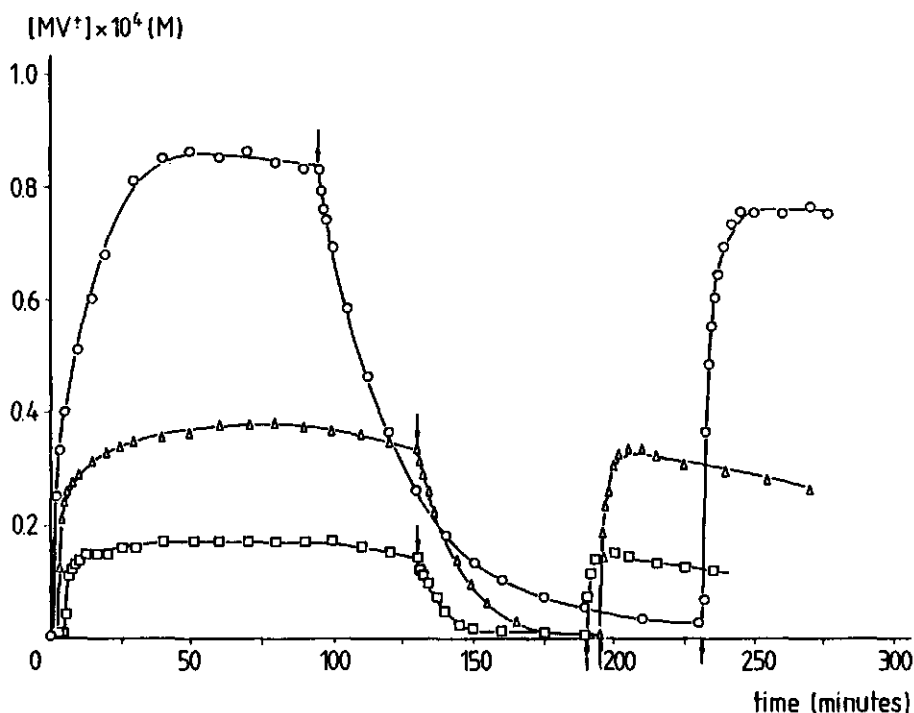


FIGURE 5.4: Formation and disappearance of $MV^{\cdot+}$ radicals in the reaction solution without catalyst. Total methylviologen concentration: $\circ - 5 \times 10^{-4}$ M, $\Delta - 2 \times 10^{-4}$ M, $\square - 1 \times 10^{-4}$ M. At time $t = 0$, irradiation of the solution starts. \downarrow indicates switching off of the light; at \uparrow the light is switched on again.

1-5 minutes of irradiation the radical is formed rapidly. The time scale on which the measurements are performed does not allow determination of the initial formation rates ($> 10^{-7}$ M/s). The $MV^{+\cdot}$ concentration reaches a plateau value which is only a fraction of the total methylviologen concentration (17-18.5 %). When the light is switched off, the radical concentration drops to zero. Under resumed illumination it returns to almost its original level. Analysis of the decay in the dark showed that, within experimental error, this process obeys first order kinetics in $MV^{+\cdot}$ concentration. The (pseudo) first order rate constant found is $1.0 \pm 0.3 \times 10^{-3} \text{ s}^{-1}$ (average value for four different methylviologen concentrations).

Under prolonged illumination the $MV^{+\cdot}$ concentration decreases slowly. After more than 15 hours the presence of $MV^{+\cdot}$ cannot be detected anymore. Subsequent determination of the total methylviologen concentration revealed that all of it has been destructed.

5.3.3 Influence of light intensity, $\text{Ru}(\text{bipy})_3^{2+}$, and EDTA concentration

The intensity of the incident light was varied by incorporating neutral density filters into the light path. The influence of the light intensity on the steady state production rate of hydrogen is displayed in figure 5.5.

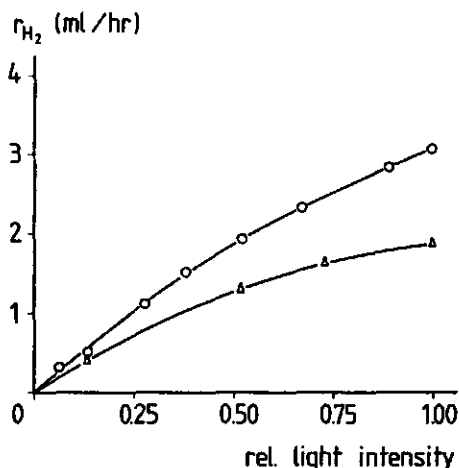


FIGURE 5.5: Influence of the light intensity on the steady state production rate of hydrogen. Δ - 3 mg RuO_2 , O - 15 mg RuO_2 .

The effect of $\text{Ru}(\text{bipy})_3^{2+}$ concentration on the hydrogen production is given in table 5.1. Under the standard conditions, the steady state production rate and MV^{+} concentration hardly depend on the sensitizer concentration.

No significant effect of varying the EDTA concentration from 0.02 to 0.2 M on the hydrogen production was observed (table 5.2). Below 0.02 M, the production rate decreases with decreasing EDTA concentration. Under extreme conditions, e.g. at relatively high concentrations of RuO_2 and methylviologen, the amount of EDTA originally present can limit the total H_2 yield, without affecting the initial production rate.

TABLE 5.1: Influence of sensitizer concentration on the steady state hydrogen production rate and MV^{+} concentration.

	$[\text{Ru}(\text{bipy})_3^{2+}]$ (M)	r_{H_2} (ml/hr)	$[\text{MV}^{+}]$ (M)
1.5 mg RuO_2	1×10^{-4}	1.1	2.9×10^{-5}
	2×10^{-4}	1.3	3.3×10^{-5}
	4×10^{-4}	1.4	3.3×10^{-5}
15 mg RuO_2	1×10^{-4}	2.2	1.3×10^{-5}
	2×10^{-4}	3.0-3.1	1.5×10^{-5}
	4×10^{-4}	3.2	1.6×10^{-5}

TABLE 5.2: Influence of EDTA concentration on the hydrogen production.

	[EDTA] (M)	r_{H_2} (ml/hr)	H_2 yield (ml)	$[\text{MV}^{+}]$ (M)
15 mg RuO_2 , 5×10^{-4} M MV	0.005	1.7-1.8	9	1.2×10^{-5}
	0.01	2.3	19	1.3×10^{-5}
	0.02	3.0-3.1	28	1.5×10^{-5}
	0.05	3.2	32	1.5×10^{-5}
	0.1	3.3	31	1.5×10^{-5}
	0.2	3.2	31	-
40 mg RuO_2 , 2×10^{-3} M MV	0.02	4.3	42	-
	0.2	4.3	60	-

5.3.4 H₂ pressure and buffer capacity

The presence of H₂ in the gas phase had a considerable influence on the performance of the system. Flushing with H₂ instead of N₂ lowered the steady state production rate in the standard solution (15 mg RuO₂) from ca. 3 to 1.8 ml/hr and the total yield decreased from 28 to 13.5 ml. No effect on the induction time has been observed.

Lowering the buffer capacity while keeping the total ionic strength of the solution constant (by addition of KNO₃), does not significantly affect the steady state production rate (table 5.3). During hydrogen evolution from the standard solution, the pH increases from 4.6 to ca. 5. For the lower buffer concentrations, the pH increases to ca. pH 6.5, at which EDTA is an efficient buffer ($pK_2 \approx 6.2$ [22]).

TABLE 5.3: Influence of the buffer capacity on the hydrogen production. The total ionic strength of the reaction solution is constant. The amount of RuO₂ is 15 mg.

conc. buffer (M)	r_{H_2} (ml/hr)	H ₂ yield (ml)	final pH
0	2.8	23	6.5
2×10^{-3}	3.0	23	6.5
5×10^{-3}	2.9	22	6.4
0.05	3.0-3.1	28	4.8-5.2

5.3.5 Hydrogen production as a function of RuO₂ amount and methylviologen concentration

The effects of the amount of catalyst on the hydrogen production rate, the total hydrogen yield, and the steady state MV^{+} concentration are shown in figure 5.6. The production rate and total yield increase with the RuO₂ quantity until a plateau is reached. At high amounts of RuO₂, the catalyst particles absorb a substantial fraction of the incident light (see figure 5.2) and this probably determines the height of the plateau and causes the slight decrease above 25 mg RuO₂.

At the plateau, the steady state MV^{+} concentration is relatively low

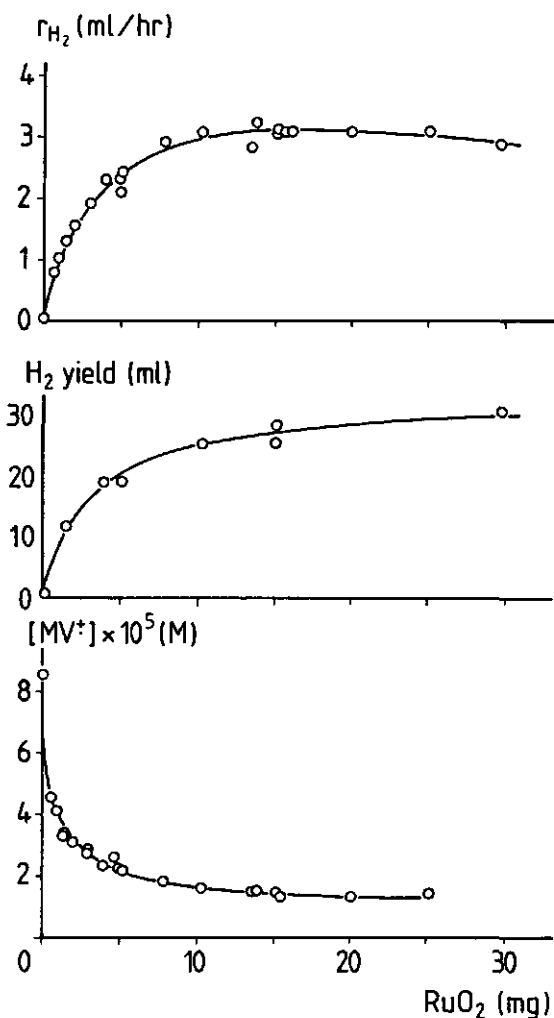


FIGURE 5.6: Steady state production rate, total hydrogen yield, and steady state MV^{+} concentration as a function of the amount of catalyst in the system.

(3 % of the total methylviologen concentration). The production rate is 3.0-3.1 ml/hr and the total H_2 yield is 28-30 ml, which corresponds to about 1.2 mmol H_2 . The turnover numbers of $\text{Ru}(\text{bipy})_3^{2+}$ and MV^{2+} (defined as the ratio of the total obtained H_2 amount to the initial amount of the considered component, both expressed in moles) are ca. 100 and 40, respectively.

At low quantities of RuO_2 , methylviologen radicals accumulate, which can also be seen with the naked eye: within a few minutes after switching on the light source, the color of the reaction mixture changes to green. By the time the production of hydrogen has stopped, the solution has adopted its original color.

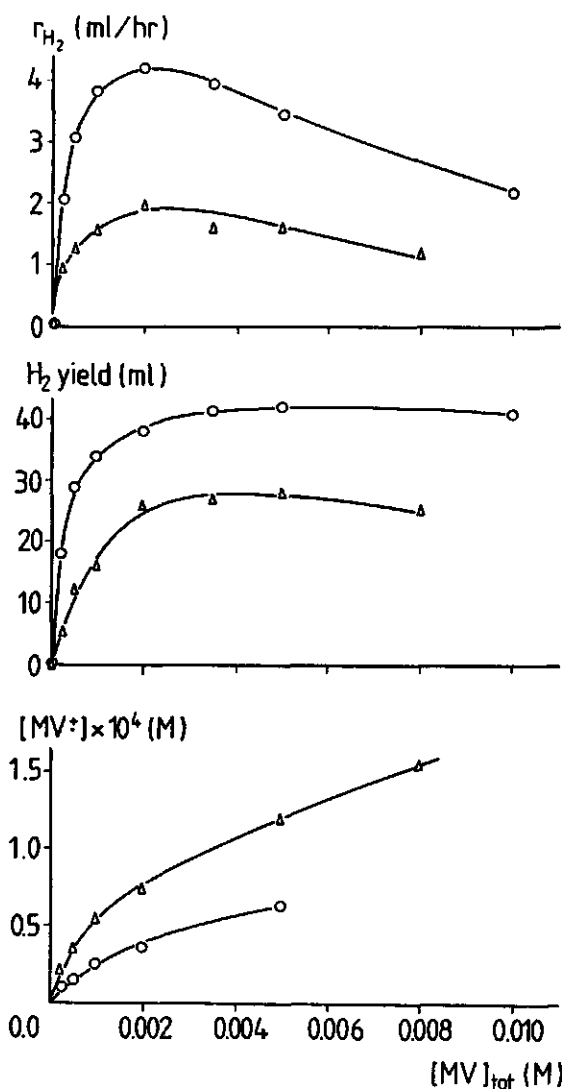


FIGURE 5.7: Steady state production rate, total hydrogen yield, and steady state MV^{\bullet} concentrations as a function of total methylviologen concentration. Δ - 1.5 mg RuO_2 , \circ - 15 mg RuO_2 .

In order to find out whether the RuO_2 particles loose their catalytic activity during evolution of hydrogen, the following experiment was performed for 3 and 10 mg RuO_2 in the standard reaction solution. After hydrogen production had stopped, the particles were given opportunity to settle in the reaction cell and the solution was removed. Fresh reaction solution was added, in which the RuO_2 was dispersed again. Under illumination H_2 evolution took place at a rate that was the same (3 mg RuO_2 : 1.9 ml/hr) or even higher than in the foregoing experiment (10 mg RuO_2 : 3.1 + 3.6 ml/hr). The induction time was for both RuO_2 quantities the same as before, i.e. about 25 minutes.

In figure 5.7 the effect of the methylviologen concentration on the H_2 evolution is given for two catalyst concentrations. An maximum in production rate is observed. In the case of 15 mg RuO_2 , the H_2 yield increases with methylviologen concentration until a plateau of ca. 42 ml is reached. This plateau production is determined by the amount of EDTA in the system. If, in the case of 10^{-2} M methylviologen, 0.02 M extra EDTA is added to the system after the H_2 formation has stopped, the production resumes at almost the original rate and another 27 ml H_2 is produced.

At the end of some of the experiments, the concentrations of $\text{Ru}(\text{bipy})_3^{2+}$ and methylviologen were determined. In all cases more than 95 % of the sensitizer was still unimpaired. However, large fractions of the electron relay appeared to be destructed. An overview is given in table 5.4. If, after the hydrogen production has come to an end, 5×10^{-4} M extra MV is added to the system (standard solution, 15 mg catalyst), the production starts again.

3.3.6 Influence of stirring rate

During the steady state period of hydrogen evolution, the rate of the magnetic stirrer was varied. Generally a higher stirring rate resulted in a modest increase in the production rate (figure 5.8). The value obtained for r_{H_2} at a given stirring rate appeared to be higher when the stirring rate was varied from high to low than in a reverse order (hysteresis).

TABLE 5.4: Breakdown of methylviologen in the reaction mixture during hydrogen evolution.

RuO ₂ (mg)	initial [MV] (M)	r _{H₂} (ml/hr)	MV destructed (%)
1.5	5 x 10 ⁻⁴	1.3	98-99
5.1	5 x 10 ⁻⁴	2.3-2.4	80-99
10	5 x 10 ⁻⁴	3.0-3.1	75
15	5 x 10 ⁻⁴	3.0-3.1	64-84
30	5 x 10 ⁻⁴	2.8	49
15	10 ⁻³	3.8	62
1.5	2 x 10 ⁻³	1.9-2.0	84
15	2 x 10 ⁻³	4.2	36

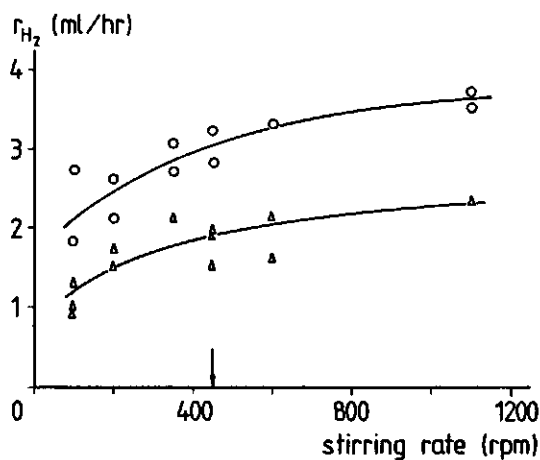


FIGURE 5.8: Effect of stirring rate on the steady state hydrogen production. Δ - 3 mg RuO₂, ○ - 15 mg RuO₂. The arrow indicates the standard rate of the magnetic stirrer.

5.3.7 Temperature dependency

The influence of the temperature on the production of H_2 was studied at a low (1.5 mg) and at a relatively high amount of RuO_2 (15 mg). In both cases increasing the temperature had a positive influence on the hydrogen production rate. In figure 5.9 this is illustrated in an Arrhenius plot. In the temperature range studied (10–40 °C) Arrhenius behavior is observed, and from the slopes of the lines, activation energies are found of 36 and 30 kJ/mol H_2 for 1.5 and 15 mg RuO_2 , respectively. For 1.5 mg of catalyst the steady state concentration MV^{+} increases slightly with temperature, whereas for 15 mg this concentration is fairly constant. Temperature also

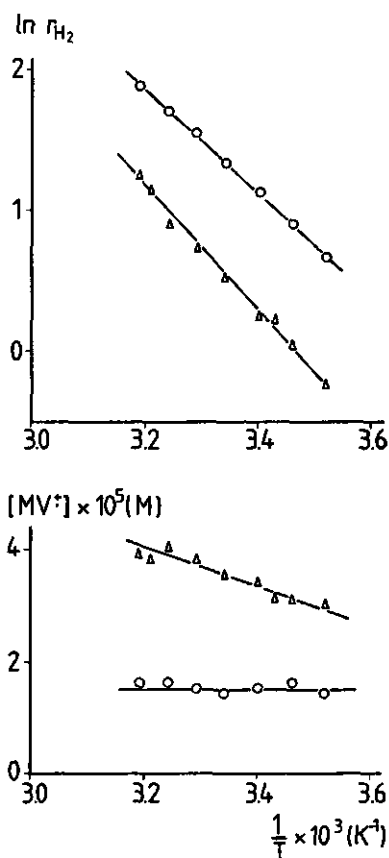


FIGURE 5.9: Arrhenius plot of H_2 evolution rates. Δ - 1.5 mg RuO_2 , \circ - 15 mg RuO_2 . For clarity, the steady state MV^{+} concentration is also plotted against $1/T$.

had a marked effect on the induction time of the process, which ranged from 45-50 minutes at 10 °C to 10 minutes at 40 °C. The total H₂ yield is rather insensitive to the temperature.

5.3.8 Influence of the presence of stabilizing agents

RuO₂ is colloid-chemically very unstable in the reaction solution, which has an ionic strength of about 0.1 M, and coagulation occurred rapidly. Several experiments were performed in which the reaction solution contained also a polymer or surfactant (PVA, PVP, dextran, or Synperonic NPE 1800). None of these agents did in fact stabilize the RuO₂ particles to an appreciable extent (see also section 2.8). The results on the H₂ production in the presence of the polymers and surfactant are summarized in table 5.5.

TABLE 5.5: Hydrogen production in the presence of stabilizing agents. The amount of RuO₂ is 15 mg. (Note: the light intensity is ca. 70 % of the standard light intensity.)

polymer	r _{H₂} (ml/hr)	H ₂ yield (ml)	remarks
-	2.5	27	
92 mg/l PVA	1.9	-	flotation of RuO ₂
457 mg/l PVA	2.1	28	
46 mg/l PVP	1.8	20	
275 mg/l dextran	2.0	19	
46 mg/l Synperonic	2.3	26	foam formation

5.4 DISCUSSION

5.4.1 The induction time

The induction time at the beginning of each experiment, is a commonly observed phenomenon in this kind of photochemical systems for hydrogen production (see for example references [2,8,13]). It is partly ascribed to the time required for saturation of the solution with hydrogen and adsorption of hydrogen at several parts of the apparatus. However, these appear

to be small effects, since flushing with H_2 instead of N_2 does not significantly decrease the induction time. Moreover, the solubility of H_2 in aqueous solutions is very low as long as the H_2 pressure is low, which is generally the case at the early stages of the experiments. (At 1 atm. H_2 pressure and 20 °C, the solubility is 0.82 mmol/l [23].)

It is rather obvious that before hydrogen production can reach a steady state, first an appropriate concentration of methylviologen radicals has to be built up. Under first time illumination this process can take tens of minutes, as can be seen from figure 5.4. Formation of $MV^{\cdot+}$ starts only after 1-5 minutes, possibly depending on the quantity of oxygen that is still present in the system, despite the nitrogen flushing. The first methylviologen radicals formed are therefore not stable [1].

Another contributing factor could be that first the RuO_2 surface must be covered with hydrogen atoms or molecules, and maybe the catalyst has to be reduced to a certain extent. However, examination of all the obtained V-t plots revealed that there is no correlation between the quantity of catalyst in the system and the time required to reach the steady state. For the standard solution containing various amounts of RuO_2 particles, the induction time varies between 18 and 26 minutes. If the same RuO_2 is used a second time as catalyst, the induction time is not shorter than the first time. This indicates that the induction period involves no reduction process of the catalyst itself.

Therefore, it is concluded that the process of building up a steady state concentration of $MV^{\cdot+}$ in the bulk solution is the leading factor that gives rise to the induction times observed. To some degree, this is confirmed by the observations that the induction time seems to decrease slightly with increasing sensitizer and EDTA concentration. With respect to the methylviologen concentration, there seems to be a minimum in the induction time around 2×10^{-3} M. However, all these variations are hardly significant relatively to the variations already found for duplicate experiments. The only variable that significantly affects the length of the induction period is the temperature.

5.4.2 Termination of the hydrogen production

There are several factors that could contribute to the termination of the hydrogen production process. First of all, the sensitizer could be

destroyed, but $\text{Ru}(\text{bipy})_3^{2+}$ is fairly stable in sacrificial water reduction systems [2,5]. After the hydrogen production has ceased, more than 95 % of the sensitizer is still unimpaired. Inactivation of the catalyst RuO_2 during hydrogen evolution does also not occur.

Neither accumulation of H_2 in the gas phase, nor the slight increase in pH during hydrogen evolution can be causes for the termination of the production. Even when the system is flushed with H_2 gas, hydrogen production takes place, albeit at a lower rate. This observation points to chemical reversibility of the hydrogen evolution reaction, corroborating the findings on RuO_2 film electrodes described in section 3.3.4. Results of Keller et al. [14,15] show that with RuO_2 as the catalyst no decrease in the hydrogen production takes place when the pH of the system is increased from pH 5 to pH 6.

In some experiments it was obvious that the total H_2 production was limited by the amount of EDTA present. The maximum volume of hydrogen produced from solutions containing 0.02 M EDTA is approximately 42 ml, which means that 3 electrons per EDTA molecule are used. Values of 2-4 electrons per EDTA molecule for systems in which $\text{Ru}(\text{bipy})_3^{2+}$ is used as the sensitizer can also be found in the literature [2,5,12,13]. Possible reaction sequences for the oxidation of EDTA at different pH values are given in references [1,5]. According to these schemes, up to 4 electrons per EDTA molecule are available. A high pH facilitates the donation of electrons by EDTA. The products are probably glyoxylic acid and ethylene-N,N'-diacetic acid.

A more general cause for termination of the hydrogen production is the irreversible destruction of the electron relay methylviologen. Its gradual disappearance during irradiation is illustrated by the data in figure 5.4 and table 5.4. No attempt was made to determine the identity of the breakdown product(s).

It is a well-known fact that MV^{2+} can be hydrogenated in the presence of H_2 and Pt [1-3,5,24,25]. The presence of the hydrogenation product in the $\text{Ru}(\text{bipy})_3^{2+}/\text{MV}^{2+}/\text{EDTA}/\text{Pt}$ system after H_2 production had ceased, was established by its isolation [2]. The formation of this substance rose dramatically upon increasing the Pt concentration, indicating a typically catalytic process. This competitive process leads to a pronounced maximum in the H_2 yield as a function of the amount of Pt catalyst present [2,3,5,6,13]. In the case of RuO_2 as the catalyst, such an maximum is not observed, con-

firming the conclusion of Keller et al. [15] that RuO_2 is not able to catalyze the hydrogenation of methylviologen. These authors established that MV^{2+} is stable in RuO_2 dispersions under hydrogen atmosphere. The destruction of methylviologen during hydrogen production was attributed to side-reactions initiated by H^\cdot intermediates, adsorbed at the RuO_2 surface. Our observation that also in the absence of RuO_2 methylviologen disappears from the reaction solution under prolonged illumination, is in contradiction with this explanation. Moreover, there is a negative correlation between the destruction of methylviologen and both the quantity of RuO_2 in the system and the hydrogen production rate (table 5.4). The steady state concentration of $\text{MV}^{+\cdot}$ radicals in the reaction mixture increases with decreasing amount of RuO_2 and hydrogen production rate (figure 5.6). Therefore, it is concluded that some side-reaction of the radical form $\text{MV}^{+\cdot}$ leads to the destruction of methylviologen, and the catalyst is not involved in this process. The observation that the total hydrogen yield, in contrast to the hydrogen production rate, does not increase with the temperature, suggests that the destruction of methylviologen is promoted by increasing temperature.

5.4.3 Limiting factors in hydrogen generation under steady state conditions

In the later stages of the experiments, the gradual breakdown of methylviologen, the exhaustion of EDTA, and the accumulation of products increasingly affect the hydrogen production rate. In this section, only the steady state production rate is considered.

The rate of hydrogen production is clearly affected by the light intensity (figure 5.5). The relevant wavelength interval for excitation of the sensitizer ranges from ca. 350 nm to ca. 600 nm. Below 350 nm no light passes through the glass components of the system, and above 600 nm light absorption by $\text{Ru}(\text{bipy})_3^{2+}$ is negligible (figure 5.2). In this interval, the RuO_2 particles and methylviologen radicals also absorb light, and therefore, part of the incident light is lost for excitation ("inner filter effect"). Light absorbance by $\text{MV}^{+\cdot}$ is not very important, since its extinction coefficient is low in the region where $\text{Ru}(\text{bipy})_3^{2+}$ exhibits an absorption maximum, and the steady state $\text{MV}^{+\cdot}$ concentration is always (considerably) less than the sensitizer concentration. On the other hand, RuO_2 absorbs a substantial part of the incident light over the whole wavelength

interval, more than 30 % for quantities higher than 10 mg. (Scattering of light by RuO_2 particles is of minor importance, because their color is almost black.) For the sake of simplicity, the inner filter effect is neglected for the moment, so that for each wavelength λ the absorption of photons by $\text{Ru}(\text{bipy})_3^{2+}$, $I_A(\lambda)$, may be expressed as:

$$I_A(\lambda) = I_0(\lambda) (1 - 10^{-\epsilon(\lambda)cl}) \quad (5.7)$$

where l is the length of the light path through the reaction cell; $\epsilon(\lambda)$ refers to the extinction coefficient of $\text{Ru}(\text{bipy})_3^{2+}$ and c to its concentration. In chapter 6 a more precise equation will be presented.

If $\epsilon(\lambda)cl > 2$, then:

$$I_A(\lambda) \approx I_0(\lambda) \quad (5.8)$$

For the standard concentration sensitizer (2×10^{-4} M) this approximation holds for $400 \text{ nm} < \lambda < 460 \text{ nm}$. The contributions to the excitation process at other wavelengths are relatively small. Therefore, almost all the light appropriate for excitation is absorbed, and increasing the sensitizer concentration hardly improves the hydrogen production rate (table 5.1). However, changing the dimensions of the reaction cell (l smaller and the illuminated area larger) should result in a higher production rate per volume of reaction solution. At very low $\text{Ru}(\text{bipy})_3^{2+}$ concentrations, the excitation reaction becomes first order in the sensitizer concentration:

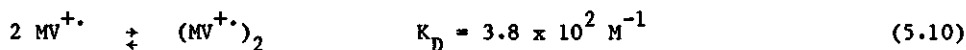
$$I_A(\lambda) \approx 2.303 I_0(\lambda) \epsilon(\lambda)cl \quad (5.9)$$

The hydrogen production rate does not depend on the EDTA concentration above 0.02 M. Only at low EDTA concentrations a positive dependence on the EDTA concentration is observed. Apparently, the undesired back-reaction (5.4) of MV^{+} with the oxidized sensitizer is successfully suppressed by the presence of 0.02 M EDTA. Reaction (5.4) is, at least under the standard conditions of our experiments, not a rate-limiting factor in the hydrogen production.

On the basis of the reaction scheme presented in the introduction of this chapter, one would expect that, in the absence of catalyst, continuous

irradiation would ultimately result in 100 % conversion of the MV^{2+} present into $MV^{+\bullet}$. Intramolecular decay of the excited sensitizer to its ground state and reaction (5.4) only slow down this process, and the latter is of minor importance due to the presence of EDTA. Therefore, it is striking that the plateau values of the $MV^{+\bullet}$ concentration in figure 5.4 are only a fraction of the total methylviologen concentration. This implies that some additional reaction takes place in the solution, resulting in reconversion of $MV^{+\bullet}$ into MV^{2+} . The decay in $MV^{+\bullet}$ concentration in the dark also reflects such a reaction. In the absence of oxygen, $MV^{+\bullet}$ is stable in alkaline, neutral, and mildly acidic solutions [26]. Therefore, probably one of the other components in the solution is involved in this reaction. Our observations might be explained after consideration of the oxidation path of EDTA, as described by Amouyal [1]: the protonated form of the first oxidation product of EDTA reacts with $MV^{+\bullet}$ to give the initial compounds EDTA and MV^{2+} . This reaction is first order in the $MV^{+\bullet}$ concentration. At pH 4.6 the protonated oxidation product of EDTA coexists with the non-protonated form. Since oxidation of EDTA only takes place under illumination, it could be that the back-reaction of $MV^{+\bullet}$ is faster in the light than in the dark. The rate of this reaction under illumination will be estimated in chapter 6.

Over the whole range of RuO_2 quantities, the rate of hydrogen production depends on the methylviologen concentration. It increases with methylviologen concentration until a maximum is reached and then decreases again (figure 5.7). Such a maximum is also found in Pt systems [27,28] and is generally attributed to adsorption of MV^{2+} on the catalyst, which would block reaction sites. This explanation does not seem to hold for our system, since we did not find any indication that MV^{2+} adsorbs to an appreciable extent on RuO_2 under the given conditions (sections 4.3.3 and 4.3.4). An alternative explanation that has to be considered, is the tendency of methylviologen radicals to form dimers [3,18]:



The dimer (presumably a diradical [18]) has a less negative standard redox potential (-0.29 V/NHE, [3]) than the monomer, thus making the evolution of hydrogen thermodynamically less favourable, if not impossible at the employed pH value ($E(H^+/H_2) = -0.27$ V/NHE at 1 atm. H_2 pressure). However,

around the observed maximum in hydrogen production rate, the $MV^{+\bullet}$ concentration is still so low, that the dimer concentration is only ca. 1.5 and 3 % of the $MV^{+\bullet}$ concentration, for RuO_2 amounts of 1.5 and 15 mg, respectively. At the highest steady state $MV^{+\bullet}$ concentration observed, i.e. 1.5×10^{-4} M (obtained in the system containing 8×10^{-3} M methylviologen and 1.5 mg RuO_2), the dimer concentration amounts to ca. 6 % of the $MV^{+\bullet}$ concentration. Therefore, it is very unlikely that the maximum results from dimerization of methylviologen radicals. Perhaps the occurrence of this maximum is due to progressive competition of reaction (5.4) and other side-reactions of the methylviologen radical with the production of hydrogen when the methylviologen concentration is increased.

The production rate increases with the amount of catalyst until a plateau is reached (figure 5.6). As outlined before, the height of the plateau is limited by (among other factors) the inner filter effect of the RuO_2 particles, which absorb a large fraction of the incident light. At the plateau, the available catalytic surface area is not a rate-determining factor. In cases with relatively small amounts of catalyst, accumulation of $MV^{+\bullet}$ is observed and one or more of the heterogeneous processes, comprised in equation (5.3), are rate-limiting. The change in the relative contributions of the bulk reactions and the heterogeneous processes to the production rate going from low to high RuO_2 quantities, is also reflected in the observed temperature effects. For both high and low RuO_2 amounts, Arrhenius behavior is observed, but there is a slight reduction in activation energy with increasing amount of catalyst (36 kJ/mol for 1.5 mg RuO_2 , 30 kJ/mol for 15 mg RuO_2). Furthermore, for high RuO_2 amounts the steady state concentration of $MV^{+\bullet}$ is constant over the temperature range studied, while for low quantities this concentration increases with temperature. Apparently, the reactions that lead to formation of $MV^{+\bullet}$ in the bulk solution are more accelerated by increasing temperature than the heterogeneous processes. The calculated activation energies are in the same order as values found for comparable systems with Pt as a catalyst (80 kJ/mol [8], 24 kJ/mol [11]).

The coagulation of RuO_2 particles in the reaction solution might have a negative influence on the photolysis efficiency by the loss of accessibility of catalytic surface area. It is likely that the plateau values of hydrogen production rate (figure 5.6) are obtained at higher RuO_2 amounts than if the colloid would be stable and better dispersed. Unfortunately,

attempts to stabilize the sol with polymers and surfactants were unsuccessful. Therefore, a positive effect of these compounds on the hydrogen production was not expected, unless they would be chemically involved in this process (catalytic effect). For the polymers and surfactant investigated (all non-ionic) there is indeed only a small negative effect on the production rate, probably due to retardation of diffusion processes at the surface or to blocking of surface sites. It must be noted that the influence of the "stabilizing" agents on the hydrogen production was investigated at relatively high (not rate-limiting) RuO_2 amounts.

It is assumed that the transfer of compounds to and from the catalyst surface is a steady state convective diffusion process of a specific type, i.e. particles in a turbulent flow [29]. The concentration of solutes is homogeneous throughout the solution, and there is only a thin diffusion layer around the catalyst particles (aggregates). The effective thickness of this layer depends on the diffusion coefficient of the compound in question, the viscosity of the solution, the size of the aggregates, and the stirring regime [29]. It is practically impossible to estimate the thickness of the diffusion layer, because the size of the RuO_2 flocs and the velocity of the liquid relative to the solid are unknown. (Taking for these parameters 1 μm and 1 m/s, respectively, and using the diffusion coefficient of MV^{2+} , which is $8 \times 10^{-10} \text{ m}^2/\text{s}$ [28], a thickness of the diffusion layer in the order of tens of nanometers is calculated). The hysteresis observed in the production rate as a function of stirring rate, is presumably due to changes in the degree of dispersion of the catalyst. For low as well as higher RuO_2 quantities, the stirring rate affects the rate of hydrogen evolution. This may be rationalized in terms of the following: a) mass transfer of MV^{+} is one of the rate-limiting steps. Mass transfer of protons is much faster, since their diffusion coefficient and effective concentration are by orders of magnitude higher than for MV^{+} . As outlined in section 3.3.4, protons associated with the buffer are also available for the hydrogen evolution reaction. b) At higher stirring rates hydrogen gas bubbles are more quickly removed, so that more catalytic surface is available. Probably, this second effect is of no consequence at higher RuO_2 quantities.

From the Stokes-Einstein equation one expects the diffusion coefficients to increase by a factor of 2.1 from 10 °C to 40 °C, corresponding to an activation free energy of ca. 18 kJ/mol. This value is too small to account

entirely for the influence of the temperature on the rate of hydrogen formation.

Lowering the buffer concentration, or even leaving the buffer out of the solution completely, does not result in a significant decrease in the hydrogen production rate. Apparently, the transfer of protons to the catalyst surface is still not rate-limiting. (At the initial pH of 4.6, EDTA is not a good buffer and will not be a labile proton donor.) This, together with the generally low ratio $[MV^{+}]/[MV^{2+}]$, indicates that the hydrogen evolution reaction takes place at a relatively low overpotential of the RuO_2 particles (see section 3.3.4). In chapter 6 this subject will be considered in more detail.

Comparison of our results with studies in the existing literature must be made with caution, since experimental conditions vary from study to study. For example, data on the incident light intensity, which has a pronounced influence on the production rate, are never reported, and catalyst characterization is frequently lacking. However, it can be established that the hydrogen production rates and yields (per volume of reaction solution) obtained in this work are in the same order as reported for other RuO_2 systems [7,14,15], and also for Pt systems [2,4,7,8,13]. For Pt systems, similar rate dependence with respect to the concentrations of $Ru(bipy)_3^{2+}$, MV^{2+} , and EDTA are found [7,8,10,13].

5.5 CONCLUSIONS

The $Ru(bipy)_3^{2+}/MV^{2+}/EDTA$ /colloidal RuO_2 system described in this chapter, represents a model system for the photochemical generation of hydrogen from water. In many aspects its performance is comparable to previously investigated systems involving colloidal Pt. An important difference is that the undesired hydrogenation of methylviologen is not catalyzed by RuO_2 , whereas this reaction limits the formation of hydrogen promoted by Pt. Hydrogen evolution is chemically reversible at RuO_2 , as it is on Pt.

An appropriate MV^{+} concentration has to be built up before the system starts to produce hydrogen at a steady state rate. This is the primary cause for the phenomenon of an induction period. The maximum attainable amount of hydrogen is determined by the amount of electron donor in the system, which is a general feature of sacrificial systems. In the system under study, three electrons per EDTA molecule are available. However, in

most experiments this maximum hydrogen yield is not attained, because of gradual destruction of methylviologen under illumination, due to a side-reaction of the radical form. The RuO_2 catalyst is not involved in this process. It therefore appears that methylviologen, albeit a relatively efficient electron relay with convenient properties for basic studies in model systems, is not suitable to be used in future commercial systems for solar energy conversion.

The hydrogen production rate in the steady state period is controlled by a complex of factors. In all our experiments, the light intensity is rate-limiting. It determines the rate of the first step in hydrogen formation, i.e. the excitation of the sensitizer. The catalyst RuO_2 itself absorbs light throughout the visible spectrum and therefore limits the hydrogen production if it is present in relatively high quantities. However, using lower quantities of this catalyst results in a decrease of hydrogen production rate, because then the available catalytic surface area becomes rate-limiting. Mass transfer of $\text{MV}^{+\cdot}$ to the catalyst surface is probably a rate-limiting step over the whole range of catalyst amounts studied.

The steady state ratio between $\text{MV}^{+\cdot}$ and MV^{2+} concentrations was found to be low under all conditions applied, even if there is no catalyst present at all. This must be the result of a yet unknown reaction in the solution, which converts $\text{MV}^{+\cdot}$ into MV^{2+} again. This reaction is competitive with hydrogen formation and makes the system less efficient.

The presence of acetate buffer is not an essential factor for the kinetics of the heterogeneous hydrogen evolution reaction. The buffer is in fact a sacrificial proton donor, which can be left out in cyclic systems. In its absence, the pH increases to about pH 6 and then EDTA sufficiently buffers the system.

In the next chapter a more quantitative interpretation of the results will be given on the basis of kinetic flux equations.

5.6 ACKNOWLEDGEMENTS

The following people are gratefully acknowledged: Ronald Wegh, Henny van Beek and Louis Verhagen for designing and making the volumeter, Erna Rouwendal for performing part of the experiments, dr. C. Laane (Department of Biochemistry) for use of the gas chromatograph, mr. A. van Hoek (Department of Molecular Physics) for helpful advices concerning optical aspects

of the work and for use of the light power meter, and Fred van Wijk (Department of Molecular Physics) for carrying out EPR experiments.

5.7 REFERENCES

1. E. Amouyal, Sci. Pap. Inst. Phys. Chem. Res. **78** (1984) 220-231
2. O. Johansen, A. Launikonis, J. W. Loder, A. Mau, W. H. Sasse, J. D. Swift, and D. Wells, Aust. J. Chem. **34** (1981) 981-991
3. A. Harriman, and G. Porter, J. Chem. Soc., Faraday Trans 2 **78** (1982) 1937-1943
4. A. Moradpour, E. Amouyal, P. Keller, and H. Kagan, Nouv. J. Chim. **2** (1978) 547-549
5. P. Keller, A. Moradpour, E. Amouyal, and H. Kagan, Nouv. J. Chim. **4** (1980) 377-384
6. P. Keller, A. Moradpour, E. Amouyal, and H. Kagan, J. Mol. Catal. **7** (1980) 539-542
7. E. Amouyal, and P. Koffi, J. Photochem. **29** (1985) 227-242
8. E. Borgarello, J. Kiwi, E. Pelizzetti, M. Visca, and M. Grätzel, J. Am. Chem. Soc. **103** (1981) 6324-6329
9. P. A. Brugger, P. Cuendet, and M. Grätzel, J. Am. Chem. Soc. **103** (1981) 2923-2927
10. A. Harriman, and A. Mills, J. Chem. Soc., Faraday Trans. 2 **77** (1981) 2111-2124
11. H. Dürr, G. Dürr, K. Zengerle, and B. Reis, Chimia **37** (1983) 245-248
12. D. N. Furlong, D. Wells, and W. H. Sasse, J. Phys. Chem. **89** (1985) 1922-1928
13. L. Loy, and E. E. Wolf, Solar Energy **34** (1985) 455-461
14. E. Amouyal, P. Keller, and A. Moradpour, J. Chem. Soc., Chem. Commun. (1980) 1019-1020
15. P. Keller, A. Moradpour, and E. Amouyal, J. Chem. Soc., Faraday Trans. **1** **78** (1982) 3331-3340
16. D. N. Furlong, and W. H. F. Sasse, Colloids Surfaces **7** (1983) 29-52
17. A. Calderbank, and S. H. Yuen, Analyst **90** (1965) 99
18. E. M. Kosower, and J. L. Cotter, J. Am. Chem. Soc. **86** (1964) 5524-5527
19. T. Watanabe, and K. Honda, J. Phys. Chem. **86** (1982) 2617-2619
20. D. Meisel, W. A. Mulac, and M. S. Matheson, J. Phys. Chem. **85** (1981) 179-187

21. W. R. Dunham, J. A. Fee, L. J. Harding, and H. J. Grande, *J. Magn. Res.* **40** (1980) 351-359
22. L. G. Sillén, and A. E. Martell, in "Stability Constants of Metal-Ion Complexes", Chem. Soc. Spec. Publ. 17, Metcalfe and Cooper Ltd., London (1964)
23. BINAS tables, Wolters-Noordhoff, Groningen (1977)
24. T. W. Ebbesen, *J. Phys. Chem.* **88** (1984) 4131-4135
25. W. J. Albery, P. N. Bartlett, and A. J. McMahon, *J. Electroanal. Chem.* **182** (1985) 7-23
26. D. R. Prasad, K. Mandal, and M. Z. Hoffman, *Coord. Chem. Rev.* **64** (1985) 175-190
27. J. Kiwi, and M. Grätzel, *J. Am. Chem. Soc.* **101** (1979) 7214-7217
28. W. J. Albery, P. N. Bartlett, and A. J. McMahon, in "Photogeneration of Hydrogen", A. Harriman, and M. A. West (eds.), Academic Press, New York (1982) 85-103
29. V. G. Levich, in "Physicochemical Hydrodynamics", Prentice-Hall Inc., Englewood Cliffs, New Jersey (1962)

CHAPTER 6

A KINETIC MODEL FOR THE $\text{Ru}(\text{bipy})_3^{2+}/\text{MV}^{2+}/\text{EDTA}/\text{colloidal RuO}_2$ SYSTEM FOR PHOTOGENERATION OF HYDROGEN

6.1 INTRODUCTION

The $\text{Ru}(\text{bipy})_3^{2+}/\text{MV}^{2+}/\text{EDTA}/\text{colloidal}$ catalyst system for hydrogen production is rather complicated, since many different chain and parallel reactions in solution and at the catalyst surface take place simultaneously. To obtain more insight into the catalytic surface reactions and their coupling with the homogeneous reactions, it is useful to work with a model.

Many kinetic models for colloid catalyzed hydrogen production treat the catalytic reaction in terms of a series of homogeneous reactions in which the colloidal particles are regarded as a "molecular" reactant (see for example references [1-4]). This kind of treatment leads to second order rate constants with very limited meaning and predictive power, since they do not allow discrimination between the catalytic properties of the surface and mass transfer effects. A better approach is to regard the colloidal particles as small electrodes ("microelectrodes").

Two redox couples form the basic elements of the reaction at the surface of these microelectrodes:



The suggestion that heterogeneous catalysis of electron transfer reactions can be interpreted in terms of the electrochemical behavior of the reactants involved, has been first proposed by Wagner and Traud [5] for corrosion reactions. Spiro [6] has developed a theory for two coupled reactions at colloidal particles, one or both being in the Tafel region, i.e. not mass transfer limited. This theory was adapted for the $\text{Ru}(\text{bipy})_3^{2+}/\text{MV}^{2+}/\text{EDTA}/\text{colloidal Pt}$ system by Miller et al. [7,8] and Albery

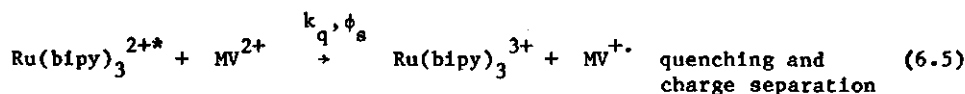
et al. [9,10]. Both groups considered the reduction of H^+ to be irreversible, i.e. back-reaction of H_2 at the catalyst surface was neglected. They underlined the effects of the pH, the redox potential and concentration of the electron relay, and the overpotential of the catalyst material for the hydrogen evolution reaction. The mathematical treatments (and experiments to test these) considered only the heterogeneous reactions. The buffer, which is generally present in sacrificial systems for hydrogen evolution, was neglected as a labile proton donor, making part of the interpretation of the supporting experiments doubtful (see section 3.3.4).

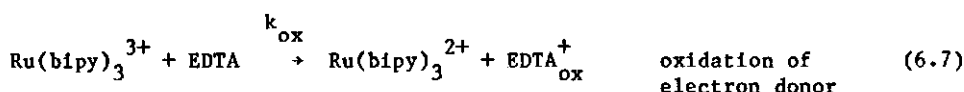
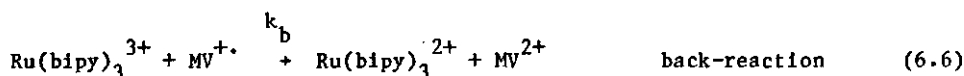
In the model presented here, both the homogeneous reactions and the heterogeneous processes which take place in the H_2 producing system, are incorporated. The reactions in solution are described with steady state kinetic equations and the heterogeneous reactions are described as electrode processes. The formation and consumption of the methylviologen radical $MV^{\cdot+}$ play a central role. The model is tested by using the experimental results of the $Ru(bipy)_3^{2+}/MV^{2+}/EDTA$ /colloidal RuO_2 system described in chapter 5.

6.2 THE MODEL

6.2.1 Flux equation for the homogeneous reactions

$Ru(bipy)_3^{2+}$, methylviologen and EDTA are the most commonly used constituents of water reducing systems, and therefore the reactions between these compounds have been thoroughly studied by several groups of researchers. The main reactions that take place in solution are:





The symbol s^* stands for the rate of the excitation reaction.

The quenching reaction does not always lead to charge separation, but can also result in formation of Ru(bipy)_3^{2+} and MV^{2+} . The term ϕ_s refers to the quantum yield of this reaction (the fraction of quenching acts that leads to electron transfer) and is concerned with the extent of product separation from a "solvent caged ion pair" [11]. At pH 4.7, the value of ϕ_s is lower than 0.25 [11].

The symbols "EDTA" and "EDTA_{ox}" represent all the forms of these substances present in the solution. The donation of electrons by EDTA is described by only one effective reaction and rate constant k_{ox} , a simplification of the real situation, where each EDTA species can oxidize up to three Ru(bipy)_3^{3+} ions (see chapter 5).

The rate constants k_i , k_q , and k_b are well-established, and there appears to be little controversy about their values. The natural life-time of Ru(bipy)_3^{2+*} in deaerated aqueous solution is 0.60 μs ; $k_i \approx 1.6 \times 10^6 \text{ s}^{-1}$ [12-15]. Values reported for k_q vary from 5×10^8 to $1.5 \times 10^9 \text{ M}^{-1}\text{s}^{-1}$ [11,13,16], and for k_b from 2.6×10^9 to $2.8 \times 10^9 \text{ M}^{-1}\text{s}^{-1}$ [12,13,17,18]. The value of k_{ox} is not so well known and depends strongly on the pH of the solution. Values of about $10^8 \text{ M}^{-1}\text{s}^{-1}$ at pH 4.7-5 have been reported [11,13], but also much lower values have been published, ranging from $8 \times 10^3 \text{ M}^{-1}\text{s}^{-1}$ at pH 4 [19] to $2 \times 10^6 \text{ M}^{-1}\text{s}^{-1}$ at pH 8.2 [20].

Methylviologen, especially its reduced form $\text{MV}^{+\cdot}$, is involved in various side-reactions, which are poorly documented in the literature. As outlined in section 5.4.3, there has to be at least one other homogeneous reaction in which $\text{MV}^{+\cdot}$ is reconverted into MV^{2+} :



This unidentified reaction cannot be neglected in a model for the system under study, because it leads to relatively low steady state $\text{MV}^{+\cdot}$ concentrations in the reaction mixture. The observed low ratios of $[\text{MV}^{+\cdot}]/[\text{MV}^{2+}]$

in the absence of catalyst cannot be explained if reaction (6.8) is not included in the reaction scheme. For the moment, the rate of this unknown reaction will be denoted as v_u .

In chapter 5 it was demonstrated that on top of the abovementioned reactions a gradual destruction of methylviologen takes place. However, the rate of this process is too slow to play an important role in the steady state period of hydrogen production. Thus, $[MV^{2+}] + [MV^{+\cdot}]$ is considered to be constant and equal to the initial concentration of methylviologen.

The rate of formation and consumption of $MV^{+\cdot}$ in solution is given by:

$$\frac{d[MV^{+\cdot}]}{dt} = \phi_s k_q [MV^{2+}][Ru(bipy)_3^{2+*}] - k_b [MV^{+\cdot}][Ru(bipy)_3^{3+}] - v_u \quad (6.9)$$

At the steady state, the net formation rate of $MV^{+\cdot}$ in solution equals its net consumption rate at the catalyst surface, and is designated as v_H (expressed in moles per unit volume of reaction mixture, per second); v_H is twice the formation rate of H_2 , assuming that no other redox reactions than (6.1) and (6.2) take place at the surface. The concentrations of all intermediate species are constant. Therefore, $[Ru(bipy)_3^{2+*}]$ and $[Ru(bipy)_3^{3+}]$ can be eliminated from equation (6.9), using:

$$\frac{d[Ru(bipy)_3^{2+*}]}{dt} = s^* - k_1 [Ru(bipy)_3^{2+*}] - k_q [MV^{2+}][Ru(bipy)_3^{2+*}] \quad (6.10)$$

$$\begin{aligned} \frac{d[Ru(bipy)_3^{3+}]}{dt} = & \phi_s k_q [MV^{2+}][Ru(bipy)_3^{2+*}] - k_b [MV^{+\cdot}][Ru(bipy)_3^{3+}] \\ & - k_{ox} [Ru(bipy)_3^{3+}][EDTA] \end{aligned} \quad (6.11)$$

if the time derivatives are set to zero. The (excess) concentration EDTA is approximately constant and therefore $k_{ox}[EDTA]$ may be replaced by a pseudo first order rate constant k'_{ox} . Rearrangement of equations (6.9)-(6.11) yields a flux equation for the homogeneous reactions:

$$v_H = \frac{s^* \phi_s k_q k'_{ox} [MV^{2+}]}{(k_i + k_q [MV^{2+}]) (k'_{ox} + k_b [MV^{+}])} - v_u \quad (6.12)$$

This equation illustrates that in the absence of catalyst ($v_H = 0$) all the MV^{2+} would be converted into MV^{+} , if reaction (6.8) were not included in the reaction scheme.

6.2.2 The rate of the excitation reaction

The quantum yield of reaction (6.3) is close to unity [21], which means that the rate of excitation, s^* , is equal to the number of photons absorbed by the sensitizer $Ru(bipy)_3^{2+}$ (expressed in moles per unit volume of reaction mixture, per second). As already mentioned in section 5.4.3, the excitation rate depends on the light intensity in the reaction cell, the concentration and the absorption spectrum of the sensitizer, and also on the light absorption by MV^{+} and RuO_2 ("inner filter effect"). At each wavelength λ , the effective light intensity in the cell is, according to Beer's law:

$$I(x, \lambda) = I_0(\lambda) 10^{-(\epsilon_1(\lambda)c_1 + \epsilon_2(\lambda)c_2 + \epsilon_3(\lambda)c_3) x} \quad (6.13)$$

x being the distance from the front window of the reaction cell and $I_0(\lambda)$ the incident light intensity; $\epsilon_1(\lambda)$, $\epsilon_2(\lambda)$, $\epsilon_3(\lambda)$, and c_1 , c_2 , c_3 stand for the extinction coefficients and concentrations of $Ru(bipy)_3^{2+}$, MV^{+} , and RuO_2 , respectively. The absorption of photons by $Ru(bipy)_3^{2+}$, $I_A(\lambda)$, can be found from equation (6.13) together with:

$$\frac{dI_A(\lambda)}{dx} = I(x, \lambda) 2.303 \epsilon_1(\lambda)c_1 \quad (6.14)$$

Integration over x from 0 to l (l is the length of the light path through the reaction cell) yields:

$$I_A(\lambda) = I_0(\lambda) \frac{\epsilon_1 c_1}{\epsilon_1 c_1 + \epsilon_2 c_2 + \epsilon_3 c_3} \{1 - 10^{-(\epsilon_1 c_1 + \epsilon_2 c_2 + \epsilon_3 c_3)l}\} \quad (6.15)$$

For convenience, $\epsilon_1(\lambda)$ is now simply written as ϵ_1 . Equation (6.15) is more general than equation (5.7), in which the inner filter effect has been neglected. The rate of excitation is found by subsequent integration over the wavelength interval of interest:

$$s^* = \frac{A}{V N_{av}} \int_{350}^{600 \text{ nm}} I_A(\lambda) d\lambda \quad (6.16)$$

where N_{av} denotes Avogadro's Number, A the illuminated area, and V the volume of the reaction solution (for a flat reaction cell, $V/A = l$). As will be shown in section 6.3.4, the concentrations of $\text{Ru}(\text{bipy})_3^{2+*}$ and $\text{Ru}(\text{bipy})_3^{3+}$ are very much lower than the total sensitizer concentration, so that $c_1 (= [\text{Ru}(\text{bipy})_3^{2+}]) \approx [\text{Ru}(\text{bipy})_3]_{\text{tot}}$.

6.2.3 Flux equations for the heterogeneous reactions

The heterogeneous processes in the hydrogen production system may be described by an electrochemical model for heterogeneous catalysis [6]. The colloidal catalyst is regarded as an assembly of microelectrodes. In the system under study, the microelectrodes are in fact aggregates of RuO_2 particles.

Figure 6.1 shows schematically the current density-potential curves of the two individual redox couples H^+/H_2 and $\text{MV}^{2+}/\text{MV}^{\cdot+}$ at the surface of the catalyst. At any given potential, the total current is the algebraic sum of the currents developed by the individual couples [5,6]. At the steady state of hydrogen production, the net oxidation and the net reduction currents at the surface must be the same. Thus, the microelectrodes attain a so-called mixed potential E_m , at which the two partial current densities have the same numerical magnitude i_m .

It has already been shown that the i - E curve for the H^+/H_2 couple can be described by the Butler-Volmer equation (see sections 3.3.4 and 5.4.3). At the steady state, the net reduction current density is given by:

$$i_m = i_o (e^{-\alpha_1 f \eta} - e^{(1-\alpha_1) f \eta}) \quad (6.17)$$

where η stands for the overpotential for hydrogen evolution, α_1 for the transfer coefficient, i_o for the exchange current density, and $f = F/RT$. The overpotential is equal to $E_m - E_{eq}$, with E_{eq} being the equilibrium potential for the H^+/H_2 couple.

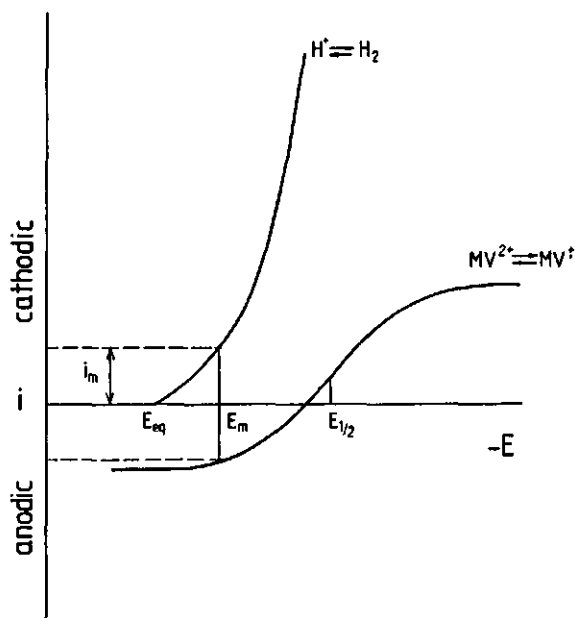


FIGURE 6.1: Schematic representation of the i - E curves for the individual redox couples reacting at the microelectrodes. For details see the text.

For the oxidation of MV^{+} at the catalyst surface, the rates of both electron transfer and mass transfer have to be taken into account (see sections 4.3.4 and 5.4.3). The net oxidation current density of the methylviologen couple at the steady state is given by [22]:

$$i_m = F k^o \left\{ [MV^{+}]_s e^{(1-\alpha_2)f(E_m - E^o)} - [MV^{2+}]_s e^{-\alpha_2 f(E_m - E^o)} \right\} \quad (6.18)$$

E^0 is the standard redox potential of the MV^{2+}/MV^{+} couple, α_2 the transfer coefficient, k^0 the standard heterogeneous rate constant, and $[MV^{+}]_s$ and $[MV^{2+}]_s$ are the concentrations of MV^{+} and MV^{2+} at the surface of the catalyst. $[MV^{+}]_s$ and $[MV^{2+}]_s$ can be related to their corresponding bulk concentrations, considering that the mass transfer of these compounds to and from the surface is equal to the rate of the surface reaction:

$$\frac{i_m}{F} = m ([MV^{2+}]_s - [MV^{2+}]) = m ([MV^{+}] - [MV^{+}]_s) \quad (6.19)$$

The mass transfer coefficients m for MV^{2+} and for MV^{+} are approximately the same; m is a function of the diffusion coefficient D_{MV} , the viscosity of the solution, the size and geometry of the microelectrodes, and the stirring regime. Furthermore, the mass transfer coefficient involves the loss of accessibility of the surface by aggregation of the RuO_2 particles.

Combination of equations (6.18) and (6.19) results into:

$$i_m = F \frac{[MV^{+}] e^{(1-\alpha_2)f(E_m-E^0)} - [MV^{2+}] e^{-\alpha_2 f(E_m-E^0)}}{\frac{1}{k^0} + \frac{1}{m} \left[e^{(1-\alpha_2)f(E_m-E^0)} + e^{-\alpha_2 f(E_m-E^0)} \right]} \quad (6.20)$$

The steady state current density i_m is related to the rate of formation of H_2 , via:

$$i_m = \frac{F V}{A_c} v_H \quad (6.21)$$

where A_c is the total catalytically active surface area in the system, and V is the volume of the reaction mixture.

6.2.4 Overall picture

Combination of the steady state flux equation for the homogeneous reactions with those for the heterogeneous reactions, gives a set of three equations for v_H :

$$v_H = \frac{s^* \phi_s k_q k'_{ox} ([MV]_{tot} - [MV^{+}])}{\{ k_1 + k_q ([MV]_{tot} - [MV^{+}]) \} \{ k'_{ox} + k_b [MV^{+}] \}} - v_u \quad (6.22)$$

$$v_H = \frac{A_c}{F V} i_o (e^{-\alpha_1 f \eta} - e^{(1-\alpha_1) f \eta}) \quad (6.23)$$

$$v_H = \frac{A_c}{V} \frac{[MV^{+}] e^{(1-\alpha_2) f (\eta + \Delta E)} - ([MV]_{tot} - [MV^{+}]) e^{-\alpha_2 f (\eta + \Delta E)}}{\frac{1}{k^o} + \frac{1}{m} \left\{ e^{(1-\alpha_2) f (\eta + \Delta E)} + e^{-\alpha_2 f (\eta + \Delta E)} \right\}} \quad (6.24)$$

where η refers, as before, to the overpotential of the microelectrodes for the hydrogen evolution reaction. The term $\eta + \Delta E$ is equal to $E_m - E^o$, the potential of the microelectrodes relative to the standard redox potential of the MV^{2+}/MV^{+} couple. (Thus, $\Delta E = E_{eq} - E^o$, in which E_{eq} is the equilibrium potential for the H^{+}/H_2 couple.)

Equations (6.22)-(6.24) have been used for numerical simulations of the steady state in the hydrogen production system. Under given "experimental" conditions (i.e. amount of RuO_2 , and concentrations of $Ru(bipy)_3^{2+}$, methylviologen, and EDTA), and using appropriate values for the various parameters, the rate of hydrogen formation, the concentration MV^{+} , and the overpotential of the RuO_2 microelectrodes can be calculated. The hydrogen production rate in ml/hr, r_{H_2} , can in a simple way be obtained from v_H .

The rate of the parasitic reaction (6.8), v_u , is a function of the MV^{+} concentration and will be estimated in the next section. The rate of the excitation reaction can be obtained using equations (6.15) and (6.16); $I_o(\lambda)$ and the extinction coefficients of $Ru(bipy)_3^{2+}$, MV^{+} , and RuO_2 are given in figure 5.2. Since the steady state concentration MV^{+} is not known beforehand, in the numerical simulations iterations have been performed to correct s^* for the inner filter effect of MV^{+} .

The exchange current density for the hydrogen evolution reaction and the standard heterogeneous rate constant for the MV^{2+}/MV^{+} couple are known for RuO_2 film electrodes (sections 3.3.4 and 4.3.4), and are here indicated as $i_{o, film}$ and k_{film}^o . The corresponding quantities for the RuO_2 microelectrodes can be written as:

$$i_o = \frac{i_{o, \text{film}}}{b} \quad (6.25a)$$

$$k^o = \frac{k_{\text{film}}^o}{b} \quad (6.25b)$$

where $i_{o, \text{film}}$ and k_{film}^o refer to the geometrical surface area of the RuO_2 film electrodes; b accounts for the surface roughness of these electrodes and for any change of the kinetic parameters of the RuO_2 due to the process of sintering the films at 700°C (see section 3.2.4).

The catalytically active surface area A_c is taken as the amount of RuO_2 multiplied by its BET specific surface area, i.e. the total surface area of the RuO_2 particles. However, there might be loss of active surface area due to aggregation and the presence of hydrogen gas bubbles at the surface. The model parameters b and m also include these effects. Under given stirring conditions and at a given ionic strength of the reaction solution, b and m should be fairly constant.

In the numerical simulations only ϕ_s , b , and m have been used as adjustable parameters. The other parameters have fixed values and these are given in table 6.1. The calculations have been performed on a Digital PDP11/73 computer.

TABLE 6.1: Parameters used in the numerical simulations of the steady state in the hydrogen production system.

parameter	value used	source	remarks
k_1	$1.6 \times 10^6 \text{ s}^{-1}$	ref. [12-15]	
k_q	$1.0 \times 10^9 \text{ M}^{-1}\text{s}^{-1}$	ref. [13]	
k_b	$2.8 \times 10^9 \text{ M}^{-1}\text{s}^{-1}$	ref. [13]	
k_{ox}	$1.0 \times 10^7 \text{ M}^{-1}\text{s}^{-1}$	ref. [28]	"typical value"
k_u/ϕ_s	0.1 s^{-1}	section 6.3.1	
α_1	0.33	section 3.3.4	0.05 M acetate buffer, pH 4.6
$i_{o, \text{film}}$	0.91 A/m^2	,,	,,
α_2	0.35	section 4.3.4	
k_{film}^o	$1.4 \times 10^{-5} \text{ m/s}$,,	
E^o	-0.446 V/NHE	ref. [25,29]	
E_{eq}	-0.267 V/NHE		$E_{eq} = -0.058 \times \text{pH}$; p_{H_2} at the RuO_2 surface is 1 atm.
S_{BET}	$21.5 \text{ m}^2/\text{g}$	section 2.6	for the batch used in the experiments of chapter 5.

6.3 RESULTS AND DISCUSSION

6.3.1 The rate of the unidentified side-reaction of MV^{+} .

It is possible to estimate the rate of reaction (6.8) from the experimentally determined steady state concentrations MV^{+} in the absence of catalyst. In that case (see equation (6.22)):

$$v_u = \frac{s^* \phi_s k_q k'_{ox} ([MV]_{tot} - [MV^{+}])}{\{ k_i + k_q ([MV]_{tot} - [MV^{+}]) \} \{ k'_{ox} + k_b [MV^{+}] \}} \quad (6.26)$$

The results for four different methylviologen concentrations are given in table 6.2. The excitation rate decreases with increasing MV^{+} concentration, due to the inner filter effect.

The quotient $v_u/(\phi_s [MV^{+}])$ represents the rate constant for reaction (6.8), assuming this process is first order in MV^{+} concentration. Since this quotient systematically decreases with increasing methylviologen concentration, it could be concluded that either reaction (6.8) is less than first order in $[MV^{+}]$ or that another species is involved for which the steady state concentration also varies with total methylviologen concentration (e.g. one of the oxidation products of EDTA, see section 5.4.3 and reference [23]). We will not speculate about this any further, since the obtained relationship between v_u and the MV^{+} concentration depends on the choice of the rate constants for the other reactions. A reasonable approach

TABLE 6.2: Experimentally determined steady state MV^{+} concentrations in the absence of catalyst, and calculated rates of the excitation reaction and reaction (6.8); 2×10^{-4} M $Ru(bipy)_3^{2+}$, 0.02 M EDTA, 0.05 M acetate buffer pH 4.6.

$[MV]_{tot}$ (M)	$[MV^{+}]$ (M)	s^* (M/s)	v_u/ϕ_s (M/s)	$v_u/(\phi_s [MV^{+}])$ (s ⁻¹)
1×10^{-4}	1.7×10^{-5}	6.15×10^{-5}	2.45×10^{-6}	0.14
2×10^{-4}	3.8×10^{-5}	5.64×10^{-5}	3.38×10^{-6}	0.09
3×10^{-4}	5.3×10^{-5}	5.35×10^{-5}	4.11×10^{-6}	0.08
5×10^{-4}	8.6×10^{-5}	4.85×10^{-5}	4.52×10^{-6}	0.05

to take reaction (6.8) into account in the simulations of the steady state, is to describe it with a (pseudo) first order rate constant k_u : $v_u = k_u [MV^{+}]$, with $k_u = 0.1 \phi_s \text{ s}^{-1}$.

6.3.2 Effects of the model parameters ϕ_s , b , and m

The influences of the parameters ϕ_s , b , and m on the simulated steady state hydrogen production rate, the MV^{+} concentration, and the overpotential of the RuO_2 microelectrodes are illustrated by figure 6.2.

The parameter ϕ_s affects the homogeneous reactions. It should be noted that in our model the value of k_u is adjusted upon changing ϕ_s (see previous section). Therefore, at low amount of catalyst, ϕ_s has hardly any influence on the MV^{+} concentration. In the limiting case of no catalyst present, $[MV^{+}]$ is constant over the whole range of ϕ_s values. (If the value of k_u would be fixed, then the steady state MV^{+} concentration would increase with ϕ_s .) In the presence of catalyst, a higher value for ϕ_s results in higher steady state MV^{+} concentrations, which allows the hydrogen production to take place at a higher rate and overpotential.

The parameters b and m both affect the heterogeneous processes: m controls the rate of mass transfer of methylviologen species to and from the surface of the microelectrodes, whereas b determines the effective values of the interfacial reaction rates. Increasing b means slowing down the interfacial processes, i.e. both i_0 and k^0 get a lower value. The hydrogen production rate decreases and will finally become zero, as if there were no catalyst at all. With decreasing hydrogen production rate, the MV^{+} concentration in the bulk solution increases. The same effects are generated by decreasing m , which implies slowing down the mass transfer of MV^{+} to the catalyst surface.

If mass transfer of the methylviologen species is much slower than the interfacial reactions (i.e. at low values for m or at low values for b), hydrogen production takes place at the mass transport limited current density of the methylviologen couple and at a low overpotential. This is illustrated in figure 6.3.

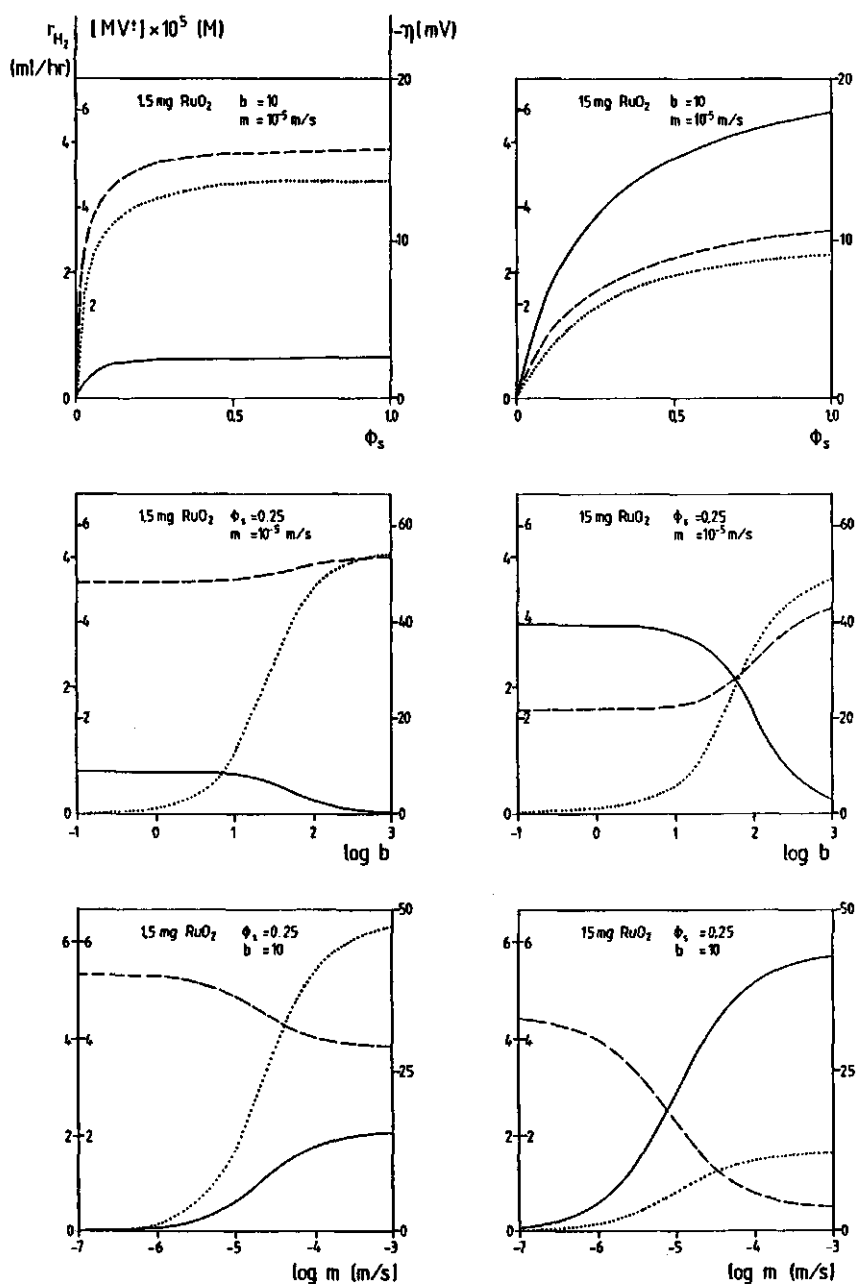


FIGURE 6.2: Simulated steady state situations in the hydrogen production system as a function of the model parameters ϕ_s , b , and m .

— r_{H_2} , --- $[MV^{+}]$, η .

Standard "experimental" conditions (2×10^{-4} M $Ru(bipy)_3^{2+}$, 5×10^{-4} M MV, 0.02 M EDTA).

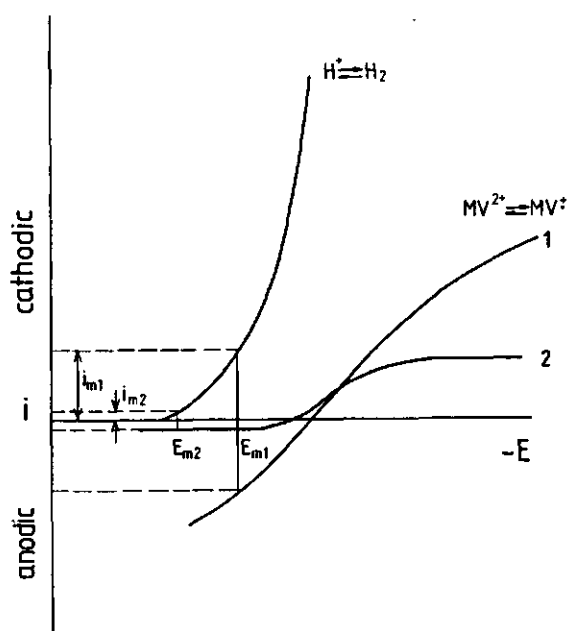


FIGURE 6.3: Schematic plots of the i - E curves for the individual redox couples reacting at the microelectrodes. Curve 1 represents the situation in which $m \times b$ is large, curve 2 stands for the situation in which $m \times b$ is relatively small. In the latter case, mass transfer of MV^{+} dominates the heterogeneous processes.

6.3.3 Parameter ranges

To determine the ranges in which the values for ϕ_s , m , and b for the $Ru(bipy)_3^{2+}/MV^{2+}/EDTA/RuO_2$ system can be found, the experimentally obtained relationships between the steady state hydrogen production rate, the MV^{+} concentration, and the amount of RuO_2 were used (displayed in figure 5.6).

The parameter ϕ_s was found by first calculating s^* for a given amount of RuO_2 and the corresponding experimentally determined MV^{+} concentration, and then calculating r_{H_2} , using equation (6.22) and taking $\phi_s = 1$. The experimental value for r_{H_2} was divided by the calculated value, which yields ϕ_s . Over the whole range of RuO_2 amounts (0.6-30 mg), the value found for ϕ_s was rather constant: $\phi_s = 0.16 \pm 0.03$. This is a satisfactory result, regarding the finding of Prasad et al. [11] (at pH 4.7, $\phi_s < 0.25$). It should be noted that the value obtained here includes the uncertainty in the light intensity $I_0(\lambda)$ and any deviations of the rate constants k_1 , k_q ,

k_b , and k_{ox} from their fixed values.

Using $\phi_s = 0.16$, it follows that $k_u \approx 0.02 \text{ s}^{-1}$. For the decay of the MV^{+} concentration after switching off the light source, a pseudo first order rate constant of about 10^{-3} s^{-1} had been found (section 5.3.2). Apparently, the conversion of MV^{+} into MV^{2+} via unknown side-reactions under illumination is ca. 20 times faster than in the dark. This points to the involvement of a photogenerated species in reaction (6.8), which could indeed be an oxidation product of EDTA, as suggested above.

For determination of ranges for the parameters b and m , a similar procedure was followed, now using the flux equations for the heterogeneous processes. From the experimentally obtained rate of hydrogen production the corresponding value of v_H was calculated. Subsequently, η was determined for various values of b , using equation (6.23). Substitution of v_H , η , and the experimental value for $\{MV^{+}\}$ in equation (6.24), yields a value for the mass transfer coefficient m .

Taking $b > 100$ results in high overpotentials, which are for the lower RuO_2 amounts physically unrealistic, in the sense that E_m is more negative than the standard redox potential of the MV^{2+}/MV^{+} couple (see figure 6.1, $E_1 = E^0$). Furthermore, for $b > 11$ negative values for m are obtained, which means that the MV^{+} concentration near the surface of the microelectrodes would be higher than in the bulk solution. This is also a physically unrealistic situation. In other words, for $b > 11$ the interfacial processes are too slow to account for the observed hydrogen production rates at the given (low) MV^{+} concentrations. Considering the roughness factor of the RuO_2 film electrodes, which is in the order of several hundreds (section 3.3.4), and the fact that the electrochemical surface area of the RuO_2 particles found from the acid-base potentiometric titrations equals the BET surface area (section 3.3.1), the value of b is surprisingly small.

Taking $b < 11$, m was generally found to be in the range of $1-3 \times 10^{-5} \text{ m/s}$, which seems to be quite reasonable: Miller et al. [7,8] estimate the mass transfer coefficient for methylviologen in hydrogen production systems to be 10^{-5} m/s .

6.3.4 Simulation of the steady state as a function of RuO_2 amount

Having established in which ranges appropriate values for ϕ_s , b , and m can be found, the complete set of equations (6.22)-(6.24) was used to simu-

late the steady state as a function of amount of RuO_2 under standard "experimental" conditions. An acceptable agreement between the experimentally determined hydrogen production rate and MV^{+} concentration and the corresponding calculated values, is obtained with $\phi_s = 0.16$, $b = 8$, and $m = 3 \times 10^{-5}$ m/s. This is shown in figure 6.4. In the absence of catalyst, the calculated MV^{+} concentration is lower than the experimental value, resulting from the fact that for k_u an average value for four different methylviologen concentrations has been taken. Also for the higher RuO_2 amounts, the quantitative agreement between the calculated and the experimentally found MV^{+} concentrations is not perfect.

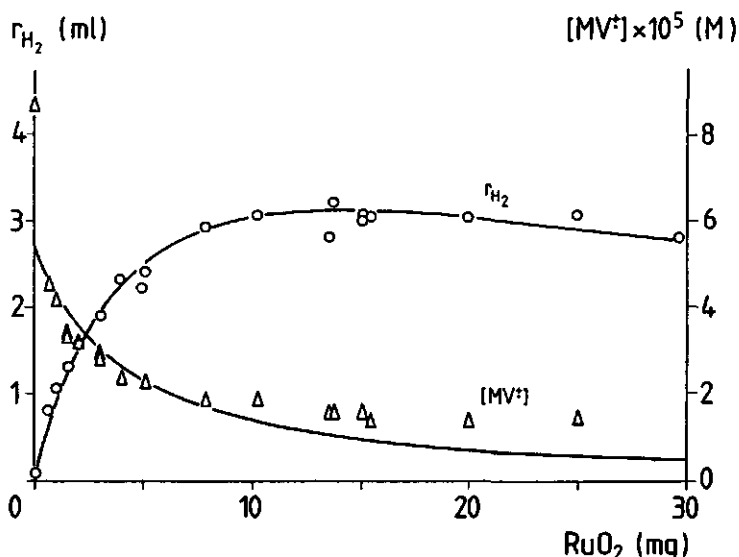


FIGURE 6.4: Numerical simulations (drawn curves) and experimental results (points) for the steady state hydrogen production rate and MV^{+} concentration as a function of amount of RuO_2 . The other experimental conditions are standard.

In table 6.3 the corresponding overpotentials of the RuO_2 microelectrodes are given. Over the whole range of RuO_2 quantities, the overpotential is low. Therefore, back-reaction of MV^{2+} at the catalyst surface is negligible (see figure 6.1 and equation (6.24)). At high amounts of catalyst, the hydrogen evolution takes place very close to the equilibrium potential of the H^{+}/H_2 couple.

TABLE 6.3: Simulated steady state situation in the hydrogen production system; 2×10^{-4} M $\text{Ru}(\text{bipy})_3^{2+}$, 5×10^{-4} M MV, 0.02 M EDTA. For further details see the text.

RuO_2 (mg)	η (mV)	Q	ϕ_H	$s^* \times 10^5$ (M/s)
0.1	-28	2.9	0.0008	5.35
1	-23	3.3	0.007	5.39
2	-19	3.6	0.011	5.39
3	-16	3.9	0.014	5.35
5	-12	4.3	0.019	5.21
7	-10	4.6	0.022	5.04
10	-7	4.9	0.026	4.67
15	-5	5.2	0.029	4.32
20	-4	5.4	0.031	3.93
30	-2	5.6	0.033	3.32
100	0	5.8	0.036	1.64

The importance of mass transfer of $\text{MV}^{+\bullet}$ to the microelectrode relative to the electron transfer reaction at the surface, can be expressed in terms of the reversibility quotient Q:

$$Q = \frac{1}{m} \left\{ e^{(1-\alpha_2)f(\eta+\Delta E)} + e^{-\alpha_2 f(\eta+\Delta E)} \right\} / \frac{1}{k^0} \quad (6.27)$$

If $Q \gg 1$, the results of the simulations are independent of k^0 , and the electron transfer reaction would be essentially a Nernstian reaction (electrochemically reversible). Values for Q are given in table 6.3. They show that mass transfer dominates as rate-determining factor over electron transfer, but the latter cannot be neglected. With increasing RuO_2 amount, mass transfer becomes even more important, as may be expected.

The quantum yield of hydrogen production, ϕ_H , is defined as the fraction of photons absorbed by the sensitizer which actually results in formation of hydrogen, i.e. $\phi_H = v_H/s^*$. It increases with amount of catalyst (see table 6.3), and its limiting value is completely determined by the homogeneous reactions. From equation (6.22), it can be deduced that under

the standard conditions of our experiments, this limiting value is ca. 0.04. Less than 4 % (!) of the photons absorbed by the sensitizer is efficiently used for hydrogen production.

Although ϕ_H increases with the amount of catalyst, the hydrogen production rate itself exhibits a maximum. This is due to the inner filter effect of RuO_2 and is illustrated by the values for s^* in table 6.3. If there would be no light absorption by RuO_2 , nor by $\text{MV}^{+\cdot}$, the rate of excitation at a sensitizer concentration of 2×10^{-4} M would be ca. 6.7×10^{-5} M/s.

To conclude this section, a final word about the steady state concentrations $\text{Ru}(\text{bipy})_3^{2+\cdot}$ and $\text{Ru}(\text{bipy})_3^{3+}$. From equations (6.10) and (6.11), it can be derived that for $s^* \approx 5 \times 10^{-5}$ M/s and the standard concentrations methylviologen and EDTA, $[\text{Ru}(\text{bipy})_3^{2+}] \approx 2 \times 10^{-11}$ M and $[\text{Ru}(\text{bipy})_3^{3+}] \approx 8 \times 10^{-12}$ M. Therefore, the assumption that the sensitizer is mainly present in the form $\text{Ru}(\text{bipy})_3^{2+}$ is justified.

6.5.3 Steady state simulations as a function of light intensity and composition of the reaction solution

In this section, the model parameters ϕ_s , m , and b are fixed at the values found in the previous section, which are 0.16, 3×10^{-5} m/s, and 8, respectively.

In figures 6.5-6.7 the effects of the light intensity, the $\text{Ru}(\text{bipy})_3^{2+}$ concentration, and the EDTA concentration on the steady state hydrogen production rate and $\text{MV}^{+\cdot}$ concentration are shown. For comparison, the experimentally obtained results are also indicated. Although there is no complete quantitative accordance, the numerical simulations are in fair agreement with the experimental results and the model describes all the effects observed.

With increasing light intensity or $\text{Ru}(\text{bipy})_3^{2+}$ concentration, the potential of the microelectrodes becomes more negative and mass transfer of $\text{MV}^{+\cdot}$ to the surface of the catalyst becomes a less important rate-determining factor. Both effects are the result of a higher $\text{MV}^{+\cdot}$ concentration in solution. The quantum yield for hydrogen formation decreases: the increase in photon absorption by the sensitizer does not result in a proportional increase in hydrogen production, due to progressive competition of side-reactions of $\text{MV}^{+\cdot}$ with the production of hydrogen.

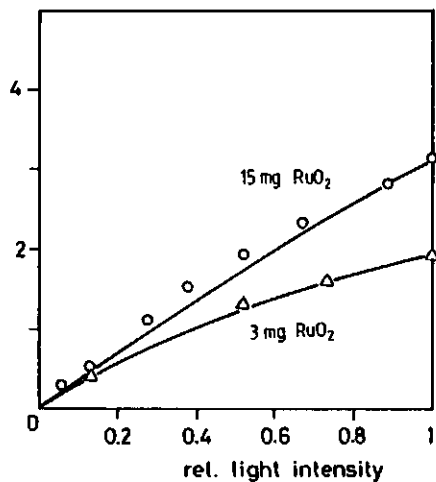
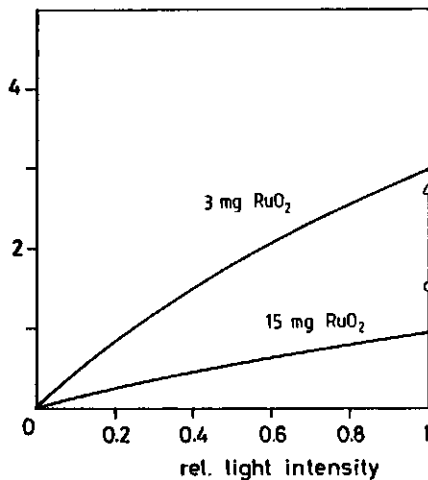
r_{H_2} (ml/hr) $[MV^+]\times 10^5$ (M)

FIGURE 6.5: Numerical simulations (drawn curves) and experimental results (points) for the steady state rate of hydrogen production and MV^+ concentration as a function of light intensity. (Standard reaction mixture.)

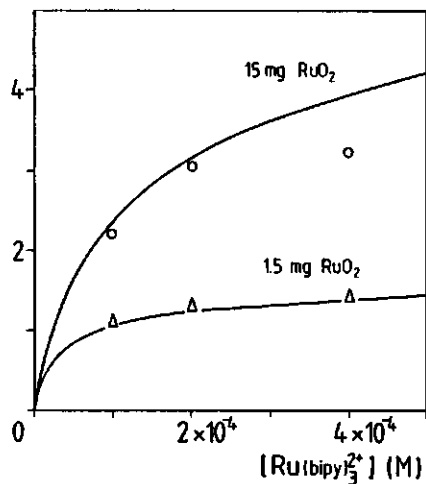
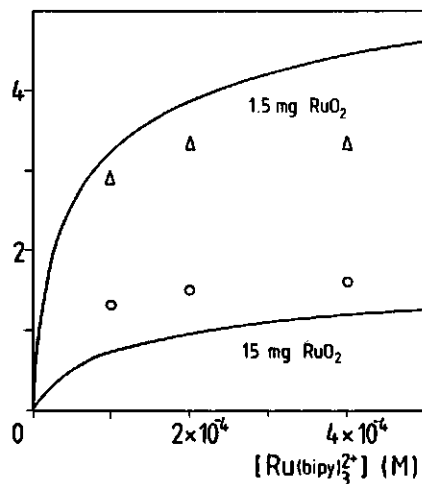
 r_{H_2} (ml/hr) $[MV^+]\times 10^5$ (M)

FIGURE 6.6: Numerical simulations (drawn curves) and experimental results (points) for the steady state hydrogen production rate and MV^+ concentration as a function of sensitizer concentration. The other conditions are standard.

With increasing EDTA concentration, the same effects are observed, except for the quantum yield of the hydrogen production process, which now becomes higher. The influence of the EDTA concentration is negligible above a concentration of about 0.02 M, as was found in the experiments. Apparently, for the rate constant k_{ox} , which is not as well-defined as the other rate constants for the homogeneous reactions, $10^7 \text{ M}^{-1}\text{s}^{-1}$ is an appropriate value.

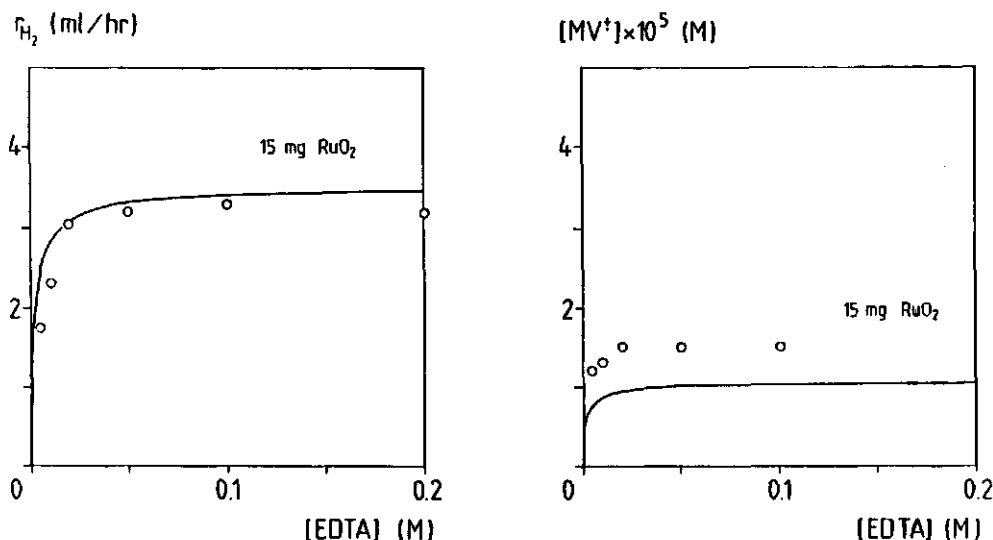


FIGURE 6.7: Numerical simulations (drawn curves) and experimental results (points) for the steady state hydrogen production rate and MV^{+} concentration as a function of EDTA concentration. The other conditions are standard.

The numerical simulations and the experimental results for the steady state rate of hydrogen production and MV^{+} concentration as a function of methylviologen concentration are shown in figure 6.8. The model predicts an increase of the production rate with methylviologen concentration, until a plateau is reached. For 1.5 mg RuO_2 a slight decrease in r_{H_2} above 5×10^{-3} M is predicted. The overpotential for the hydrogen evolution reaction of the RuO_2 microelectrodes and the quantum yield for hydrogen formation increase with the methylviologen concentration. At the plateau, ϕ_H is ca. 0.017 for 1.5 mg RuO_2 and ca. 0.075 for 15 mg RuO_2 .

At low methylviologen concentrations ($< 2 \times 10^{-3}$ M for 1.5 mg RuO_2 , $< 10^{-3}$ M for 15 mg RuO_2), the numerical simulations are in agreement with

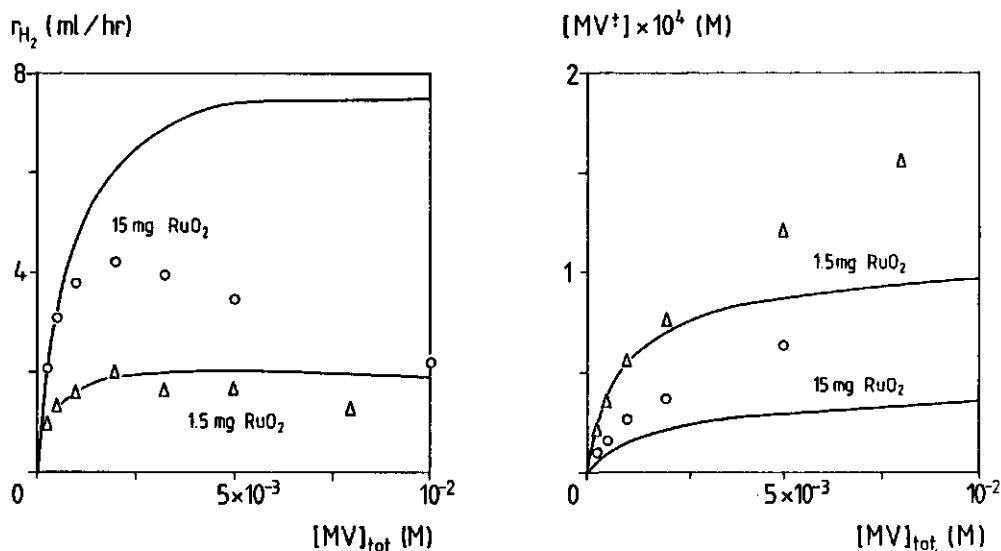


FIGURE 6.8: Numerical simulations (drawn curves) and experimental results (points) for the hydrogen production rate and MV^{+} concentration as a function of the total methylviologen concentration. The other experimental conditions are standard.

the experimental results. However, the model does not account for the experimentally observed maximum in the hydrogen production rate as a function of methylviologen concentration; changing the values of ϕ_B , m , and b does not result in a more acceptable description of the experiments. Therefore, it seems that this maximum is not due to reaction (6.6) becoming competitive with reaction (6.7), nor to the progressive competition of the other undesired side-reaction of MV^{+} with the hydrogen production. Even if k_{ox} is lowered or k_u is increased by a factor of 100, still no maximum is found. Doing so decreases all the calculated values for r_{H_2} .

To investigate whether the maximum in production rate as a function of methylviologen concentration could be caused by dimerization of the methylviologen radical, this phenomenon was incorporated in the model. It was assumed that the dimer is always in equilibrium with MV^{+} , according to equation (5.10), and that the dimer neither reacts with the other compounds in solution, nor gives rise to hydrogen production at the catalyst surface. Using the literature value for the equilibrium constant K_D ($3.8 \times 10^2 \text{ M}^{-1}$ [24,25]), the dimerization has no significant effect on the calculated production rates, nor on the steady state MV^{+} concentrations. In all cases

only a very small fraction of the radical is present in the dimer form. Increasing K_D , up to 1000 times its literature value, results in a decrease of r_{H_2} and $[MV^{+\cdot}]$, but does not give a maximum in r_{H_2} as a function of the methylviologen concentration. Therefore, the maximum cannot be ascribed to dimerization of $MV^{+\cdot}$, and, assuming the literature value for K_D to be correct, the dimerization equilibrium can be left out of the model.

The differences in the experimental and the calculated $MV^{+\cdot}$ concentrations (the former increasing more strongly with increasing methylviologen concentration than the latter), suggest that MV^{2+} slows down the heterogeneous reactions by adsorption on the catalyst surface, a phenomenon that has been reported for Pt catalysts [4,10,26,27]. If the heterogeneous reactions are progressively inhibited with increasing methylviologen concentration, the bulk concentration $MV^{+\cdot}$ would indeed increase more strongly than the model predicts. (To simulate this, b should be made a function of the methylviologen concentration.) However, the deviations between the experimental and the calculated r_{H_2} and $[MV^{+\cdot}]$ start already below $1-2 \times 10^{-3}$ M methylviologen. For such and even higher concentration levels, no indications have been found for any significant adsorption of MV^{2+} on RuO_2 under the conditions applied in the hydrogen production system (see chapter 4). Therefore, the cause of the phenomenon of a maximum in the hydrogen production rate as a function of methylviologen concentration is as yet an open question.

6.3.6 Time-evolution of the $MV^{+\cdot}$ concentration upon illumination

In the previous chapter, it was concluded that the building up of the steady state concentration $MV^{+\cdot}$ is probably the main factor that determines the induction times for the hydrogen production process. Here, the time-evolution of the $MV^{+\cdot}$ concentration in the standard reaction solution is simulated numerically, for the case that no catalyst is present. The simulation is carried out using equations (6.9)-(6.11), in which $\phi_s = 0.16$ and $v_u = k_u [MV^{+\cdot}]$, with $k_u = 0.02 \text{ s}^{-1}$. The calculations were performed on a Digital VAX/8600 computer. To save computer time, the concentration of MV^{2+} and the excitation rate s^* were considered to be constant. In the real situation, both quantities decrease with increasing $MV^{+\cdot}$ concentration, but the variation is not strong (at the steady state more than 80 % of the methylviologen is still present as MV^{2+} , and s^* is 0.7 times its original

value).

Figure 6.9 shows the results of the numerical simulation. The steady state concentration of MV^{+} is reached within a few minutes. In the experiments, when the solution is illuminated for the first time, the building up of the MV^{+} concentration starts only after a few minutes and it can take up to 20 minutes to reach the steady state (see figure 5.4). Probably, the process is delayed by the presence of residual oxygen, which reacts with the first methylviologen radicals formed [23]. When the light is switched off, after having reached the steady state concentration of MV^{+} , and the MV^{+} concentration has decayed to zero, repeated irradiation leads to a much faster approach of a steady state. The experimentally observed increase in MV^{+} concentration during this second irradiation period is also given in figure 6.9. There is a significant difference between this experimental result and the simulation. The cause of this might again be related to the poor treatment of the unidentified parasitic reaction (6.8).

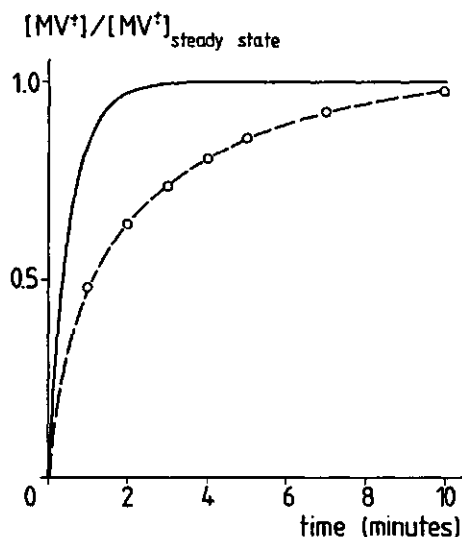


FIGURE 6.9: Simulated (drawn curve) and experimentally observed time-evolution (points) of the MV^{+} concentration in the standard reaction solution upon illumination.

6.4 CONCLUSIONS

The present chapter provides a quantitative theory for the steady state in the $\text{Ru}(\text{bipy})_3^{2+}/\text{MV}^{2+}/\text{EDTA}/\text{RuO}_2$ system for photoproduction of hydrogen. It is shown that the catalytic properties of colloidal RuO_2 can be understood and predicted by using a fairly simple electrochemical model. Both the homogeneous and the heterogeneous processes are taken into account, allowing a satisfactory interpretation of most of the results reported in chapter 5. Extensions of this approach should assist the rational design of catalytic systems for solar energy conversion.

The parameter ϕ_s , which indicates the probability of the quenching of $\text{Ru}(\text{bipy})_3^{2+}$ by MV^{2+} to result in charge separation, has been found to be about 0.16, in accordance with literature. The mass transfer coefficient for methylviologen, m , is in the order of 10^{-5} m/s. For the model parameter b , which incorporates among other effects the roughness factor of the RuO_2 film electrodes, an unexpectedly low value of ca. 10 has been found. This finding deserves further study.

The effects of amount of catalyst, light intensity, concentration sensitizer, and concentration electron donor are satisfactorily described by the model. The application of a numerical optimization procedure, in which all model parameters are involved, could result in an even better quantitative agreement between model predictions and experimental results. The model calculations confirm that hydrogen evolution at the catalyst surface takes place at low overpotentials, even at small amounts of catalyst. The overall rate of the heterogeneous processes is dominated by mass transport of MV^{+} to the catalyst surface.

The model is limited by lack of insight into the various break-down and other side-reactions of the electron relay methylviologen. The experimental results on the steady state hydrogen production rate and MV^{+} concentration at higher methylviologen concentrations cannot be simulated by the model, making further refinements necessary. The differences between model predictions and experiments point to a progressive inhibition of the heterogeneous processes with increasing methylviologen concentration. This appears to be in contradiction with our findings that MV^{2+} does not significantly adsorb on RuO_2 under the conditions of hydrogen production. This problem will be the subject of further investigations in our laboratory.

6.5 REFERENCES

1. A. J. Henglein, *J. Phys. Chem.* **83** (1979) 2209-2216
2. D. Meisel, W. Mulac, and M. S. Matheson, *J. Phys. Chem.* **85** (1981) 179-187
3. A. Harriman, and A. Mills, *J. Chem. Soc., Faraday Trans. 2* **77** (1981) 2111-2124
4. W. J. Albery, P.N. Bartlett, and A. J. McMahon, in "Photogeneration of Hydrogen", A. Harriman, and M. A. West (eds.), Academic Press, New York (1982) 85-103
5. C. Wagner, and W. Traud, *Z. Elektrochem.* **44** (1938) 391-402
6. M. Spiro, *J. Chem. Soc., Faraday Trans. 1* **75** (1979) 1507-1512
7. D. S. Miller, A. J. Bard, G. McLendon, and J. Ferguson, *J. Am. Chem. Soc.* **103** (1981) 5336-5341
8. D. S. Miller, and G. McLendon, *J. Am. Chem. Soc.* **103** (1981) 6791-6791
9. W. J. Albery, and A. J. McMahon, *J. Electroanal. Chem.* **182** (1985) 1-6
10. W. J. Albery, P. N. Bartlett, and A. J. McMahon, *J. Electroanal. Chem.* **182** (1985) 7-23
11. D. R. Prasad, K. Mandal, and M. Z. Hoffman, *Coord. Chem. Rev.* **64** (1985) 175-190
12. K. Kalyansundaram, J. Kiwi, and M. Grätzel, *Helv. Chim. Acta* **61** (1978) 2720-2730
13. P. Keller, A. Moradpour, E. Amouyal, and H. B. Kagan, *Nouv. J. Chim.* **4** (1980) 377-384
14. Y. Kawanashi, N. Kitamura, Y. Kim, and S. Tazuke, *Sci. Pap. Inst. Phys. Chem. Res.* **78** (1984) 212-219
15. E.-I. Ochiai, D. I. Schaffer, D. L. Wampler, and P. D. Schettler, *Trans. Met. Chem.* **11** (1986) 241-246
16. P. A. Brugger, and M. Grätzel, *J. Am. Chem. Soc.* **102** (1980) 2461-2466
17. E. Amouyal and B. Zidler, *Isr. J. Chem.* **22** (1982) 133-137
18. P. C. Lee, M. S. Matheson, and D. Meisel, *Isr. J. Chem.* **22** (1982) 133-137
19. D. S. Miller, and G. McLendon, *Inorg. Chem.* **20** (1981) 950-953
20. N. Sutin, *J. Photochem.* **10** (1979) 19-40
21. J. N. Demas, and D. G. Taylor, *Inorg. Chem.* **18** (1979) 3177-3179
22. A. J. Bard, and L. R. Faulkner, in "Electrochemical Methods, Fundamentals and Applications", John Wiley and Sons, New York (1980)

23. E. Amouyal, *Sci. Papers Inst. Phys. Chem. Res.* **78** (1984) 220-231
24. E. M. Kosower, and J. L. Cotter, *J. Am. Chem. Soc.* **86** (1964) 5524-5527
25. A. Harriman, and G. Porter, *J. Chem. Soc., Faraday Trans. 2* **78** (1982) 1937-1943
26. B. Beden, O. Enea, F. Hahn, and C. Lamy, *J. Electroanal. Chem.* **170** (1984) 357-361
27. O. Enea, *Electrochim. Acta* **30** (1985) 13-16
28. T. W. Ebbesen, *J. Phys. Chem.* **88** (1984) 4131-4135
29. E. Amouyal, P. Keller, and A. Moradpour, *J. Chem. Soc., Chem. Commun.* (1980) 1019-1020

CHAPTER 7

SUMMARY, CONCLUSIONS, AND PERSPECTIVES

The formation of hydrogen from water using solar energy is a very attractive research topic, because of the potential use of hydrogen as an alternative, clean fuel. It has been shown by many workers in the field that photochemical hydrogen generation can be achieved in an aqueous system, containing a sensitizer (a light absorbing solute), an electron relay, and a dispersed catalyst. The electron relay transfers electrons from the light-excited sensitizer to the surface of the catalyst, where subsequent reduction of H^+ takes place. In an ideal photochemical system for solar energy conversion, water itself would ultimately provide the necessary electrons for hydrogen formation, under simultaneous oxygen evolution. However, complete ("cyclic") photodissociation of water involves a number of complications, like the recombination of intermediate photoproducts. To separately study the formation of hydrogen, these additional problems can be bypassed by adding an electron donor, which decomposes after having reduced the oxidized sensitizer. Such simplified systems are known as "sacrificial".

The present thesis is concerned with the generation of hydrogen in such a sacrificial photochemical system. The main purpose has been to gain insight into the processes that take place at the catalyst/solution interface. Because of its wide application in photochemical model systems for hydrogen production, methylviologen (MV^{2+}) was chosen as the electron relay. Via its reduced form $MV^{\cdot+}$, electrons are transferred from the sensitizer to the catalyst. Colloidal ruthenium dioxide (RuO_2) was used as the catalyst compound. It has the advantage over the more commonly used Pt catalysts, that it does not catalyze the undesired, irreversible hydrogenation of MV^{2+} .

The heterogeneous processes in a hydrogen photoproduction system cannot be investigated without taking into account the reactions in solution too. Therefore, ruthenium trisbipyridyl ($Ru(bipy)_3^{2+}$) and EDTA were chosen as photosensitizer and sacrificial electron donor, respectively: most of

the (light-induced) homogeneous reactions that take place in the $\text{Ru}(\text{bipy})_3^{2+}/\text{MV}^{2+}/\text{EDTA}/\text{colloidal catalyst system}$ have been studied extensively by different groups of researchers. In our experiments, the standard reaction mixture (58 ml) for photogeneration of hydrogen contained 2×10^{-4} M $\text{Ru}(\text{bipy})_3^{2+}$, 5×10^{-4} M MV^{2+} , 0.02 M EDTA, and 0.05 M acetate buffer (pH 4.6).

Colloidal RuO_2 was prepared by thermal decomposition of RuCl_3 at ca. 400 °C. The material obtained is crystalline and only slightly contaminated with residual Cl, which is mainly present at the surface of the particles. The BET surface area is 20–30 m^2/g . Dispersions of RuO_2 are colloid-chemically very unstable, even in the presence of polymers or surfactants. They manifest the same electric double layer characteristics as many other oxide dispersions. The point of zero charge (p.z.c.) in indifferent electrolyte (KNO_3) is positioned at pH 5.7–5.8.

Experiments with RuO_2 film electrodes, prepared from the same colloidal material and sintered at 700 °C, revealed that the hydrogen evolution reaction is chemically reversible. Hydrogen evolution at moderate overpotentials does not modify the RuO_2 . In the presence of 0.05 M acetate buffer (pH 4.6), the mass transport limited current density for H^+ reduction is high since it is related to the buffer capacity and not to the actual proton activity. In the potential range studied, the hydrogen evolution reaction can be described by the Butler-Volmer equation, with a transfer coefficient α of about 0.33, and an exchange current density i_0 of ca. 0.09 mA/cm^2 geometrical surface area. The true exchange current density is smaller by a factor depending on the surface roughness of the film electrodes.

Adsorption of MV^{2+} at the $\text{RuO}_2/\text{solution}$ interface is mainly a result of attractive coulombic interactions (above the p.z.c. of RuO_2), but it has been shown that there are also more specific interactions. However, the specific adsorption is weak and not noticeable at high concentrations of back-ground electrolyte and pH values below the p.z.c. of RuO_2 . No indications were found that MV^{2+} adsorbs at the catalyst surface under operational conditions of hydrogen evolution. Under these conditions, the sensitizer $\text{Ru}(\text{bipy})_3^{2+}$ does not adsorb either. On the other hand, the electron donor EDTA strongly adsorbs on RuO_2 from a 0.05 M acetate buffer solution of pH 4.6. However, this seems not to affect the electron transfer between methylviologen and RuO_2 film electrodes, a process which takes place with a

transfer coefficient α of ca. 0.35 and a standard heterogeneous rate constant k^0 of ca. 1.4×10^{-5} m/s (referred to the geometrical surface area).

The colloidal RuO_2 turned out to be a good catalyst for photoproduction of hydrogen, in spite of the strong tendency of the particles to form aggregates. During the hydrogen evolution process, it does not lose its catalytic properties. It was confirmed that RuO_2 does not catalyze the hydrogenation of methylviologen. A disadvantage of RuO_2 is that it absorbs light throughout the entire visible region.

Upon illumination of the reaction dispersion and after a certain induction time, hydrogen production takes place at a constant rate (steady state). After several hours, the production rate gradually decreases to zero. The maximum attainable amount of H_2 is determined by the initial amount of electron donor: each EDTA species can regenerate three oxidized sensitizer ions. However, in most experiments the total H_2 yield was less due to gradual destruction of methylviologen in the bulk solution.

The steady state ratio $[\text{MV}^{\cdot+}]/[\text{MV}^{2+}]$ appeared to be always low, even in the absence of catalyst. This must be the result of a yet unspecified reaction which reconverts $\text{MV}^{\cdot+}$ into MV^{2+} . Probably, a photogenerated intermediate species is involved in this process.

In all the experiments with the hydrogen photoproduction system, the incident light intensity was a rate-determining factor. The steady state rate of hydrogen production depends also, but to a lower extent, on the sensitizer concentration. It has been shown in a simple way that the first step in the hydrogen evolution process, i.e. the excitation of $\text{Ru}(\text{bipy})_3^{2+}$, is first order in the light intensity and less than first order in the sensitizer concentration.

The hydrogen production rate increases with EDTA concentration up to a plateau above ca. 0.02 M. At the plateau, the oxidized sensitizer is regenerated efficiently, preventing back-reaction with $\text{MV}^{\cdot+}$. As a function of methylviologen concentration, the production rate exhibits a maximum around 2×10^{-3} M.

At low quantities of RuO_2 (< 10 mg), the available catalytic surface area is rate-limiting. At higher catalyst amounts, the production rate is fairly constant; it decreases slightly with increasing RuO_2 amount due to the absorption of light by the RuO_2 particles.

For any amount of RuO_2 , the stirring rate affects the rate of hydrogen evolution. Mass transfer of H^+ to the catalyst surface is not rate-

limiting, as is also confirmed by the insensitivity of the production rate to the buffer concentration. This implies that the mass transfer of MV^{+} to the catalyst surface is a rate-determining factor.

Most of the abovementioned experimental results can be satisfactorily simulated using a quantitative model, in which the homogeneous reactions are described by steady state kinetic equations and the heterogeneous processes as electrode reactions. The catalytic properties of RuO_2 can be understood and predicted by considering the RuO_2 aggregates as microelectrodes. Probably, the electrical conductivity of RuO_2 -on the level of a metallic conductor- is essential for its catalytic performance.

Hydrogen evolution at the catalyst surface takes place near the equilibrium potential of the H^+/H_2 couple. At these potentials, reconversion of MV^{2+} into MV^{+} at the catalyst surface is negligible. The rate of the heterogeneous processes is determined by the rate of mass transfer of MV^{+} to the surface and, to a lower degree, by the rate of interfacial electron transfer. The mass transfer coefficient of methylviologen, under the standard stirring conditions, appeared to be in the order of 10^{-5} m/s.

Mass transfer of methylviologen would undoubtedly be favoured by a better dispersion of the catalyst, since aggregation of the RuO_2 particles makes the surface less accessible. If the same or higher hydrogen production rates could be reached with lower catalyst amounts, the disadvantage of light absorption by the RuO_2 particles would become less important. Therefore, it seems worth trying again to stabilize dispersions of RuO_2 , for example by covalently linking polymers to the oxide surface.

The simulations further indicate that, if the total surface area of the RuO_2 particles is assumed to be catalytically active, the kinetic parameters i_0 and k^0 are only ca. 10 times lower than the corresponding values found for the RuO_2 film electrodes per unit geometrical surface area. This is surprising, because the roughness factor of these electrodes was estimated to be in the order of several hundreds. This point deserves further attention. Aspects that could be investigated, are the influence of heat treatments on the reductive catalytic properties of RuO_2 and the comparison with kinetic parameters for single crystal RuO_2 electrodes.

The presented model for the hydrogen production system does not account for the maximum in hydrogen production rate as a function of methylviologen concentration. The differences between model predictions and experimental results point to a progressive inhibition of the heterogeneous

processes with increasing MV^{2+} concentration. This aspect will be the subject of further study, including investigation of the dependency of the electron transfer rate constant on the bulk concentration of methylviologen.

The overall quantum yield of the hydrogen production in our standard system is low; even with an excess of catalyst, it is less than 4 %. Since reconversion of MV^{2+} into MV^{+} at the catalyst surface does not take place (each MV^{+} species that reaches the surface is used for hydrogen production), the low efficiency of the system results from the homogeneous processes. Reconversion of MV^{+} into MV^{2+} in solution is competitive with the production of hydrogen and makes the system less efficient. The quantum yield is also limited by the low efficiency of the quenching of the excited sensitizer by methylviologen. At pH 4.6, less than 25 % of the quenching acts results in charge separation (according to our numerical simulations ca. 16 %). Furthermore, the gradual destruction of methylviologen under illumination of the reaction mixture, makes this compound unsuitable for use in any practical device for photogeneration of hydrogen.

Combination of information regarding the homogeneous and interfacial aspects of the hydrogen production system leads to a picture that is at least semiquantitatively, and in many aspects quantitatively consistent. Extensions of this approach could be useful for the rational design of catalytic systems for solar energy conversion.

SAMENVATTING

Sinds de oliecrisis van de jaren zeventig is er over de hele wereld veel onderzoek gedaan om alternatieve energiebronnen aan te boren. Een van deze alternatieve bronnen is de zon. Echter, voordat zonne-energie gebruikt kan worden voor praktische doeleinden, moet ze eerst omgezet worden in warmte of elektrische energie, of moet ze vastgelegd worden in de vorm van een brandstof. De zonnecellen die al enige jaren commercieel verkrijgbaar zijn, zetten zonlicht om in elektriciteit.

Het onderzoek dat in dit proefschrift beschreven wordt, houdt verband met het omzetten van zonne-energie in brandstofenergie. Met behulp van zonlicht kan water (H_2O) gesplitst worden in waterstof (H_2) en zuurstof (O_2). Als de waterstof verbrand wordt, komt de opgeslagen zonne-energie weer vrij en ontstaat er alleen maar water. Waterstofgas is dus een erg schone brandstof.

De vraag is nu hoe zonlicht gebruikt kan worden om water te splitsen. Het grote voorbeeld is het fotosynthese-proces in de plant. Dit proces speelt zich af in ingewikkelde, hoog-gespecialiseerde onderdelen van de plant, de "chloroplasten". Hierbij speelt het licht-invangende (lichtabsorberende) pigment chlorofyl, dat de bladeren hun groene kleur geeft, een centrale rol. Het hele proces komt er uiteindelijk op neer dat aan water elektronen worden onttrokken, waardoor zuurstof vrijkomt. De elektronen en overgebleven protonen (positief geladen waterstofatomen, H^+) worden gebruikt om koolzuurgas uit de lucht om te zetten in suikers en andere energierijke materialen die de plant nodig heeft voor zijn groei en onderhoud.

Van het fotosynthese-proces heeft men afgekeken welke onderdelen er nodig zijn om in een kunstmatig systeem water te splitsen. Dat zijn:

- een lichtabsorberende stof (een pigment),
- een stof die elektronen kan transporteren (elektonenmediator),
- twee katalysatoren, één voor H_2 vorming en één voor O_2 vorming.

Het pigment en de elektonenmediator zijn opgelost in water; de katalysatoren zijn meestal vaste stoffen, die in de vorm van kleine deeltjes verspreid zijn door die oplossing. Een katalysator is in het algemeen een stof die ervoor zorgt dat scheikundige reacties sneller kunnen verlopen, zonder

daarbij zelf verbruikt te worden.

Door de absorptie van licht wordt een elektron van het pigment in een toestand van hogere energie gebracht ("aangeslagen toestand"), waardoor het lossier komt te zitten en kan worden overgedragen aan de elektronenmediator. De elektronenmediator brengt het elektron naar het oppervlak van de katalysator voor H_2 produktie. De katalysator zorgt ervoor dat de afgeleverde elektronen worden overgedragen op de H^+ ionen van water, zodat waterstof kan ontstaan.

Ondertussen is het pigment een van zijn elektronen kwijtgeraakt en kan zo niet meer funktionieren. In het ideale geval zou het via de andere katalysator een elektron moeten krijgen van water, onder vorming van zuurstof. Het systeem zou dan tegelijk zuurstof en waterstof maken, terwijl er netto alleen water wordt verbruikt. Het zou in principe eeuwig kunnen werken, als er op tijd "met de gieter" langs wordt gegaan en de zon zou blijven schijnen.

Helaas blijkt in de praktijk dat het pigment en de elektronenmediator toch geleidelijk aan worden afgebroken, zodat de systemen maar een beperkte levensduur hebben (enige uren tot, op z'n hoogst, dagen). Verder verlopen de gelijktijdige vorming van waterstof en zuurstof in één systeem niet zonder problemen; het gevormde waterstof bemoeilijkt de vorming van zuurstof en andersom. Een ander probleem is de explosiviteit van het gevormde gasmengsel ("knaalgas").

Om deze bijkomende problemen te omzeilen bij de bestudering van de waterstofvorming, gebruikt men vaak systemen met maar één katalysator. Er wordt dan een stof toegevoegd die elektronen kan leveren aan de pigmentmolekulen. Deze elektronendonator wordt verder afgebroken en dus opgeofferd voor de produktie van waterstof.

In dit werk is ook zo'n vereenvoudigd systeem met één katalysator gebruikt. Het voornaamste doel van het onderzoek was het verkrijgen van inzicht in wat er zich afspeelt in het grensvlak tussen de katalysator en de oplossing, en welke factoren daar de snelheid van de waterstofvorming bepalen. De stof methylviologeen (MV^{2+}) werd gekozen als de elektronenmediator, omdat die het meest gebruikt wordt in dit soort systemen. (Methylviologeen is ook wel bekend als onkruidbestrijdingsmiddel onder de naam paraquat.) Als katalysator werd rutheniumdioxide (RuO_2) gebruikt. Het was al door een andere groep onderzoekers aangetoond dat dit een goede katalysator is voor waterstofproduktie.

Als lichtabsorberend pigment werd rutheniumtrisbipyridine ($\text{Ru}(\text{bipy})_3^{2+}$) gebruikt, en als elektronendonator ethyleendiaminetetra-azijnzuur (EDTA).

Het RuO_2 dat werd gebruikt, bestaat uit heel kleine deeltjes (ongeveer 30 nm klein, d.w.z. 30 miljoenste delen van een millimeter). Het effectieve oppervlak van de deeltjes is daardoor tamelijk groot, namelijk 20-30 m² per gram RuO_2 . Als de deeltjes in water worden gebracht, hebben ze sterk de neiging om samen te klonteren. Hierdoor wordt een deel van het katalysatoroppervlak slecht bereikbaar voor de elektronenmediator en kan zelfs verloren gaan voor waterstofproductie. Wij hebben geprobeerd de deeltjes te stabiliseren (los van elkaar in de oplossing te houden) door polymeren of zeep toe te voegen, maar dat hielp niet. Het is niet duidelijk geworden waarom dat niet werkt.

Door de RuO_2 deeltjes te laten neerslaan op een platina elektrode, zodat een dun filmpje RuO_2 ontstond, en deze elektrode in een oplossing te steken, konden we de snelheid van de H_2 vorming aan het RuO_2 oppervlak bestuderen. Deze snelheid hing af van de elektrische spanning die door ons op de RuO_2 -filmelektrode werd gezet en van de concentratie H^+ ionen in de oplossing (zuurgraad of pH).

Voor de elektronenoverdracht van methylviologeën naar RuO_2 en de vorming van waterstof aan het RuO_2 oppervlak kan de ophoping (adsorptie) van de verschillende componenten van het systeem in het grensvlak RuO_2 /oplossing van belang zijn. Immers, zo'n ophoping zou de processen aan het oppervlak kunnen vertragen. Daarom is de adsorptie van $\text{Ru}(\text{bipy})_3^{2+}$, MV^{2+} en EDTA aan RuO_2 bestudeerd onder de omstandigheden die in het waterstofproductiesysteem heersen. Het bleek dat er niet of nauwelijks sprake is van ophoping van $\text{Ru}(\text{bipy})_3^{2+}$ of MV^{2+} , maar EDTA heeft wel sterk de neiging in het grensvlak te gaan zitten. Uit experimenten met de RuO_2 -filmelektroden bleek echter dat de aanwezigheid van EDTA in het grensvlak de snelheid van elektronenoverdracht tussen methylviologeën en RuO_2 niet beïnvloedt.

Omdat in ons land de zon lang niet iedere dag volop schijnt, werd in de experimenten met het waterstofsysteem een diaprojektor met een sterke lamp (250 W) gebruikt als lichtbron. Uit deze experimenten bleek dat RuO_2 inderdaad een goede katalysator is, ondanks de bovenvermelde sterke neiging van de deeltjes om samen te klonteren. Tijdens de waterstofproductie treedt geen achteruitgang op in de katalytische werking van RuO_2 . Een nadeel van de katalysator is dat de RuO_2 deeltjes zichtbaar licht absorberen (ze zijn donkerblauw, vandaar de kleur van dit proefschrift). Het door RuO_2 geabsor-

beerde licht kan niet gebruikt worden voor waterstofproductie.

Nadat het systeem een tijd lang (een paar uur) waterstof had geproduceerd met een konstante snelheid, bleek de produktie langzamerhand af te nemen. In sommige gevallen kwam dit gewoon doordat de elektronendonor EDTA opdraakte. Maar veel vaker hield de produktie op doordat de elektronenmediator methylviologeen kapot ging. Dit betekent dat methylviologeen geen erg geschikte stof is om gebruikt te gaan worden in eventuele toekomstige commerciële waterstofproductiesystemen.

De snelheid van de waterstofproductie werd bestudeerd onder verschillende omstandigheden. We varieerden onder andere de lichtintensiteit, de hoeveelheid katalysator en de concentraties $\text{Ru}(\text{bipy})_3^{2+}$, MV^{2+} en EDTA in de reaktieoplossing. De waterstofproductiesnelheid bleek erg sterk af te hangen van de lichtintensiteit. Als er maar een beetje RuO_2 in het systeem zit, kan de produktiesnelheid nog verhoogd worden door méér RuO_2 toe te voegen. Maar bij wat grotere hoeveelheden RuO_2 maakte méér toevoegen niet uit; de produktiesnelheid werd er niet hoger van. Zoiets bleek ook te gelden voor de concentraties $\text{Ru}(\text{bipy})_3^{2+}$ en EDTA.

Als we steeds hogere concentraties methylviologeen gebruikten, nam de produktiesnelheid eerst toe, maar later weer af. Bij een bepaalde concentratie MV^{2+} was er dus een maximum in de snelheid van H_2 vorming.

Om de resultaten van de experimenten met het waterstofsysteem beter te begrijpen, werd er een model (een processchema) gemaakt voor het systeem. We gingen na welke scheikundige reacties er allemaal plaats konden vinden tussen $\text{Ru}(\text{bipy})_3^{2+}$, MV^{2+} en EDTA. De gegevens die verkregen waren uit de experimenten met de RuO_2 -filmelektroden werden gebruikt om te beschrijven wat er zich in het grensvlak tussen RuO_2 en de oplossing afspeelt.

Dit model werd gebruikt om een computer de experimenten met het waterstofsysteem na te laten doen (te simuleren). Als de computer werd verteld wat de samenstelling van het reaktiemengsel was (hoeveelheid RuO_2 , concentratie $\text{Ru}(\text{bipy})_3^{2+}$ enz.), rekende hij uit hoe snel er waterstof zou worden gemaakt. De computer gaf bijna altijd dezelfde resultaten als we in de experimenten hadden gevonden. Alleen het maximum in de waterstofproductiesnelheid bij variëren van de MV^{2+} concentratie werd niet door de computer gevonden. Daaruit konkludeerden we dat we met een nog onbekend proces dat zich in het grensvlak RuO_2 /oplossing afspeelt, geen rekening gehouden hebben. Dit zal nog verder onderzocht worden.

Uit de computerberekeningen bleek dat vooral de aanvoersnelheid van

methylviologeen naar het katalysatoroppervlak de snelheid van de waterstofvorming bepaalt. De aanvoer van elektronen door methylviologeen is de langzaamste stap in de processen die zich afspelen in het grensvlak. Als een methylviologeenion eenmaal bij het oppervlak is, geeft hij redelijk snel het meegebrachte elektron af. De aanvoer van H^+ ionen die nodig zijn voor H_2 vorming, gaat heel erg snel.

Verder werd door de computer berekend dat de vorming van waterstof in ons systeem helemaal niet efficiënt is: nog geen 4 % van het licht dat door $Ru(bipy)_3^{2+}$ ingevangen wordt, wordt uiteindelijk vastgelegd in de vorm van brandstofenergie. In planten wordt maar liefst 95 % van de opgevangen zonne-energie vastgelegd in energierijke materialen. De lage waterstofopbrengt in ons systeem wordt niet veroorzaakt doordat de katalysator niet goed zou werken, maar door allerlei vervelende extra reacties in de oplossing, waarbij energie verloren gaat voor de vorming van H_2 . Bij die ongewenste reacties is methylviologeen steeds betrokken. Al met al is het belangrijk om te zoeken naar stoffen die beter dan methylviologeen kunnen optreden als elektronenmediator.

Het zal nog wel even duren voordat er een economisch rendabel (duurzaam en niet te duur) systeem is ontwikkeld. Een auto die rijdt op waterstofgas gemaakt uit water en zonlicht, zullen we voorlopig nog niet tegenkomen in het verkeer. Toch komen we stap voor stap wel verder. Er is al veel bekend over de werking van watersplitsende systemen, en dit onderzoek heeft daar een steentje aan bijgedragen.

CURRICULUM VITAE

Mieke Kleijn werd op 6 december 1956 geboren in Zeist. In 1975 behaalde zij het diploma gymnasium B aan het St. Bonaventura College te Leiden. Na gedurende twee jaar de opleiding diëtetiek in Den Haag te hebben gevolgd, besloot zij te gaan studeren aan de Landbouwhogeschool te Wageningen.

In 1981 behaalde zij het kandidaatsdiploma voor de studierichting Moleculaire Wetenschappen. De daaropvolgende ingenieursstudie omvatte de volgende vakken: kolloïdchemie (hoofdvak), moleculaire fysica (hoofdvak) en bodemscheikunde (bijvak). Haar praktijktijd bracht zij door in Engeland, aan de School of Chemistry van de Universiteit van Bristol. Het ingenieurs-examen werd afgelegd in maart 1983.

Vanaf maart 1983 tot maart 1987 werkte zij als wetenschappelijk medewerkster aan de vakgroep Fysische en Kolloïdchemie van de Landbouwhogeschool/universiteit. In deze periode werd het werk verricht dat leidde tot dit proefschrift. Inmiddels werkt zij als universitair docente in vaste dienst bij de eerder genoemde vakgroep.